Process-Level and Systems Models of Groundwater Flow and Transport Beneath the Pajarito Plateau: Migration of High Explosives from Technical Area 16

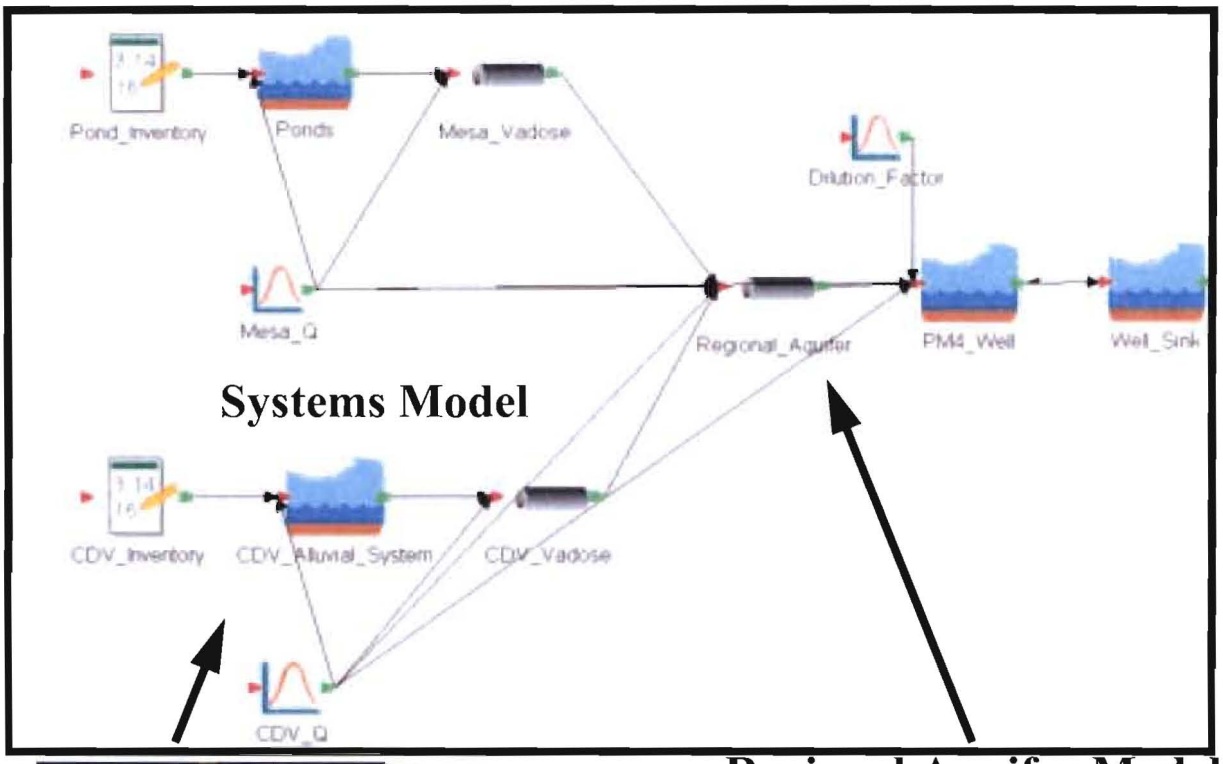

Systems Model

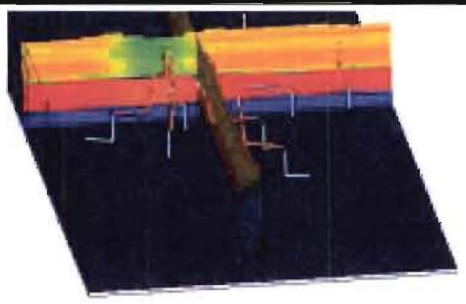

Vadose Zone Model

Regional Aquifer Model

LA-UR-07-5752

Bruce Robinson, Elizabeth Keating, Brent Newman, Kay Birdsell, Bill Carey, Marc Witkowski, Zhiming Lu, April Idar, Mark Haagenstad, George Zyvoloski, Velimir Vesselinov

October 6, 2000

Milestone report submitted to ALDSSR Office to fulfill reporting requirements for the FY 2000 Pajarito Plateau Groundwater Modeling Project

1.0 - Abstract

This report outlines and implements an approach for carrying out process-level and systems models for groundwater flow and contaminant transport on the Pajarito Plateau. The study augments ongoing modeling activities under the Laboratory's Hydrogeologic Workplan and Environmental Restoration Project activities. The primary goal of this new modeling initiative is to develop a methodology for the application of detailed numerical models of contaminant fate and transport to predict current and future potential adverse impacts to the regional aquifer groundwater resource. The modeling methodology is demonstrated to predict the migration of contaminants away from a site of current interest, TA-16. High explosives (HE) detected in well R-25 are modeled several scales using detailed, process-level models. In addition, a probabilistic systems model is used to examine potential future contamination associated with groundwater pumped from the regional aquifer. A critical element of the approach is an iterative process of process model development and prediction, assessment of the uncertainty in the predictions, collection of new data, refinement of the detailed process-level models, and re-assessment of the prediction of the behavior of the system. To implement this plan for HE migration from Technical Area 16 (TA-16), the current data associated with the site has been summarized, and models of flow and transport in the vadose zone (from the ground surface to the regional water table) and the regional aquifer have been developed. To tie the modeling results together, a probabilistic systems model has also been developed. This model includes abstracted representations of the vadose zone and regional aquifer models, as well as an estimate of the HE source term and the dilution associated with extraction of HE-contaminated water in a pumping well. The first phase of model development is presented in this report; subsequent work is needed to implement the iterative process of modeling, data collection, and refinement of groundwater contamination predictions envisioned by the method. Although this study is specific to TA-16, the overall methodology, as well as the specific results obtained from the process-level models, are expected to be relevant to other sites across the Laboratory.

2.0 - Executive Summary

This report outlines and implements an approach for carrying out process-level and systems models for groundwater flow and contaminant transport on the Pajarito Plateau. The modeling methodology is used to predict current and potential future adverse impact to the regional aquifer groundwater resource posed by High Explosives (HE) contaminants released from TA-16. This site is a Los Alamos National Laboratory facility established in the 1940s to develop explosive formulations, and to assemble and test explosive components for the U.S. nuclear weapons program. Although the methodology is implemented for TA-16, the approach should have widespread applicability for providing groundwater impact estimates for other contaminated sites at the Laboratory. This executive summary outlines the approach and highlights the key results of the study.

2.1 Modeling Approach

Figure 2-1 illustrates the approach developed in this study for applying modeling at various scales to estimate impact to groundwater posed by contamination. The systems model is a high-level model that pieces together simplified representations of the various sub-models needed to describe contaminant transport from source to potential receptor. The critical aspect of the systems model is that it is probabilistic: uncertain parameters are given distributions of values, and the Monte Carlo approach is used to predict a family of results, such as the contaminant concentration versus time in a pumping well. This approach yields a range of estimates and a guide to which parts of the system are most important to study to reduce the uncertainty. The simplified sub-models are informed by the process-level models, typically complex numerical models developed to synthesize field and laboratory data to provide a description of the transport pathways. The entire process is envisioned to be iterative: the systems model is used to provide a “bottom-line” metric and to guide future process model development and data collection activities, which, in theory, should serve to reduce the uncertainty to levels deemed sufficient for decision makers. In the present study, the process-level models for HE transport from TA-16 include one- and three-dimensional models of flow and transport through the vadose zone to the regional aquifer, and transport in the regional aquifer. These models are described in the sections below, along with the probabilistic systems model.

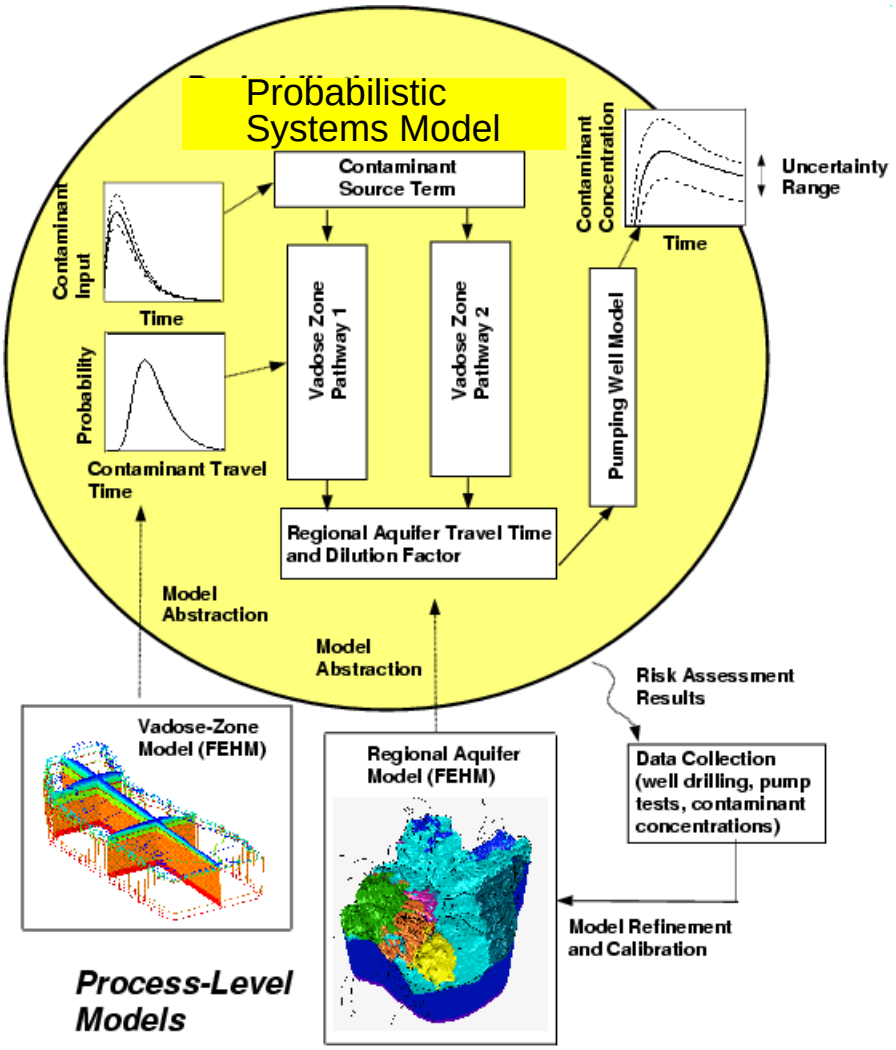

Figure 2-1. Schematic diagram of the probabilistic systems modeling approach for groundwater contamination.

2.2 Vadose Zone Flow and Transport Modeling

TA-16, located in the Western portion of the Laboratory, is one of the most complex sites at the Laboratory in terms of hydrologic behavior and contaminant fate and transport. In the present study, we use the site geologic model to construct one- and three-dimensional models of flow and transport in the vadose zone, the region between the ground surface and the water table of the regional aquifer. To do this, we first outline a conceptual model to describe the observations of complex lateral flow and transport in the uppermost rock strata. This model suggests that the primary pathways through the vadose zone probably occur either from the bottom of retention ponds in which HE has been discharged, or from the bottom of Cañon de Valle. The one-

dimensional modeling results, as well as the data collected in wells drilled at the site, suggest that simple, one-dimensional vertical pathways cannot explain the data thoroughly. Moisture profiles in the shallow subsurface are consistent with infiltration rates on the order of 1 mm/y, whereas in the deeper subsurface, much wetter conditions exist, including the presence of perched groundwater. This is the case even for well R-25, which is located on the mesa. Therefore, lateral flow is indicated by these results. The three-dimensional model was used to explore various mechanisms for explaining the data, including lateral spreading of water at high recharge rates from Cañon de Valle. Figure 2-2 shows that lateral diversion can occur due to the slope of the rock units underneath the site.

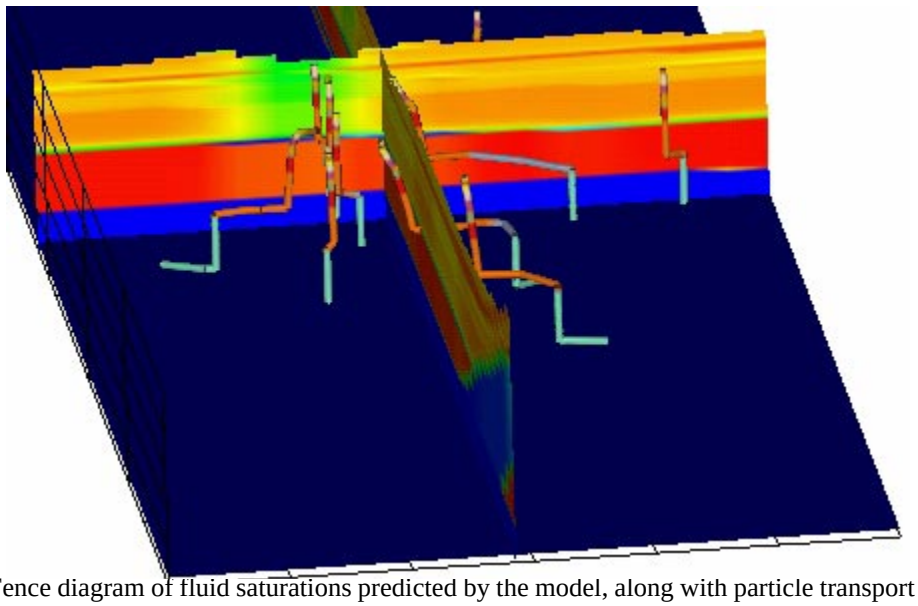

Figure 2-2. Fence diagram of fluid saturations predicted by the model, along with particle transport pathways. Colors on the pathlines represent the hydrogeologic units through which the particles are traveling.

The infiltration rate in Cañon de Valle is an uncertainty that cannot be reduced with the present data. At present, we can use travel times of HE to depth to bound the infiltration rate if we assume that the water traveled from Cañon de Valle. Figure 2-3 shows the predicted travel time to various depths, illustrating the dramatic difference in travel time depending on whether the release is on the mesa at a location where infiltration rates are low, versus in Cañon de Valle. Initial simulations used a Cañon de Valle infiltration rate of 300 mm/y, consistent with values estimated for Los Alamos canyon, but travel times suggest that perhaps larger infiltration rates (1000 to 2000 mm/y) are possible. The modeling shows that moisture content measurements in relatively shallow wells drilled into the bedrock could allow us to reduce the uncertainty of infiltration rate.

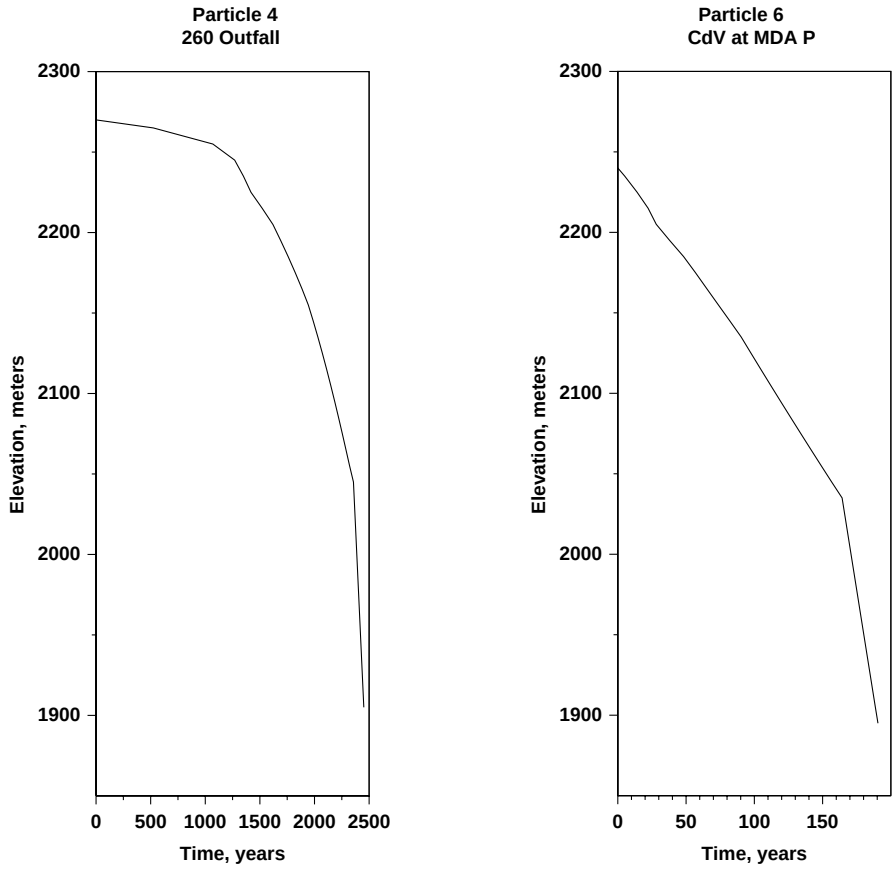

Figure 2-3. Travel time to depth predicted by the model for releases from the mesa (left) and from Cañon de Valle (right).

We have also used the three-dimensional model to explore alternative computational and conceptual approaches for simulating the behavior of the vadose zone. A promising approach is to develop a combined unsaturated/saturated (UZ/SZ) model to simultaneously resolve flow and transport in the vadose zone and in the regional aquifer (see Figure 2-4 for a figure showing the particle pathways resulting from such a model). Model results are preliminary because the numerical challenges of such an approach have not been fully studied and resolved. However, the approach holds promise for providing a realistic depiction of the transport behavior of contaminants in the shallow saturated zone, including the effects of pumping wells. Using the combined UZ/SZ model approach, an alternate conceptual model was explored for explaining the hydrogeology of the site. In this model, water generally interpreted as perched is assumed to be the top of the regional aquifer. This results in shorter travel times in the vadose zone (due to the shallower water table) and steeper gradients in the regional aquifer under the site.

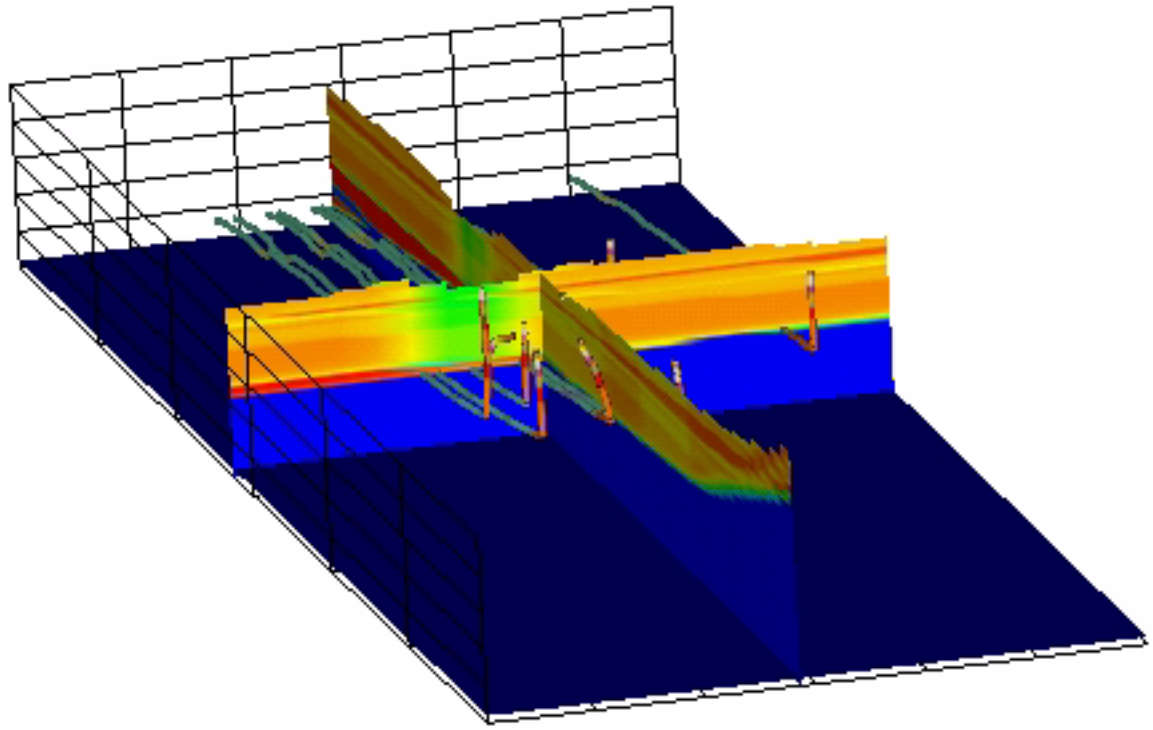

Figure 2-4. Particle pathlines for the combined UZ/SZ model, illustrating the near-vertical transport to the water table, followed by easterly transport in the regional aquifer.

2.3 Regional Aquifer Flow and Transport Modeling

2.3.1 Approach

This year's modeling of HE transport in the regional aquifer builds on the initial effort described by Keating et al.(1999), who performed particle tracking simulations using a relatively coarse numerical mesh. One important result of the previous work was to highlight the importance of the hydraulic properties of the Puye Formation, the shallowest hydrostratigraphic unit in the aquifer in the vicinity of R-25. According to the site-wide geologic model, the Puye Formation is subdivided into two hydrostratigraphic zones (fanglomerate and Totavi Lentil) (Carey et al. 1999). These initial HE transport simulations highlighted the dominant role of the permeable Totavi Lentil hydrostratigraphic unit, which, as defined by the site-wide geologic model (Carey et al. 1999) provided a continuous conduit for relatively fast transport away from TA-16. In fact, the spatial continuity of the Totavi Lentil is not certain. More generally, we believe it is important to address the inherent uncertainty in spatial definition of hydrofacies within the Puye Formation. Thus, we have begun the development of a stochastic facies-based model of hydraulic conductivity variation for this important unit. The elements of the stochastic approach are: (1) identification of key

hydrofacies within the Puye, (2) estimation of the statistics of facies dimensions (e.g. minimum, maximum, mean thickness; minimum, maximum lateral continuity) and spatial relations between facies, using outcrop and borehole data, (3) generation of facies-based stochastic hydraulic conductivity fields within the Puye Formation.

Although field characterization and compilation of previous field work has begun, we were not able to collect as much new data as expected due to the Cerro Grande fire, which greatly limited our access to those canyons where the Puye is well exposed. The composite dataset on facies in the Puye is, at present, is insufficient to adequately parameterize a facies-based stochastic model. Therefore, we have incorporated the limited available data into a relatively simple stochastic model and have examined the influence of fine-scale heterogeneity within the Puye on HE transport in the regional aquifer. As more data are collected from the Puye, we will develop a more realistic facies-based stochastic model.

In order to investigate the possible importance of fine-scale heterogeneity within the Puye, we created a separate numerical mesh for the Pajarito Plateau (a small fraction of the area of the basin-scale model) with increased vertical resolution. For this model, the water flux estimates from the basin-scale model were mapped onto the submodel. In addition, recharge applied at the water table and outflow at the Rio Grande was accomplished in the same manner as the basin-scale model (see Keating et al., 1999 for details). This submodel provides a suitable platform for simulating HE transport.

2.3.2 Flow and Transport Simulations

The transport simulation results described below are based on a simulated steady state flow field for the Pajarito Plateau, assuming that pumping rates in municipal supply wells continue into the future at approximately the same rates as were measured in 1996. Since transport results will be very dependent on the accuracy of the flow field simulations, it is important to evaluate the consistency of the flow model with available data (permeability, water level, and flux data). Figure Figure 2-5, presents the predicted flow field for pre development conditions and associated residuals. Overall, the degree of agreement with predicted and measured water levels in this portion of the laboratory is very good. Matching water level declines is more difficult, and is the subject of current investigations.

To address sensitivity of the transport results to various degrees of heterogeneity within the Puye Formation, we generated a number of stochastic hydraulic conductivity fields for this

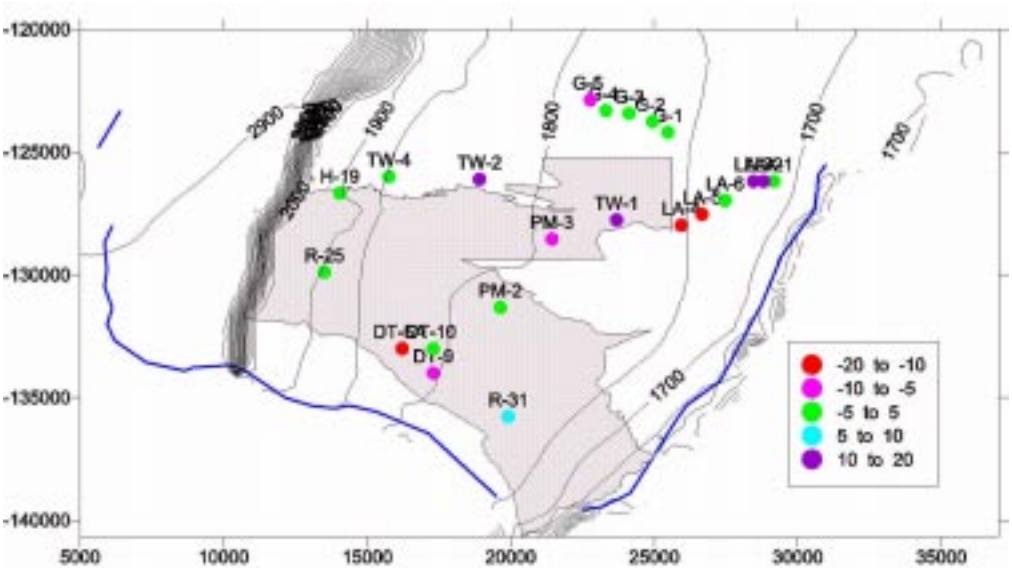

Figure 2-5. Predicted future water level contours, assuming 1996 pumping rates continue indefinately.

hydrostratigraphic unit. Since the number of measurements is limited and the estimated values have relatively large uncertainties, it is necessary to analyze the sensitivity of modeling results on the input parameters. We conduct several sets of numerical experiments to explore the importance of each parameter on simulation results. To predict HE transport beginning in 1945 and continuing hundreds of years into the future, we assume that 1996 pumping rates for all LANL area wells are sustained for the duration of the simulation. A particle tracking transport model is used to simulate conservative transport of HE from its source at the water table at R-25 to its eventual destination. Figure 2-6 shows the transport to the municipal well PM-4, and to the Rio Grande for a representative case. The fate of HE in these simulations is predicted to be to these wells and the Rio Grande, in proportions and with travel times that are functions of the specific stochastic permeability fields and porosity.

2.3.3 Summary of HE Transport Simulation Results

By developing a stochastic approach to simulating heterogeneity within the Puye Formation, we are able to examine a relatively large number of cases and provide meaningful bounds to the range of possible travel times between R-25 and the PM well field. For the case we consider to be among the most realistic, given the present dataset available to constrain the transport model, we conducted 19 simulations for different stochastic realizations. Ensemble breakthrough curves are presented in Figure 2-7; the average mean breakthrough time for the 19

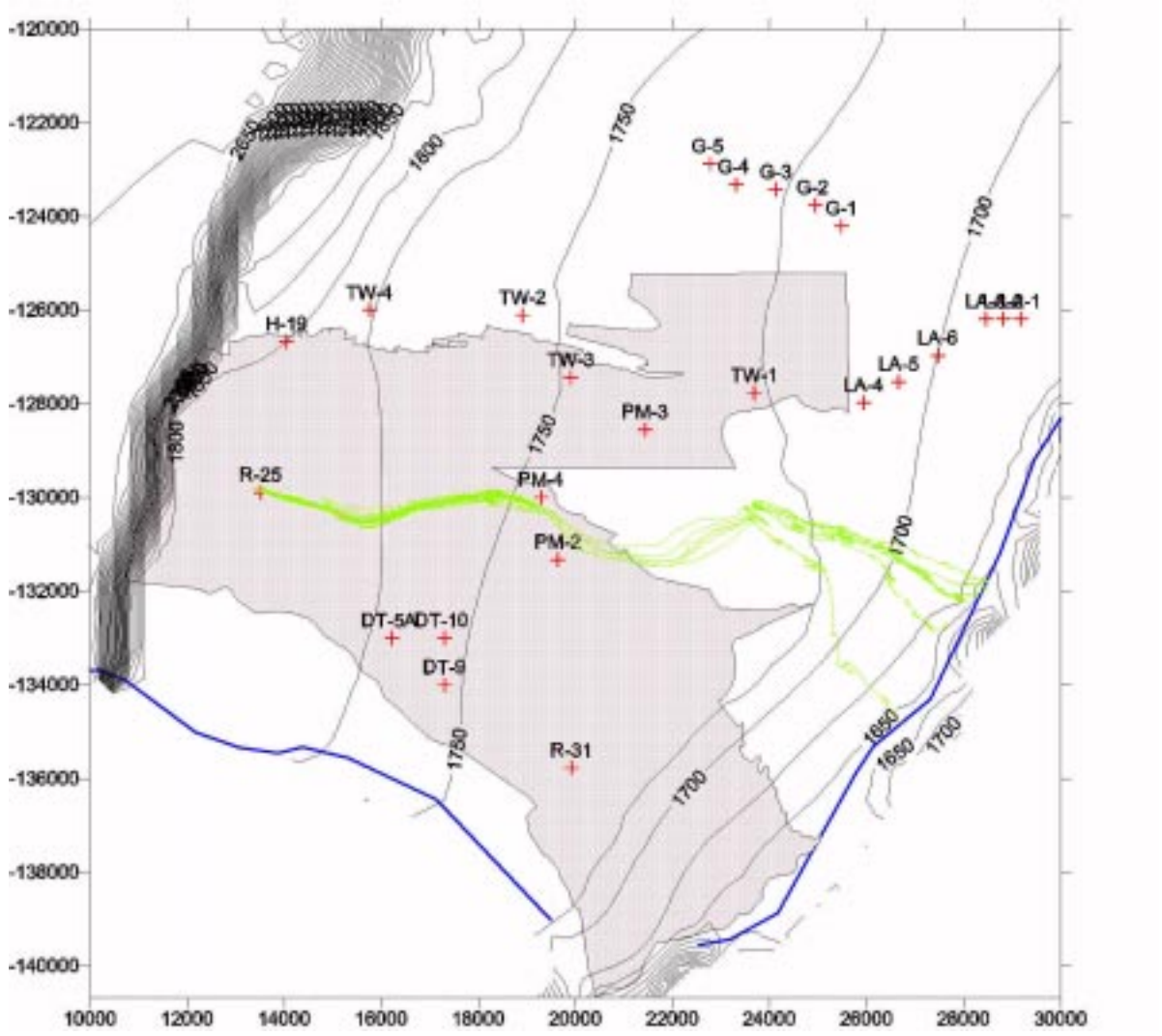

Figure 2-6. Particle tracking simulation of HE transport from the water table at R-25 to municipal well PM-4 and the Rio Grande.

cases was 286 years (PM4) and 477 years (PM2). Other simulations illustrate the importance of the porosity of the medium in controlling transport times. To estimate this parameter, we recommend that interwell tracer experiments be performed, in which the breakthrough curve of a solute under pumping conditions is determined. Accompanying modeling at the scale of the field site would aid in the interpretation and provide a partial demonstration of the validity of the transport modeling approach being taken to characterize transport in the regional aquifer.

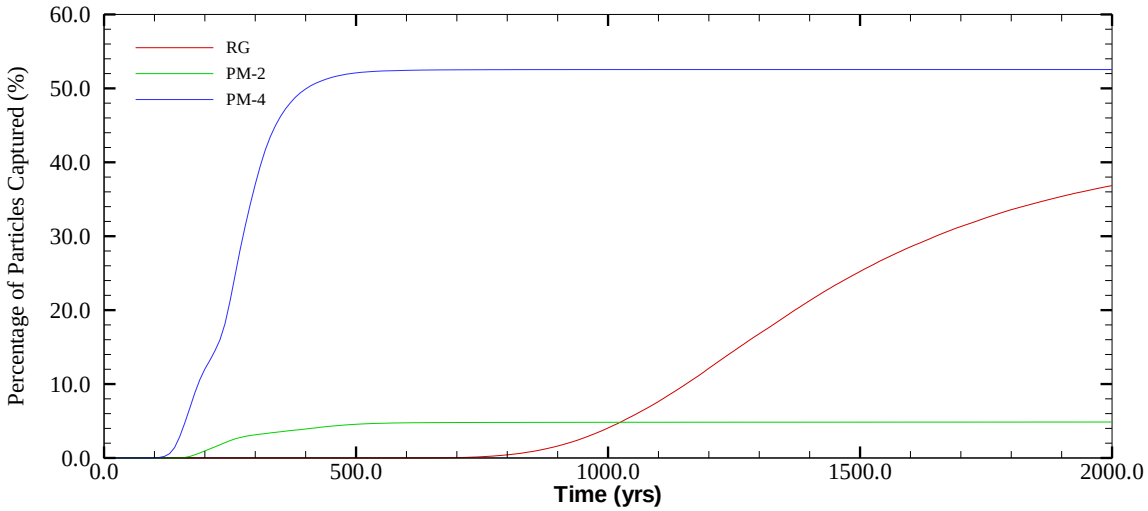

Figure 2-7. Ensemble breakthrough curve for Case 9, computed from 19 realizations.

2.4 Probabilistic Groundwater Flow and Transport Model

The systems model developed in this section applies probabilistic concepts to assessing the uncertainty in parameters and their impact on groundwater contaminant transport. In this portion of the study we use the commercial software GoldSim (Golder Associates, 2000) code to construct a model for HE transport from TA-16. We also include barium in the analysis, as it is an additional contaminant of interest at the site. The TA-16 GoldSim groundwater transport model includes two vadose-zone pathways, one that represents sources from ponds located on the mesa top and the other from the alluvial aquifer located in Cañon de Valle, as shown in Figure 2-8. Royal Demolition eXplosive (RDX) and barium travel through these two vadose-zone pathways to combine and flow through the regional aquifer into Los Alamos County Municipal Well PM-4, where an uncertain dilution factor is applied to account for the mixing of contaminants with clean water at the well. RDX was selected as a worst-case HE contaminant because of its relatively high solubility, conservative (nonsorbing) behavior, and resistance to biodegradation. Barium was selected because it is the dominant inorganic contaminant at TA-16 and because it represents a species with strong adsorption. The model uses an unlimited source term and stochastic distributions to describe RDX source concentrations, vadose-zone flow rates, regional aquifer flow rates, porosities, and well dilution factors. The results are based on analysis of 100 Monte Carlo realizations for a 1000-year transport period.

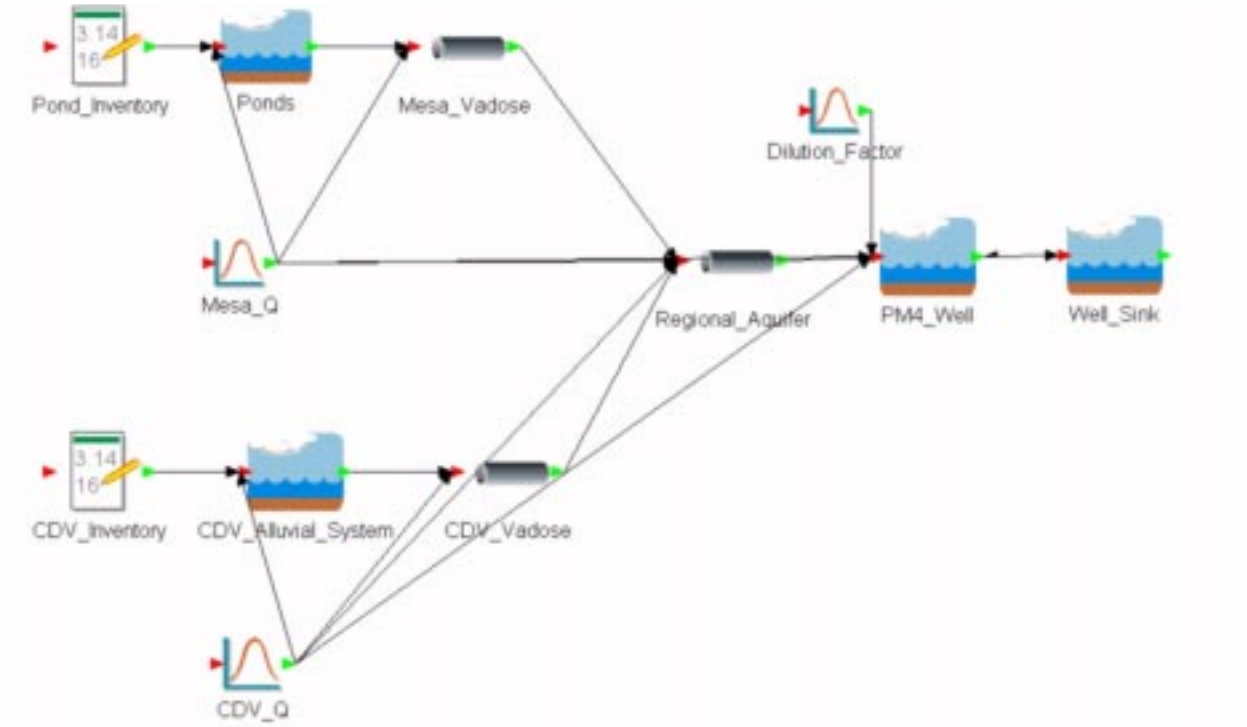

Figure 2-8. GoldSim model flowchart for TA-16. The figure shows the graphical elements and pathways used to model RDX and barium transport at TA-16.

The transport of RDX and barium can be examined either in the individual paths or as the composite behavior, which considers the source areas, the vadose zone pathways, the regional aquifer, and finally, the PM-4 well. In general, the vadose zone pathway results suggest that RDX concentrations exhibit rapid transport with breakthrough curves reaching concentration limits in less than forty years. This is consistent with the information from well R-25. Barium transport in the mesa is apparently minimal. Concentrations for all of the realizations do not reach analytically detectable levels in the 1000-year time frame. The magnitude of the concentrations reflect low solubility of barium, and the long travel times are the result of sorption.

Concentrations of RDX at the end of the regional aquifer flow path represent inputs from both mesa and Cañon de Valle sources. Figure 2-9 shows the range of concentration breakthrough curves of the fluid at the end of the regional aquifer predicted by the stochastic model. First arrivals of RDX at the end of the regional aquifer pathway range from about 110 to over 1000 years, depending on the stochastic parameters selected by the GoldSim code. Because of the unlimited source inventories, and large RDX concentration limits, some of the realizations show fairly rapid and large concentration increases after first arrival. Finally, the PM-4 pumping well results show

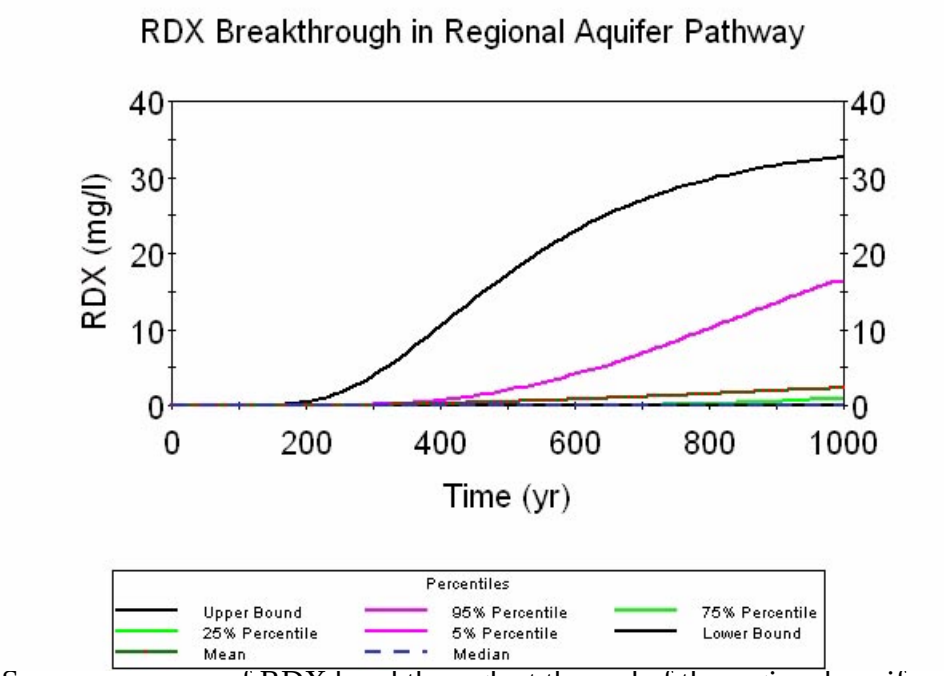

Figure 2-9. Summary curves of RDX breakthrough at the end of the regional aquifer pathway.

that substantial reductions in RDX concentrations can occur if the well pumps from both contaminated and uncontaminated parts of the regional aquifer (Figure 2-10).

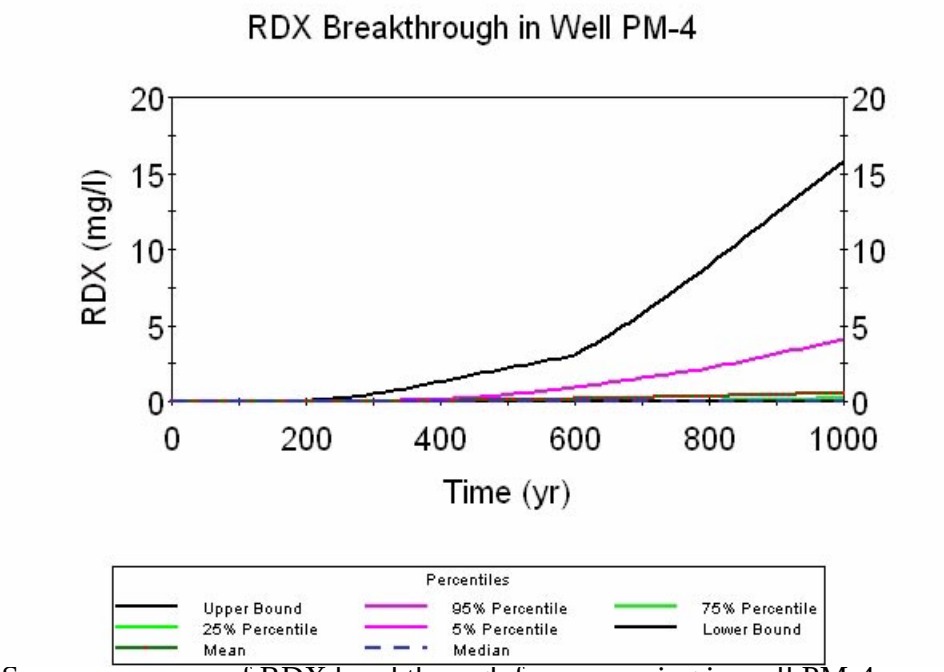

Figure 2-10. Summary curves of RDX breakthrough from pumping in well PM-4.

Results presented for the GoldSim model show a wide range of possible behaviors, much of which is due to the ranges used in the various stochastic distributions in the model. However,

under the current conservative estimates applied in this initial modeling effort, predicted concentrations reaching well PM-4 for the worst cases are higher than acceptable from a human health standpoint. However, we stress that in several instances, conservative assumptions have been made, and that further work will likely reduce the highest predicted concentrations. Furthermore, the modeling suggests that concentrations will not begin to rise in PM-4 for many decades, illustrating that this is a long-term issue rather than one that demands immediate remedial action.

Top-down modeling approaches such as the one used here can typically be refined (reducing uncertainty) from the initial simulations by collecting and applying additional information about how the system behaves. A high-level sensitivity analysis of the current model reveals the following key uncertainties requiring attention in order to reduce uncertainty and significantly lower the projected concentrations in the pumping well:

- *The HE inventory and source term.* On-going work at TA-16 by the LANL Environmental Restoration Project will provide improved inventory estimates that may allow us to relax the unlimited inventory assumption. If the forthcoming inventory estimates are low enough, the model estimates will show much lower concentrations predicted for the regional aquifer and PM-4 water. In addition, ongoing surface clean-up efforts should improve the predictions.
- *The flow rates for the various model elements.* The stochastic distributions of flow rates are based on best available data and in some cases are probably realistic site-specific values. Nevertheless, additional data collection should reduce the uncertainty of the vadose zone and regional aquifer transport velocities.
- *The cross-sectional areas of the vadose and regional aquifer pathways.* The area of recharge through the vadose zone could be smaller than that used in the model because of localized or preferential flow, or could be larger because we did not include some of the historic ditches and ponds that are no longer at the site. Like the flow rates, reduction of the cross-sectional area uncertainty can be achieved through on-going site characterization work and additional process modeling.
- *Dilution of contaminant in the pumping well.* This process was treated with a purely stochastic parameter, the dilution factor. In wells screened over hundreds of feet, contaminant plumes

may be diluted dramatically from their *in situ* concentrations. A mechanistic model of this process is required to place the results on a scientifically defensible basis.

2.5 Recommendations

We have demonstrated that the methodology proposed to examine flow and contaminant transport in the groundwater beneath the Pajarito Plateau can provide important insights into the potential impact associated with particular contaminants. A two-pronged effort of process-level and probabilistic systems modeling is the recommended course of attack for understanding the system and performing focused studies to determine future impact. An important element of the probabilistic systems modeling approach is that it must be iterative. A single iteration does not capitalize on one of the biggest advantages of the approach, the ability of the results to guide future modeling and data collection activities. A more practical issue is that in the first iteration, we may not have enough of the right type of data, and the process-level models will not be refined enough, to enable us to make an argument of minimal impact to groundwater. In the present study, conservative assumptions about the HE source term and transport properties were required. Consequently, the worst of the Monte Carlo realizations yielded maximum concentrations at well PM-4 which, if taken out of context, might be regarded as alarming. The proper perspective is that these concentrations are unlikely to occur for at least many decades, and that many realizations predict much lower concentration. The worst cases reflect the actual outcome only if several pessimistic parameters simultaneously turn out to be true. In an iterative approach, we identify which of these parameters control the results, and work to reduce those uncertainties.

With regard to HE migration from TA-16, the GoldSim modeling revealed that the following uncertainties were most important to the “bottom line:”

- The HE inventory and source term.
- The flow rates for the various model elements.
- The cross-sectional areas of the vadose and regional aquifer pathways.
- Dilution at the pumping well.

Therefore, future modeling and characterization efforts should focus on obtaining a better understanding of these elements. With this in mind, in the report we discuss specific recommended ac-

tivities that should be embarked on in the next iteration of modeling. For the vadose zone model, the next iteration will allow for a better incorporation of the source term, more accurate flow velocities through the vadose zone, and an improved understanding of the perched water and its connection to the regional aquifer. Another iteration on the regional aquifer model will provide better estimates of transport velocities and plume dimensions through the development of the facies-based permeability model. In addition, dilution at the pumping well will be better understood. Finally, the next iteration of the systems model will use the process-level models more directly, providing a more integrated set of models, and probably a narrowing of the range possible results.

3.0 - Introduction

The Laboratory's Hydrogeologic Workplan (LANL, 1998) specifies a wide range of drilling, site characterization, data management, and groundwater modeling activities. One of the primary goals of these efforts is to develop a detailed understanding of the groundwater flow and transport system for the purpose of assessing the impact associated with past, current, and future releases of contaminants and to propose remedial action where necessary for public safety. One of the main site characterization activities is the ongoing deep-drilling program, in which a network wells are currently planned over the next several years. Data collected from recently drilled boreholes, as well as ongoing modeling activities, has led to improved understanding of the nature of fluid flow and contaminant transport through the vadose zone, and has allowed us to refine the conceptual models describing groundwater flow and contaminant transport processes at the site.

The ongoing groundwater flow and transport modeling activities fall into three categories:

- Vadose zone models of flow and transport at the scale of an MDA. Currently, models exist for MDA G, MDA AB (TA-49), and MDA L (adjacent to Area G).
- Vadose zone models of flow and transport at the scale of a canyon, incorporating multiple water and contaminant source terms. Currently, the model of Los Alamos canyon extends approximately from Los Alamos Reservoir to State Road 4.
- A saturated zone model of flow at the scale of the regional aquifer (Espanola Basin). To date, a preliminary model of the groundwater flow system has been developed. Currently, the model is being updated to include newly collected data and geologic interpretations of existing data, and will incorporate geochemical information to further constrain the model. In addition, a finely resolved site scale model of the regional aquifer beneath the Pajarito Plateau is being inserted within the Basin-scale model to provide a platform for contaminant transport calculations.

In this study, a method is implemented for integrating the results of these models and other on-going hydrologic studies via probabilistic systems modeling of contaminant transport in groundwater. This approach will accomplish two important objectives: 1) better feedback between on-going data gathering and modeling activities, and 2) improved predictions of the fate and transport of contaminants over multiple scales, so that contaminants can be traced from their source

to potential receptors in the regional aquifer. The study uses HE migration from TA-16 as the test case, but the method developed is applicable to any contaminated site, and is intended to be used at other sites at the Laboratory. In addition to putting in place methods that will benefit the Laboratory's groundwater investigations, general scientific issues are addressed by this modeling work, including:

- Further confirmation of the Laboratory’s conceptual model of vadose zone flow, which consists of slow percolation through mesas and rapid percolation from focussed infiltration in canyons;
- The interaction and mixing of a contaminated plume in the vadose zone with the regional aquifer;
- The migration and dispersion of a contaminant plume within the regional aquifer as influenced by heterogeneities in aquifer hydrologic properties;

These results are described in the individual chapters associated with each model.

4.0 - Probabilistic Systems Modeling Approach

Figure 4-1 summarizes the approach being developed and implemented to assess the impact to groundwater from contaminants introduced from past Laboratory releases. To provide a comprehensive analysis of groundwater contaminant impacts, a hierarchy of models will be employed to carry out the top-down groundwater modeling strategy outlined in this study. To describe the approach succinctly, we first need to define two classes of models:

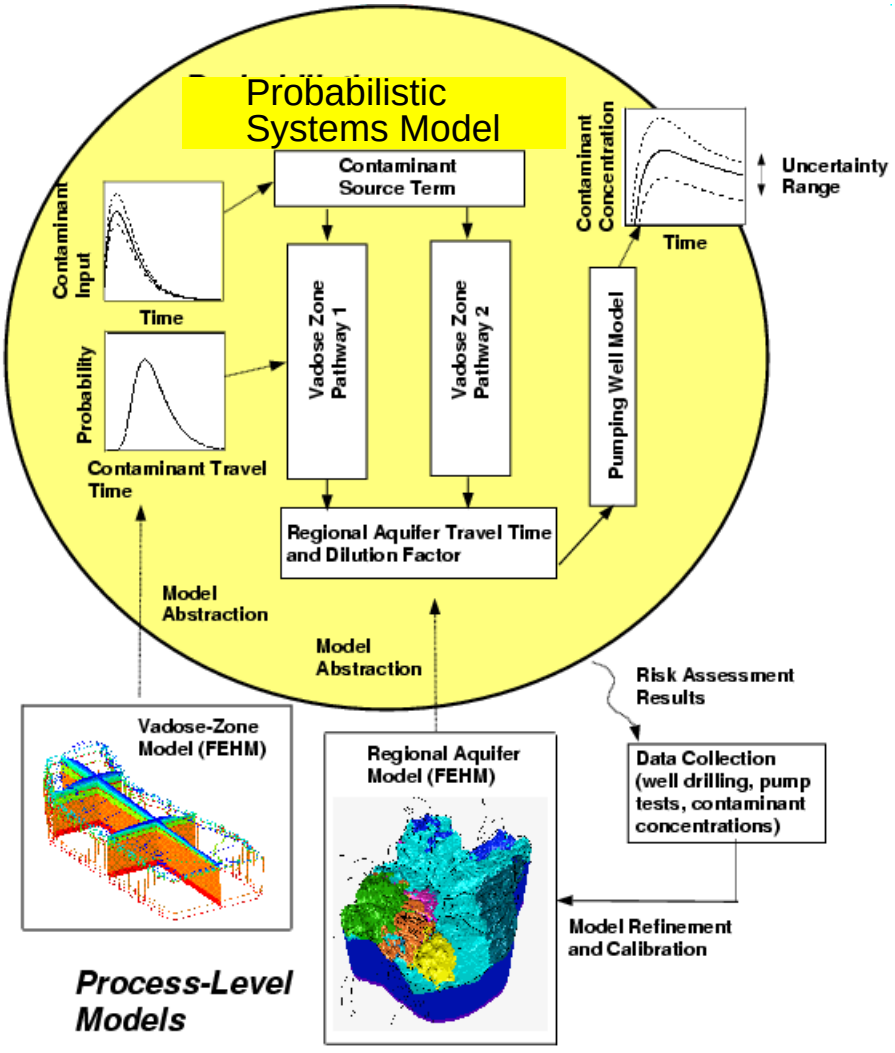

Figure 4-1. Schematic diagram of the probabilistic systems modeling approach for groundwater contamination.

Probabilistic systems model: a high-level model incorporating all relevant aspects of the contaminant transport system from source to potential receptor. For groundwater flow and contaminant migration, sub-models would typically be required for the contaminant source term, transport

through the vadose zone, plume migration in the regional aquifer, and capture and potential dilution at a pumping-well. This model stitches together sub-models, each of which involve complex processes. For practical reasons, the sub-models must be abstracted versions that "capture the essence" of the behavior of the actual process. Furthermore, in the probabilistic systems model, each of the sub-models has uncertainty ascribed to it. The results from such an overall model are therefore probabilistic, yielding a range of possible outcomes for a desired quantity (concentration in the pumped water, for example) rather than a single "answer." Sensitivity analyses can be performed to define which sub-models and which uncertain parameters are most important to study in order to reduce the uncertainty in the behavior of the system. The commercial software package GoldSim (Golder associates, 2000) is being used to perform this element of the modeling.

Process-level model: a detailed numerical model (typically a finite difference or finite element model) of a portion of the contaminant flow and transport system. These models are best used to understand in detail the behavior of a groundwater flow and transport system. The models incorporate existing hydrologic and transport information and use fluid and solute mass conservation equations to simulate the movement of fluids and contaminants. Model results are compared to field measurements and the models are "calibrated" to match the field results. The models are then run in the forward mode to predict transport behavior in the future. The models currently being developed in support of the Hydrogeologic Workplan fall into this category.

In the present study, the probabilistic system model is intended to be a tool to guide the development of the process-level models and future data collection. The process-level models are required to study the flow and transport system in detail, and the results are "abstracted" to represent the sub-models. When probabilistic model results are generated, such as the range of contaminant concentrations represented in Figure 4-1, one of the outputs will be a sensitivity analysis identifying the key uncertainties. This information will then be used to guide data collection and subsequent model refinement and calibration.

In this study, we implement an integrated methodology for modeling fate and transport of contaminants away from a site of current interest, TA-16. High explosives (HE) transport is modeled several scales using detailed, process-level models. In addition, a probabilistic systems model is developed to examine potential future impact associated with groundwater pumped from

the regional aquifer. The modeling would answer key questions on HE transport, and, perhaps more importantly, would provide a testbed for a methodology that can be applied to the Laboratory's other groundwater investigations.

Thus, the overall goal of this modeling study is to develop a methodology for the application of detailed numerical models of contaminant fate and transport to predict current and future potential impact to the regional aquifer groundwater resource. When this result is achieved and applied throughout the site, the modeling performed in support of Hydrogeologic Workplan will have a more direct tie to the site characterization program, and future modeling can be used, for example, to guide the drilling program in terms of placement of wells and recommendations of the data to be collected in the wells.

The plan for achieving this global objective includes the development of process-level models and a probabilistic systems model for contaminants originating at a particular site of interest to the Laboratory, namely TA-16. In a sense, TA-16 is a “testbed” for the methodologies being established. In addition, the findings will apply generally to many Laboratory sites. A plan for developing a process-level model of the vadose zone flow and transport system is described in Section 2. Then, the proposed work for the modeling of transport in the regional aquifer is described in Section 3. Finally, the proposed work plan for integrating the results through the development of the probabilistic systems model for HE migration in groundwater is discussed in Section 4.

5.0 - TA-16 Site Description and Hydrologic Characteristics

TA-16, located in the Western portion of the Laboratory (Figure 5-1), is one of the most complex sites at the Laboratory in terms of hydrologic behavior and contaminant fate and transport. The combination of relatively wet mesa and canyon conditions, different geological units with varying properties, multiple flow paths, different types of flow behavior, and multiple source areas results in a conceptual model that has to consider many different pathways and processes. Large uncertainties associated with aspects of the conceptual model are the result of the complexity of the TA-16 system. The modeling work performed in this report is designed to reduce these uncertainties. Until recently, the characterization has centered primarily on the surface and near-surface hydrology. This work will form the basis for establishing shallow transport pathways associated with the HE source term. The drilling of Well R-25 and CDV-15 has provided valuable information on deep vadose zone pathways and the mixing of recharging fluids in the regional aquifer. These two data sources and past studies of the hydrologic properties of the Bandelier tuff are used in the development of an initial vadose-zone flow model for the TA-16 site. In this chapter we summarize the available information on the site.

5.1 Stratigraphy

The stratigraphy of the units located above the regional water table at TA-16 is shown in Figure 5-2 (Wohletz, 1999). A soil layer covers much of the mesa top and alluvium is present in the canyon floor. In descending order, the next eight units make up the Tshirege Member of the Bandelier tuff. The units dip gently toward Cañon de Valle. The Tsankawi Pumice Bed and Cerro Toledo tuffs lie between the Tshirege Member and the Otowi Member of the Bandelier Tuff. The Guaje Pumice and the Puye Formation lie at the base of the unsaturated zone. Not all of the units are present throughout TA-16. For example, in Cañon de Valle, some of the upper units are absent.

5.2 Contaminant Source

TA-16 was established in the 1940s to develop explosive formulations, to cast and machine explosive charges, and to assemble and test explosive components for the U.S. nuclear weapons program. Almost all of the work has been in support of the development, testing and production of

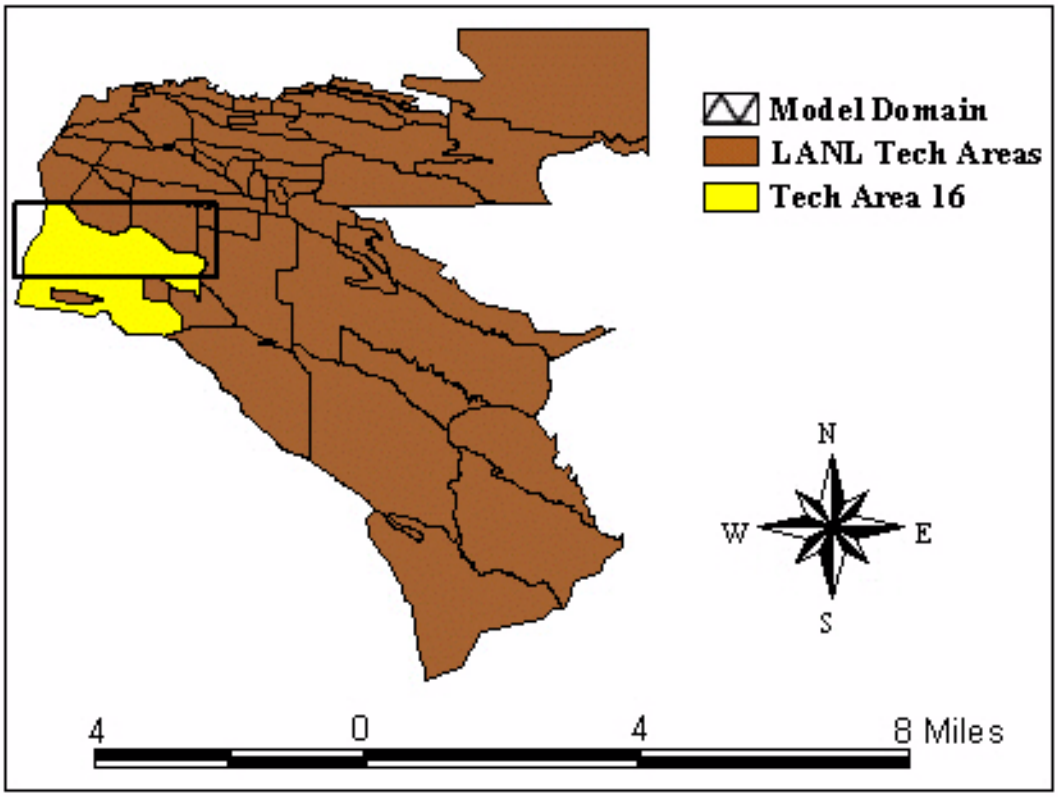

Figure 5-1. Los Alamos National Laboratory, showing TA-16 and the extent of the three-dimensional model domain.

explosive charges for the implosion method. (RFI report, 1998) Present-day use of this site is essentially unchanged, although facilities have been upgraded. As a result of the site's long history of explosives production and testing, HE contamination is wide spread.

The TA-16-260 facility, in operation since 1951, is an HE-machining building that processes large quantities of HE. Machine turning and HE wash water are routed as waste through a sump system that in turn is routed to an outfall. Discharge was historically as high as several million gallons per year. The outfall was shut off in 1996 and the 260 effluent now goes to the TA-16 treatment facility. Other HE contaminated sites include the 90's line pond, MDA R, the TA-16 Burning Ground, and MDA P. HE waste waters were routed to the 90's line pond from the 90's line buildings. MDA R was used as a burning ground for waste explosives from the mid 1940s into the 1950s. HE and HE-contaminated wastes were also burned at the TA-16 burning ground. MDA P contains waste from the processing and testing of HE and residue from HE-burning activities.

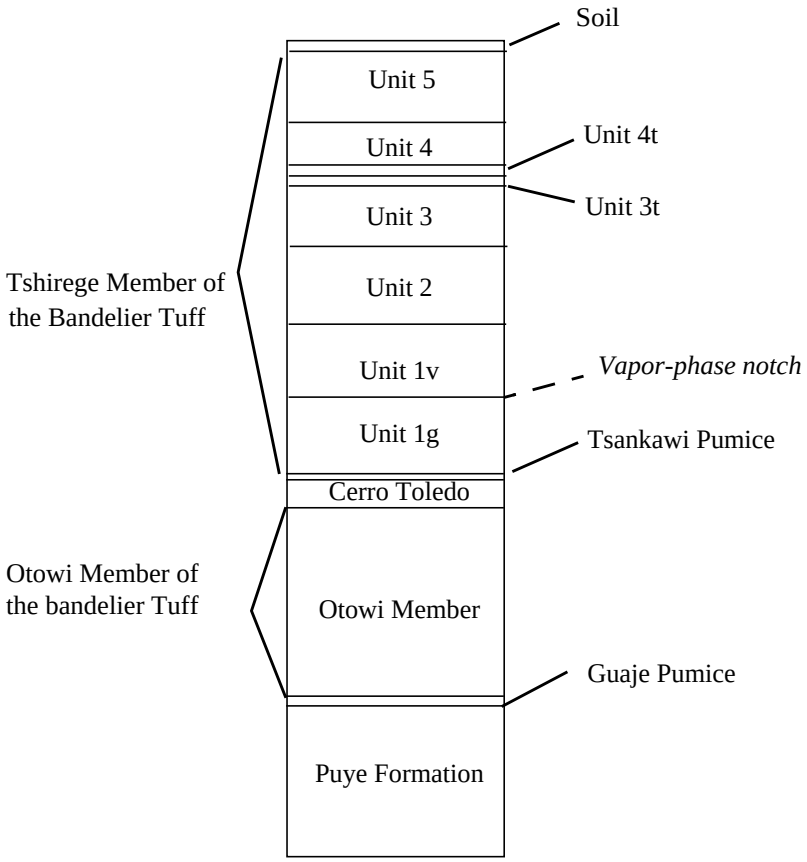

Figure 5-2. TA-16 site stratigraphy.

5.3 Vadose Zone Hydrologic Data

5.3.1 Water Content Data

Water content has been measured in several boreholes at TA-16: 16-2665 in Martin Canyon, 16-2669 near the 90's line pond, 16-2667 near SWSC spring, 16-2668 near Building 300, and the regional groundwater well R-25, which is located approximately 1700 ft east of the TA-16-260 outfall, PRS 16-021(c). These data are shown in Figures 5-3 and 5-4. Gravimetric moisture data were obtained for well R-25, and these data are roughly converted to water content assuming a bulk density of 2.0. Water contents are generally quite low, 10% by volume or less, except that zones with saturated or near saturated conditions have been observed in hole 16-2665 and 16-2669. In R-25, a major perched saturated zone was present in the Otowi Member between 747 ft and 1132 ft, and the regional aquifer extended from 1286 ft to the total depth of the borehole at 1942 ft. A zone of numerous alternating saturated zones and dry rock separates the two major saturated zones

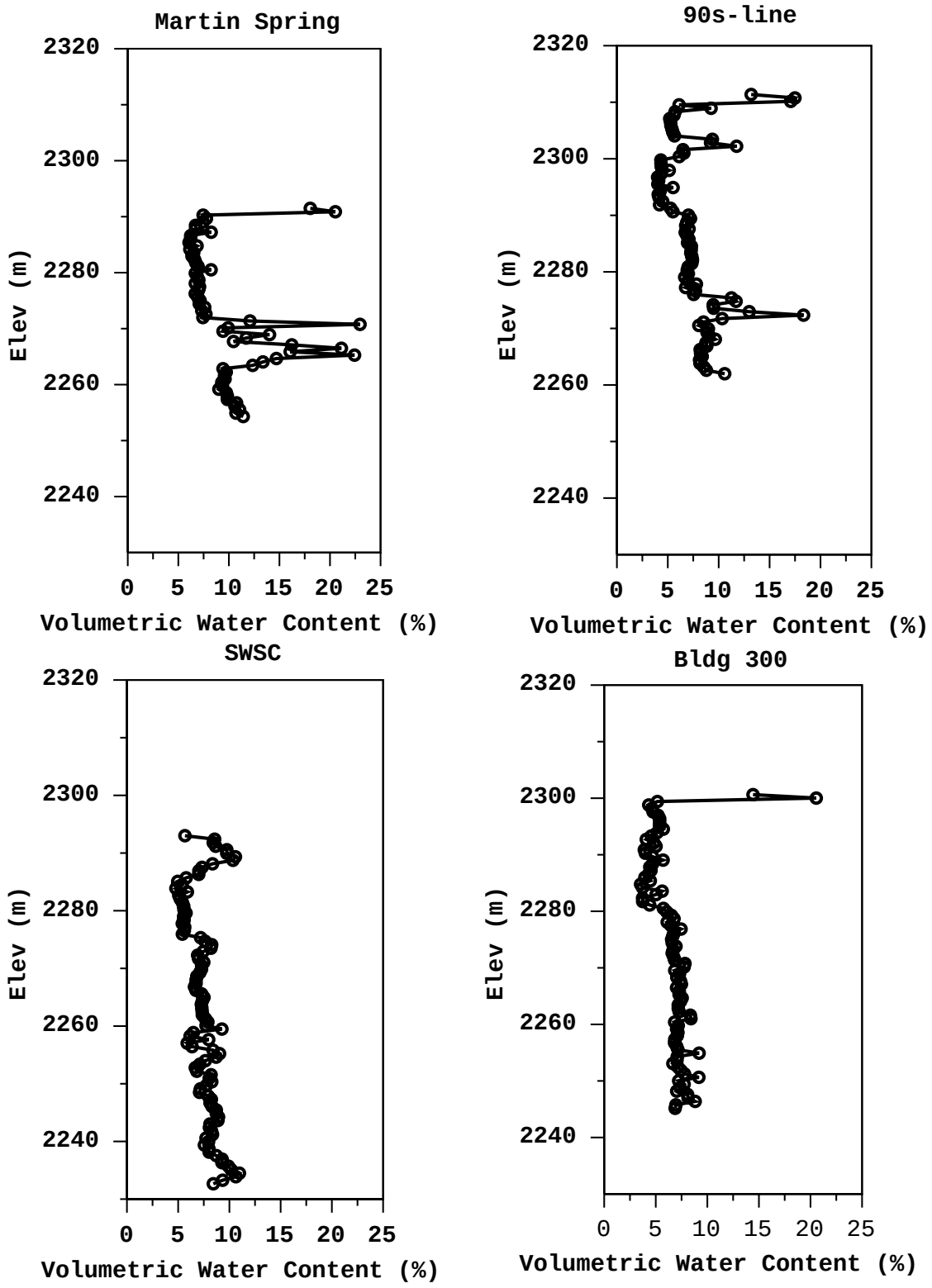

Figure 5-3. Volumetric Moisture Content data for holes 16-2665 in Martin Canyon, 16-2669 near the 90's line pond, 16-2667 near SWSC spring, 16-2668 near Building 300.

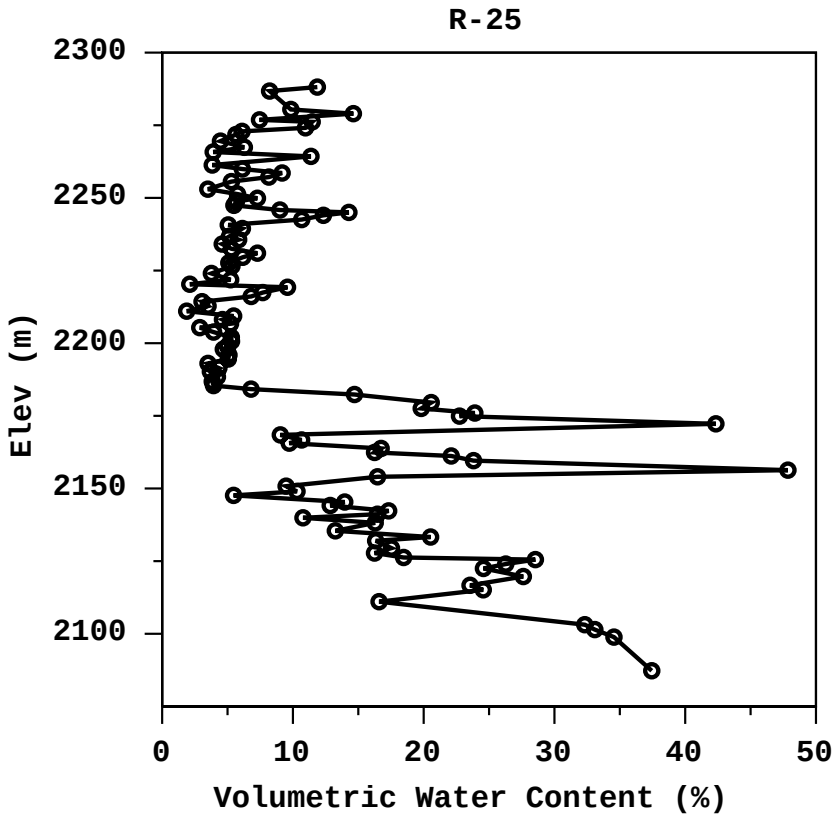

Figure 5-4. Volumetric moisture content data for regional well R-25

(Broxton et al., 1999). The nature of connectivity between these two major zones is unknown, but two conceptual models of this hydrologic condition are possible:

- The alternating wet and dry zones represent a layer upon which water perches, and the water represents downward percolation under saturated conditions; or
- The regional aquifer is represented by the top of this perched water body, and the alternating wet and dry zones are low-permeability rocks that appear relatively dry during drilling, but are actually below the water table.

5.3.2 Vadose Zone Infiltration Estimates

Chloride-based downward flux rates are estimated for the boreholes near Martin Canyon, near the 90's line pond, and near SWSC spring. These estimates are shown in Table 5-1. The flux

Table 5-1. Chloride-Based Downward Flux Rates

Borehole	Depth range (ft)	Flux Rates (mm/yr)
Martin Canyon	25-110	1.3
90's Line Pond	25-150	1.3
SWSC	5-200	1.4

estimates are too low to explain the presence of HE in the saturated zones in the Martin and 90's line boreholes. This interpretation suggests that most of the recharge to the saturated zone is occurring in up-gradient areas where fluxes are higher. If so, there must also be a lateral component to flux, which is consistent with the low hydraulic conductivities of some of the tuff units. Flux rates calculated based on chloride analyses from R-25 core suggest that downward rates are also on the order of one mm/yr.

5.3.3 Material Properties

This study focuses on the vadose-zone near the 90's line pond, the 260-outfall pond and in Cañon de Valle. The van Genuchten model (van Genuchten, 1980) is used to represent the unsaturated characteristic curves for the hydrostratigraphic units. Site-specific hydrologic properties for Unit 5, Unit 4, Unit 4t, Unit 3t, and Unit 3 were measured on core samples, as shown in Table 5-2. These hydrologic properties data show substantial variation within and between units

Table 5-2. Hydrologic properties summary for upper-most subunits of the Tshirege Member, Bandelier Tuff at TA-16

Unit	Borehole	Depth (ft)	θv	ρb	Porosity	Ks (cm/s)	welding
5	Bldg 300	10.5	6.7	1.73	0.349	1.40E-5	partly
5	Bldg 300	19	3.9	1.97	0.258	1.20E-6	partly
4	Bldg 300	31	2.4	1.3	0.51	3.80E-3	surge
4	SWSC	70.5	7.8	2.13	0.198	1.70E-8	densely
4t	90's line	90	7.2	2.17	0.18	2.00E-8	densely
4t	SWSC	89	4.6	2.21	0.165	9.80E-9	densely
3t	SWSC	100.5	7.2	2.16	0.184	2.80E-8	densely
3t	SWSC	120.5	15.4	1.42	0.466	5.00E-4	surge

Table 5-2. Hydrologic properties summary for upper-most subunits of the Tshirege Member, Bandelier Tuff at TA-16

Unit	Borehole	Depth (ft)	θv	ρb	Porosity	Ks (cm/s)	welding
3	SWSC	129.5	5.2	1.71	0.356	5.80E-5	poorly

which strongly affects flow. The denser the welding, the lower the matrix hydraulic conductivity. However, the more welded units have larger fracture porosity which is not reflected in these laboratory-scale analyses. Properties for the remaining units were obtained from the Los Alamos Canyon model (Robinson et al., 1999).

5.4 Subsurface Contaminant Distributions

High explosives were detected in regional well R-25 during fiscal year 1999 (Broxton et al., 1999). Both of the major saturated zones appeared to contain HE constituents and degradation products, including RDX, TNT, HMX, and amino-DNTs. RDX is the most abundant constituent; RDX concentrations range from non detect to above 75 μg/L. The two highest HE concentrations were in the middle of the perched zone and near the top of the regional aquifer, although until a developed well is complete it is difficult to evaluate whether any leakage from the upper zone to the lower zone has occurred.

HE contamination of shallow alluvial groundwater in Cañon de Valle and in the TA-16 springs is ubiquitous. RDX and other HE constituents are present in these media at levels greater than those observed in the R-25. HE constituents at low levels (< 10 (g/L RDX) have also been observed in springs at TA-9, in springs at TA-18, and in surface and alluvial waters within Pajarito Canyon. It is assumed that liquid discharges at the TA-16 surface constitute the primary historic source for the HE observed at R-25.

Multiple sources of high explosives contamination have been identified in soils at several technical areas in the western portion of the Laboratory through RCRA Facility Investigation (RFI) studies completed to date. Based on these RFI studies, the largest HE contaminant source term in soils appears to be at the TA-16-260 outfall. Other sites with significant (greater than a few hundred (g/g HE in soils) identified HE source terms include: the TA-16 Burning Ground and MDA P, MDA R, the TA-11 drop tower (K-Site), the 90s Line Pond, and TA-9-48 outfall at TA-9. Although these, and other yet identified, sources may all be contributing HE to deep perched and regional saturated zones, the large contaminant mass at the TA-16-260 outfall and its location

directly up-gradient from regional well R-25 suggest that it is the major source of HE in the deep perched and regional saturated zones in the TA-16 region.

5.5 VADOSE ZONE FLOW AND TRANSPORT CONCEPTUAL MODEL

This summary describes the TA-16 conceptual model for vadose zone flow and HE transport and how recent work has been used to support or revise the model. TA-16 is one of the most complex sites at the Laboratory in terms of hydrologic behavior and contaminant fate and transport. The combination of relatively wet mesa and canyon conditions, different geological units with varying properties, multiple flow paths, different types of flow behavior, and multiple source areas results in a conceptual model that has to consider many different pathways and processes. Large uncertainties associated with aspects of the conceptual model are the result of the complexity of the TA-16 system, and new data and modeling activities are focused on reducing those uncertainties. The major features of the TA-16 conceptual model are discussed below.

- The conceptual model describes key aspects of the hydrology and geology of a roughly triangular area that is bounded by Cañon de Valle on the north, Water Canyon on the south, the Pajarito Fault zone on the west, and the confluence of Cañon de Valle and Water Canyon on the east.
- Saturated flow systems occur in different forms, including the alluvial aquifer in Cañon de Valle; SWSC Spring, Burning Ground Spring, and Martin Spring; and the 90s Line Pond. All of these systems contain HE and other contaminants. Additional saturated flow systems may also be present and are discussed below.
- New investigations of 100-200 ft boreholes on the mesa suggest that ponded sources on the mesa have contributed contamination to transient saturated zones, 100-130 ft deep. These zones have RDX concentrations between 100 and 300 ppb. Samples from the 90s line pond indicate concentrations are relatively dilute. However, the dilute concentrations are likely caused by rain and snow and because no more HE is being added to the pond. During the active use period, the pond was likely saturated with HE.
- The saturated systems that feed the springs are hypothesized to be ribbon-like structures within the mesa.
- The ribbons appear to predominate at or above the Unit 4/Unit 3 contact where there is a

transition from poorly welded to strongly welded tuff. The three springs flow from or near the Unit 3/4 contact.

- In addition to the ribbons, transient saturated zones and contaminant transport in the mesa are strongly controlled by differences in the hydrologic properties between the various stratigraphic units. Newly collected data show that saturated hydraulic conductivities vary by several orders of magnitude.
- The ribbons feed the springs via localized fracture zones or high-permeability streaks. The area around the Cañon de Valle springs appears to be more fractured than the surrounding tuff. The area around Martin Spring is covered by colluvium.
- These ribbons been not been identified during drilling, so their existence is only hypothesized. Transient saturated zones have been found near the Unit 3/4 contact, which supports the saturated ribbon hypothesis. In addition, alternative hypotheses on the source of the spring water (i.e., alluvial water or artesian conditions) do not appear to be viable.
- Recharge of the saturated ribbons may occur via various sources and processes including the Pajarito Fault zone, the Steam Plant drainage, and the 90s Line Pond. Recharge may also occur via transient saturated flow.
- The presence of a 400 ft perched saturated zone in R-25 and a similar saturated zone in SHB-3 suggest the presence of a substantial recharge source to the west of TA-16. The same recharge source may also be feeding the spring/saturated ribbon system although along a different pathway than the deeper perched zone. These zones likely have a large influence on lateral and vertical transport of contaminants from TA-16.
- Transient recharge can occur via flow through fractures or other preferential flow pathways. The borrow pit located on the west-end of TA-16 is an area where transient recharge might occur.
- Transient recharge influenced by fracture flow is supported by recent moisture content measurements in two mesa top boreholes.
- The 260 outfall is a source of contamination for Cañon de Valle, SWSC spring and possibly Burning Ground spring. Bromide tracer deployed at the outfall has been observed at SWSC spring. It may have also reached Burning Ground Spring. Because the tracer reached SWSC in a relatively short time (about 4 months) under generally unsaturated conditions, transient flow

along fractures appears to be an important pathway for contaminant movement from the outfall. Matrix or porous media flow may be important as well, based on the presence of contaminants in surge beds and the powder unit. However, the wet conditions needed to verify matrix flow with the tracer have not yet developed.

- Investigations of the magnitude of the 260 outfall source term show that annual output from 1951-1996 was over 1 million gallons/year of HE saturated water (the water was also supersaturated with respect to barium).
- Pathways other than the outfall provide the bulk of the recharge to the springs. The 260 outfall has been decommissioned, yet the springs are still flowing. The outfall may have been volumetrically an important contributor to Cañon de Valle spring flow in the past, but this is no longer the case. However, this does not preclude the outfall area from being a significant contributor of contamination to the spring system.
- Surface runoff, erosion, and spring flow contribute contaminants to the Cañon de Valle alluvial aquifer. However, the effect of the springs is to dilute contamination in the alluvial aquifer. Subsurface flow may also contribute contaminants to the alluvial aquifer, however this has not yet been determined. Surface runoff, subsurface flow, and erosion can redistribute contaminants to downstream locations and ultimately to Water Canyon.

Because the 260 outfall was such a large source of HE, contaminant fate and transport from the outfall is an important aspect of the TA-16 system. Substantial inventories of contamination exist in the near surface of the outfall drainage, and contamination also exists at depth in the subsurface. Spotty contamination observed at depth in the outfall drainage boreholes indicates that contaminants are probably moving along preferential flow paths. The subsurface geology promotes preferential flow because of the large variation in hydraulic properties between and within the uppermost tuff units and also because of the fractured nature of some of the tuff units. The borehole data and tracer results also support the importance of transient flow events in controlling the fate and transport of contaminants from the outfall area into the deeper subsurface and into Cañon de Valle. This transient process can occur via fractures acting as intermittent fast flow pathways, or when large inputs of water (e.g., spring snowmelt) temporarily saturate localized zones of the subsurface resulting in matrix flow, as opposed to fracture flow. At present, because the outfall has been shut off, transient saturated zones may not develop as frequently or persist as long as they have in the past.

The impact of the outfall contamination on Cañon de Valle is substantial. The bromide tracer results show that the outfall is supplying contaminants to SWSC spring and possibly to Burning Ground Spring. Both of these springs contribute contaminants to the alluvial system in Cañon de Valle. In addition, unidentified subsurface flowpaths, overland flow, and lateral subsurface flow (interflow) may also transport contaminants from the outfall to the alluvial aquifer. The 260 outfall may not be the only source of contamination to Cañon de Valle however. Both MDA-R and MDA-P may be contributing contaminants to the canyon. Monitoring data near MDA-P suggests that its impact on the canyon is minimal. New data collected below MDA R suggest that it is a source of contaminants to Cañon de Valle in addition to the 260 outfall.

Because Cañon de Valle has both surface and subsurface flow, and because the 260 outfall and other potential contaminant sources drain into Cañon de Valle, this is the most important pathway for redistribution of contaminants away from TA-16 and into down-gradient locations such as the lower part of Water Canyon and into deeper saturated zones. During large runoff events, contaminants will move into Water Canyon. The disappearance of the Cañon de Valle alluvial aquifer down-canyon from MDA-P and the presence of HE in borehole R-25 suggest that there is subsurface transport to deeper units. The alluvial aquifer disappears shortly after it encounters Tshirege Unit 2, which is typically well fractured and could be acting as a fast flowpath to the aquifer encountered in R-25. Newly acquired discharge measurements and geophysical surveys of Cañon de Valle suggest that recharge of deeper systems may be occurring through the canyon bottom. In addition, these data provide important constraints for the FEHM and GoldSim modeling efforts.

The presence of HE in the perched saturated zone and possibly regional aquifer at borehole R-25 has led to additional investigation about recharge pathways to the system encountered by R-25 and to down-gradient locations. Flux rates calculated based on chloride analyses from R-25 core suggest that downward rates are on the order of one mm/yr, which is too low for HE to reach 700 ft in a few decades. This is a significant result, and along with flux estimates from other TA-16 holes and the FEHM vadose zone modeling presented here, indicates that for HE to travel 100 to over 700 ft though the vadose zone that recharge must be occurring from sources with higher moisture contents and/or heads. Thus, the source term focus of the modeling is on Cañon de Valle, mesa top ponds, and the 260 outfall because these are the places where the high moisture/head conditions are met. Our modeling work is consistent with the above information and should

provide insights as to the relative importance of each source term type especially in terms of controlling impact to groundwater.

6.0 - Vadose Zone Numerical Model

6.1 OVERVIEW

Two sets of calculations are performed in this section. First, a series of one-dimensional simulations at various locations around TA-16 are performed. These locations are at the deep borehole R-25, beneath the 90's line pond, and beneath the 260 outfall pond. Results from these simulations are compared to the observed water content data, chloride profile results and the conceptual model to interpret flow mechanisms at the site. The one-dimensional models serve as a simple calibration platform to examine potential recharge rates and flow patterns that are consistent with the borehole data. Then, a three-dimensional model is constructed to examine more complex flow patterns that cannot be explained with simplified one-dimensional representations. In these models, a more complete picture can be made of the relative infiltration rates across the TA-16 site.

The simulations are run with FEHM, a multi-dimensional finite-element code suitable for simulating systems with complex geometries that arise when modeling subsurface flow and transport (Zyvoloski et al., 1997). In the unsaturated zone, the governing equations for flow arise from the principles of conservation of water and air. Darcy's law is assumed to be valid for the momentum of the air and water phases in the unsaturated zone and for the water phase in the saturated zone. A number of different solute transport solution techniques are available (Zyvoloski et al., 1997, Robinson et al., 2000a).

6.2 One-Dimensional Models

6.2.1 COMPUTATIONAL GRID

Defining the site geology is the first step in grid generation. The geology for the one-dimensional unsaturated-zone columns used in this study was derived from the LANL site-wide geologic model (Vaniman et al., 1996). Grids were made at the location of R-25, beneath the 90's line pond, beneath the 260 outfall, and at two locations in Cañon de Valle. Simulations were run on the first three of these grids. The grids beneath the 90's line pond and the 260 outfall pond each have 460 nodes. The R-25 grid have 383 nodes. Node spacing varied from 0.25 feet near the surface to a maximum of 4 feet in the Otowi Member. Each of the grids ends in the Guaje Pumice.

6.2.2 BOUNDARY CONDITIONS

To bound the infiltration rate at the site, we start by applying a steady infiltration rate across the upper boundary of the computational grid. The steady-state water content that results from this boundary condition is then compared to the field data. For these preliminary runs, the infiltration rate is set to 1.0 mm/yr, based on the chloride profile analysis. The lower boundary represents the water table with a fixed saturation of 0.99.

6.2.3 One-Dimensional Flow Model Results

Figures 6-1, 6-2 and 6-3 show the resulting moisture profiles for the 1-mm/yr steady infiltration rate compared to site data for R-25, for the 90's-line pond hole, and near the 260 outfall pond, respectively. The stratigraphy for each column is also shown for reference.

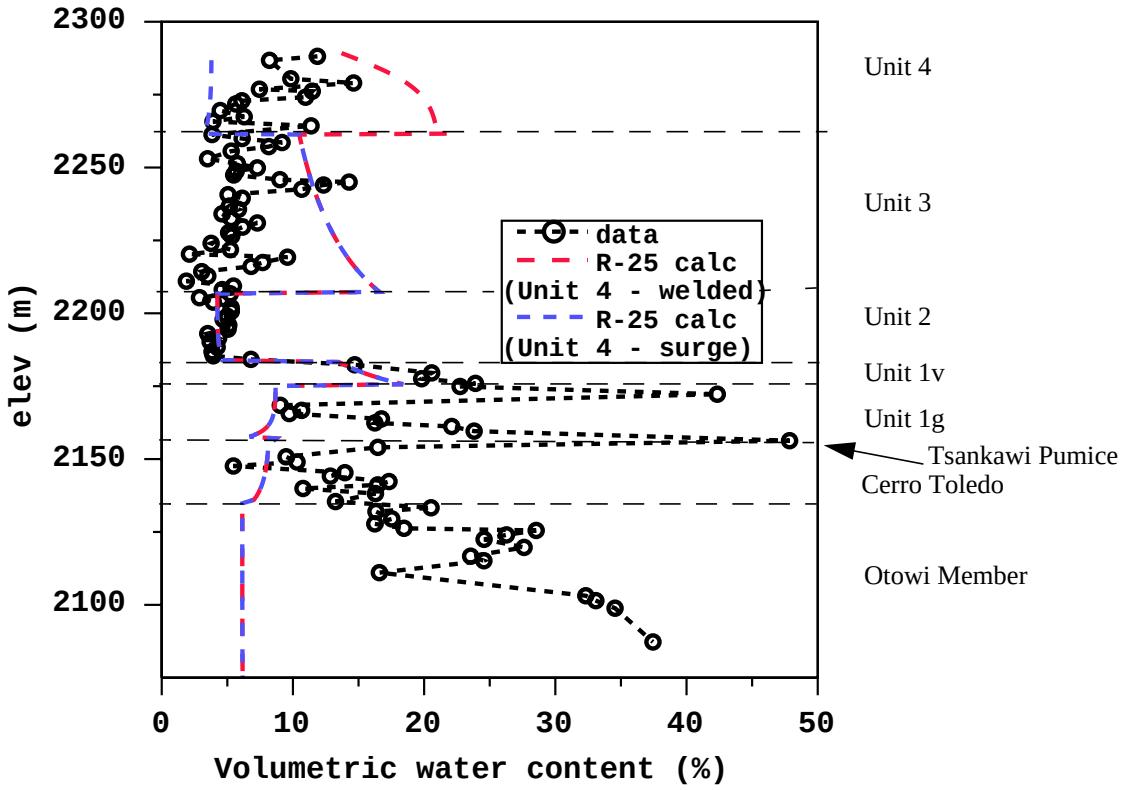

Figure 6-1. Volumetric water content data compared to simulated results for R-25. The simulations assume a constant infiltration rate of 1 mm/yr and use either welded or surge properties for Unit 4.

For well R-25, the simulated 1-mm/yr profiles match the site data fairly well in the upper units, Unit 4 through Unit 2. By simulating the column with both the welded Unit 4 and the surge Unit 4 properties, the resulting moisture profiles bound the data in that unit. The calculated water content in Unit 3 is higher than the observed water content. This result can occur either because the

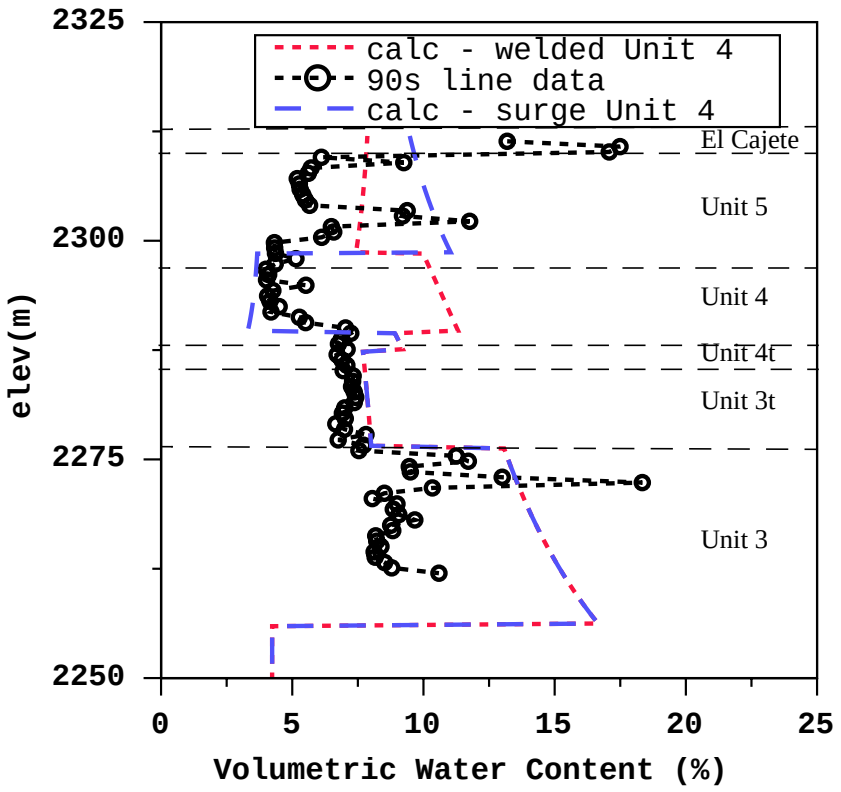

Figure 6-2. Volumetric water content data compared to simulated results for the 90's line pond hole, 16-2669. The simulations assume a constant infiltration rate of 1 mm/yr, and use either welded or surge properties for Unit 4.

simulated infiltration rate is lower than the actual rate at this location, or that the hydrologic properties used in the model do not exactly match the local values. Recall that Unit 3 is highly variable and only one set of hydrologic properties from TA-16 was available for these simulations. The simulated results and the data match extremely well for Unit 2. Below Unit 2, the one-dimensional flow model does a poor job of matching the data by considerably under predicting water content. The large moisture spikes in Unit 1g and in the Tsankawi Pumice bed are not observed in the simulation. Also, dry conditions are predicted for the Otowi member rather than the ponded conditions that were observed in R-25. The difference between the simulated results and the data indicate that recharge to the deeper units does not result directly from vertical infiltration. The moisture is thought to be the result of lateral flow from an up-gradient recharge source. Alternatively, the matrix moisture data could reflect the portion of the water that percolates through the rock matrix, whereas additional flow could be rapidly bypassing the matrix through fractures. However, this conceptual model conflicts with measurements and modeling performed on an injection test performed at TA-50 (Purtymun et al., 1989, Robinson et al., 2000b).

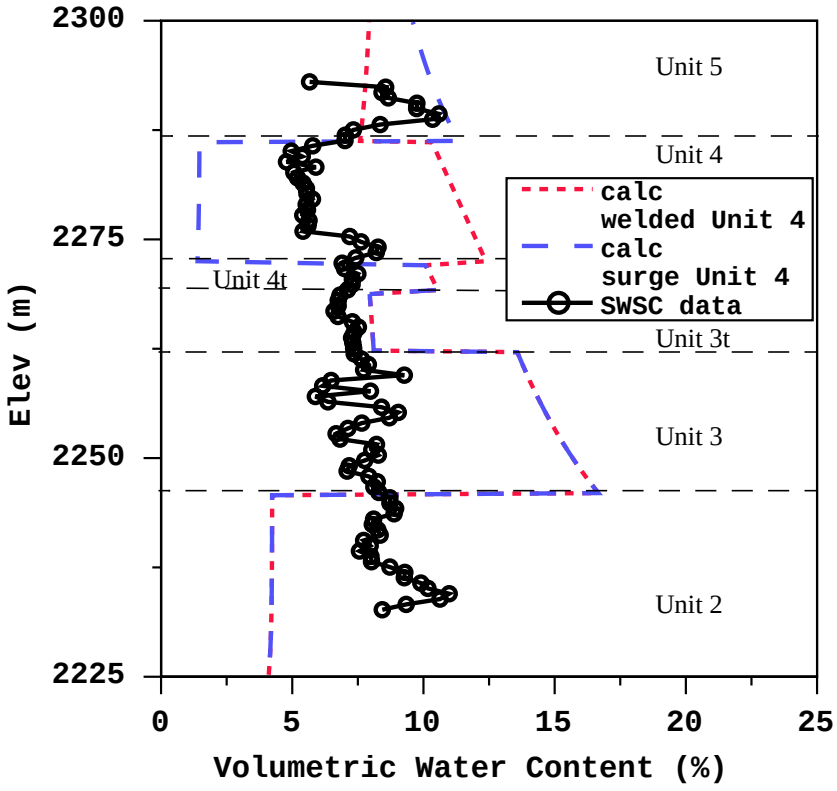

Figure 6-3. Volumetric water content data compared to simulated results for the 260 outfall one-dimensional column compared to data from the SWSC hole, 16-2667. The simulations assume a constant infiltration rate of 1 mm/yr, and use either welded or surge properties for Unit 4

For the well near the 90's line pond, the results are similar. The simulated 1-mm/yr flow matches the data quite well from Unit 5 down through Unit 3t. Unit 4 is observed to be powdery at this location, and we see that the surge properties yield a better fit to the data than do the welded Unit 4 properties. In Unit 3, the model again generally over predicts the water content, except that the near saturated condition observed in Unit 3 is not predicted by the model.

When comparing the simulated profile for the 260 outfall pond to the data from the nearby SWSC hole, the results are consistent with the other two profiles. The simulated 1-mm/yr flow matches the data fairly well for the whole profile. Again, the two sets of Unit 4 properties produce results that bound the data. The borehole log for the SWSC hole shows that the upper portion of Unit 4 is powdery (surge) while the lower portion is welded. The moisture data are consistent with the log in that the moisture content is lower in the powdery material than in the welded material. As seen in the other two profiles, the model again over predicts the water content in Unit 3. The borehole log does not show that the SWSC hole extends into Unit 2, as the one-dimensional grid

does. This explains the large difference in the simulated water content at the Unit 3/2 interface that is not present in the data.

Note that the data presented in Figures 6-2 and 6-3 are not from locations directly beneath the 90's line and 260 outfall ponds. We expect that the water content beneath these ponds is higher than at the sampled locations. To model flow beneath the ponds, a head boundary condition is more appropriate than the low, fixed-infiltration rate used in the simulations that were presented. Also, fracture flow may occur in the partly to densely welded tuff units (see Table 2), thus contributing to the observed short-circuiting of the vadose zone. Ultimately, these effects should be incorporated into the three-dimensional. However, in the three-dimensional model results presented in Section 6.3, the most effort was placed on capturing the enhanced infiltration along Cañon de Valle, so the increase in recharge at locations such as these ponds must be incorporated in an updated version of the model.

6.2.4 Conclusions: One Dimensional Modeling

The one-dimensional analyses performed to investigate the vadose zone flow and transport system at TA-16 showed that in the uppermost units of the Tshirege member of the Bandelier tuff, recharge on the mesa setting of this site receives on the order of 1 mm/yr. This conclusion is supported by a good fit to the volumetric moisture content data from several characterization wells, including the recently drilled well R-25, as well as by application of the chloride mass balance method to the chloride data from the shallow wells. This recharge rate is approximately the same as that determined by modeling of water content results from several mesa settings around the Laboratory, including TA-49, TA-54, and TA-21. This result supports a key element of the conceptual model of vadose zone flow on the Pajarito Plateau, namely the low recharge rates on mesas. This result, taken by itself, would imply that contaminant travel times through the vadose zone should be long.

However, deeper subsurface sampling at R-25 indicates that this is not the case. HE contamination was detected to great depths at this well, possibly including the regional aquifer. Furthermore, saturated or nearly saturated conditions, combined with perched water, were found in the Otowi member and the Puye formation in this well. One-dimensional models at recharge rates of 1 mm/yr cannot explain this critical observation. Therefore, we conclude that significant lateral diversion is occurring at intermediate depths, and that R-25, a mesa well, has tapped into a subsurface water body fed at the surface at a much higher recharge rate. The most likely source of this fluid is Cañon de Valle. Canyon settings have been found to exhibit focused, high recharge

rates (e.g. Los Alamos canyon) on the Plateau. Furthermore, the HE-contaminated water detected in the perched zone in R-25 would be explained as having come from the 260 outfall fluid that was discharged into Cañon de Valle.

Uncertainties related to this conceptual model include the subsurface conditions that would give rise to such lateral diversion, the rates of water movement, and the extent to which recharge at locations other than Cañon de Valle contribute to the perched water zones beneath TA-16. Multi-dimensional modeling and the drilling of additional characterization boreholes are required to address these issues. The latter is being performed under the Environmental Restoration (ER) Project and Groundwater Protection Programs. Continued monitoring of the hydrology and geochemistry of Cañon de Valle and the springs will provide additional data for modeling. In the ER project, such an approach has been shown to be an effective means for synthesizing the data for Los Alamos canyon (Robinson et al., 1999). A similar strategy is planned for the TA-16 site.

One of the purposes stated above for performing the one-dimensional modeling was to provide a means for simply extracting results from a numerical model to include in the probabilistic systems analyses. After having performed the analyses, we conclude that such a simplified modeling approach does not capture the complexity of the site's hydrologic processes. Instead, we recommend, for the first round of systems analyses, that the performance of the vadose zone be captured through abstracted, one-dimensional pathways of uncertain travel times and points of arrival at the water table. These pathways are conceived to be complex, windy rivulets of fluid that travel along regions of higher permeability. Since we are not ready to identify these pathways in detail, we instead choose to incorporate them in the systems model through a bounding analysis. The travel time can be bracketed based on the observations from R-25 as follows. The lower bound can be essentially 0 based on the fact that we cannot completely rule out a complete, rapid bypass of the vadose zone through fractures or other fast pathways. The upper bound for travel time assumes the HE reached the regional aquifer just before R-25 was drilled, so that it took roughly 50 years to reach the water table. This approach ignores the possibility that HE "detection" in the regional aquifer may be a result of borehole transport and contamination rather than vadose zone transport under undisturbed (pre-borehole) conditions. We expect, based on current opinion, that the transport occurred in the natural system, and is not a borehole artifact. If subsequent well completion information proves otherwise, we will revise the model.

6.3 Three-Dimensional Model

6.3.1 Computational Domain and Mesh Generation

A three-dimensional model of the region outlined in Figure 6-4 has been constructed to explore vadose zone flow and transport issues that the one-dimensional model results suggest must be treated in three dimensions. The model domain was selected to encompass the portion of the TA-16 site relevant to include the presumed source locations for HE releases: the stretch of Cañon de Valle starting at the 260 outfall, MDA's P and R, and the 90's line pond. Thus both Cañon de Valle and the Mesa on which the TA-16 facilities site are captured in the model. The Western most boundary of the model (State Plane Coordinate 489900 m) corresponds roughly to the location of the Pajarito Fault zone, immediately to the West of Highway 502. The dimension of the model domain in the East-West direction is 4.8 km, terminating in the East at State Plane Coordinate 494700 m. The dimension of the model in the North-South direction is 1.8 km (from State Plane Coordinate 536750 to 538550 m).

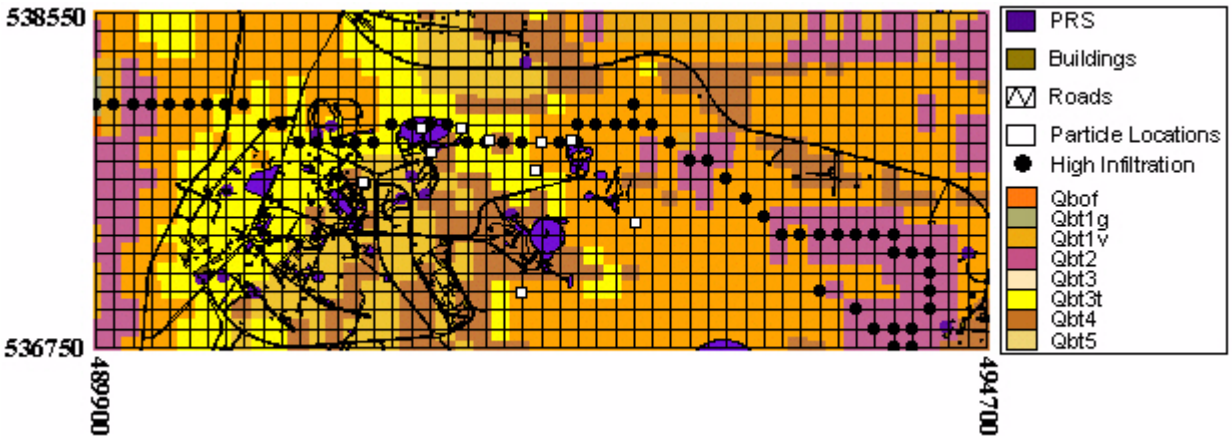

Figure 6-4. Plan view of the TA-16 model domain, showing roads, buildings, and PRS locations. Colors represent the geologic unit present at the ground surface below alluvium. Black dots represent the nodes at which high infiltration is applied in Cañon de Valle; white dots are the starting locations of particles used to map the flow paths from important surface locations.

The three-dimensional stratigraphy is based on the digital rendition of the site geology constructed by the Laboratory's Geology Group EES-1. The FY99 version of the site geology (Carey et al., 1999) is used for this model, as it is the most recent available geologic model. This

model is stored in the form of two-dimensional surfaces representing the interfaces between hydrogeologic units. To build a three-dimensional model from this data, the commercial software package Stratamodel is used. This software fills the three-dimensional space associated with the TA-16 model domain with an attribute at each location to denote the hydrogeologic unit. With this three-dimensional representation, the LaGrit mesh generation software is used to construct a three-dimensional numerical grid that conforms to the hydrogeologic representation, but also possesses computational properties suitable for performing flow and transport simulations. In the present study, two computational grids were generated, only one of which was used to perform the simulations reported. The first is a uniform grid with mesh horizontal mesh spacing of 100 m by 100 m, with an irregular upper surface to capture the topography. This grid (Figure 6-5), which consists of 45,916 nodes, extends from the ground surface to below the water table under TA-16. A second grid (Figure 6-6), a 356,045 node mesh generated but not used in the current iteration of this study, has enhanced horizontal resolution along Cañon de Valle and on the portion of the mesa where HE releases are suspected or known. Computations on this grid were postponed in favor of a series od simulations on the smaller grid. We recommend that future work extend the modeling by using the enhanced resolution grid.

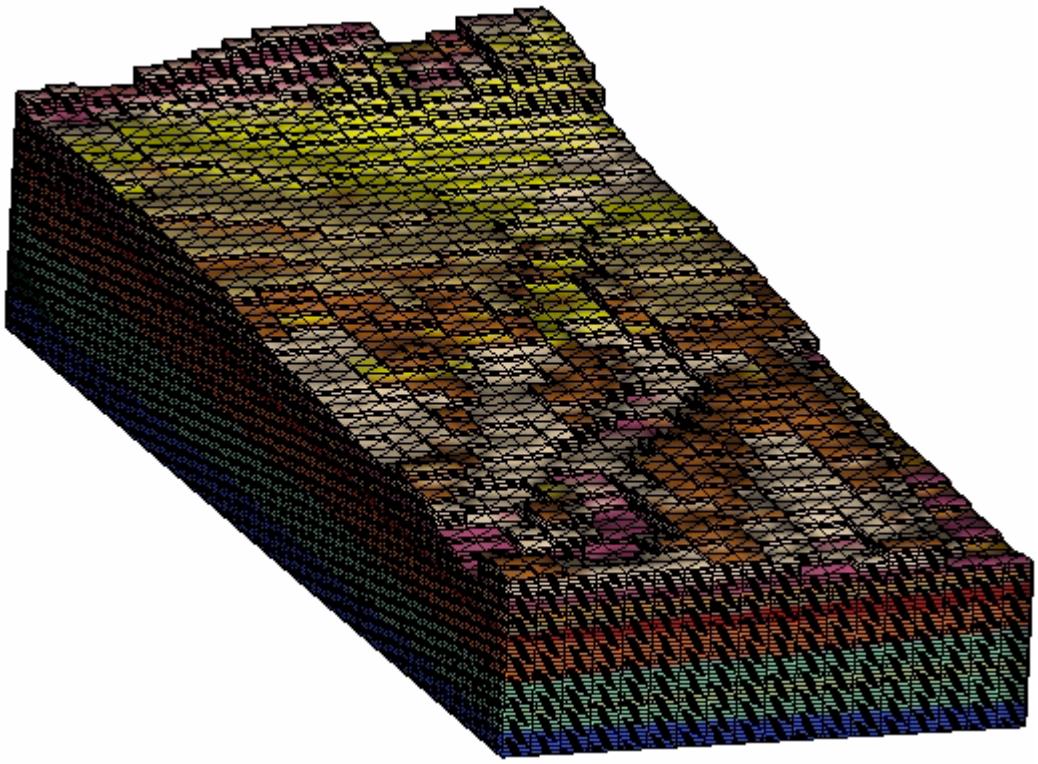

Figure 6-5. Three-dimensional grid for the TA-16 model calculations.

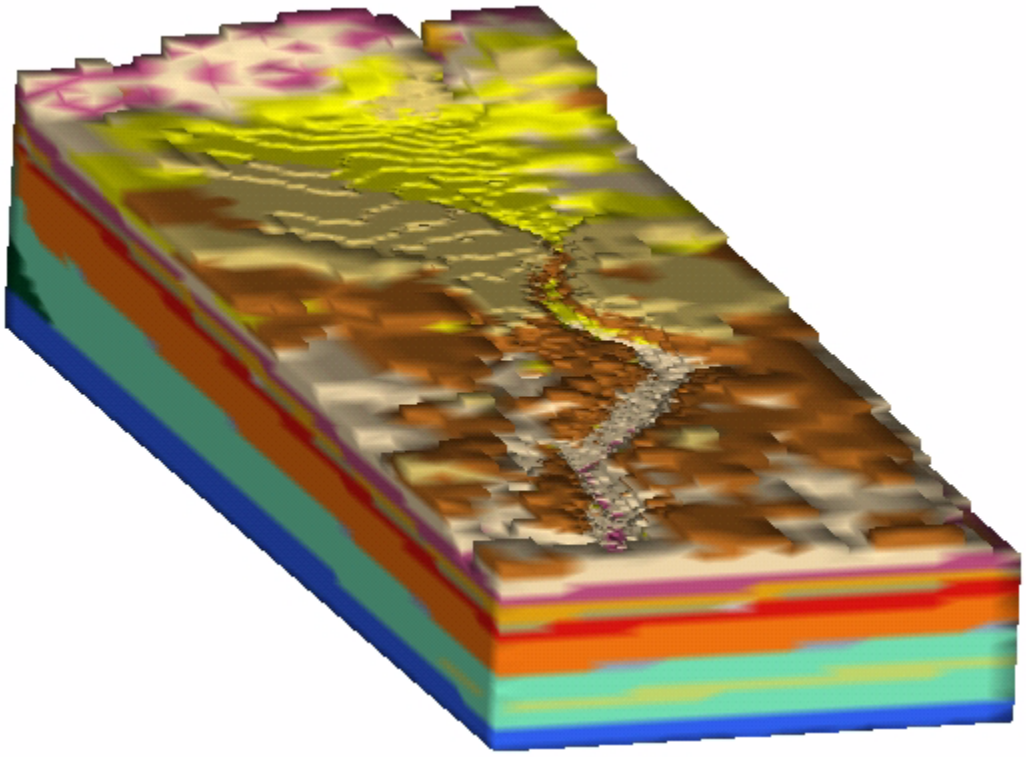

Figure 6-6. Refined three-dimensional grid generated for future modeling of the TA-16 site.

Another aspect of the three-dimensional model that requires discussion is the approach of assigning uniform properties within each hydrostratigraphic unit defined by the site geologic model. When such an approach is taken, the model cannot reproduce the complex near-surface flow patterns described in Section 5.5 because those effects are governed by heterogeneities at smaller scales than are captured by the model. Thus the three-dimensional model is designed to examine large-scale features in the flow system that extends from the ground surface to the water table. Smaller scale effects would have to be explored using stochastic models of near-surface hydrologic heterogeneity, a topic beyond the scope of this study.

6.3.2 Boundary Conditions

Boundary conditions are required to inject and produce water at locations in the model corresponding to natural locations where fluid enters and exits the model domain. For all

simulations except the combined Unsaturated/Saturated (UZ/SZ) runs described in Section 6.3.7, boundary conditions for infiltration at the ground surface and arrival at the water table are required. For infiltration at the surface, a uniform 1 mm/y infiltration is applied to all nodes except those corresponding to Cañon de Valle. This value is consistent with the one-dimensional modeling results and the chloride profile analysis presented earlier. In Cañon de Valle, model runs are performed at a variety of proposed infiltration rates. The grid points associated with the canyon were identified manually using the ArcView GIS tool. This process consists of superimposing the locations of numerical mesh points on the ArcView representation of topographic contours and cultural information, and identifying the appropriate nodes corresponding to the canyon (Figure 6-4). An auxiliary software code was then used to compute the water flow rate to inject in each of these nodes to obtain the desired infiltration rate along the canyon.

The lower boundary condition to represent the water table is set by identifying all grid points at or below the water table represented in the FY 99 site geologic model. This node list is used in the FEHM numerical simulation through the assignment of a high fluid saturation at each node. The code effectively applies the boundary condition along the water table, and all nodes below it no longer remain a part of the simulation. Therefore, the model domain for these calculations (not including the UZ/SZ model results of Section 6.3.7) extends only to the water table, and thus the model is suitable only for examining vadose zone issues.

6.3.3 Novel Modeling Approaches for Vadose Zone Flow and Transport

In this section we briefly describe several additional modeling approaches that are either used in this study or are under development that improve our ability to characterize the TA-16 site and other contaminated vadose zone sites on the Plateau.

Combined UZ/SZ Model: Most numerical models of vadose zone flow and transport utilize a boundary condition at the water table that allows water to exit the model domain. In other words, flow and transport below the water table is not simulated in such models. A consequence of this approach is that the water table elevation as a function of location is a model input, rather than a simulated result. Likewise, saturated zone models typically use the measured water table elevation as the upper boundary of the model, and the system is modeled assuming a confined aquifer upper boundary. One of the reasons for these simplifications is combined UZ/SZ systems are very difficult computational problems, and numerical convergence is slow. The difficulty arises in the sim-

ulation of the location of the water table. As a simulation proceeds, grid cells change from one-phase (water) to two-phase (air and water). This results in a discontinuity in the mass balance equations being solved. Numerical techniques usually cannot smoothly track this change, especially in large-scale models, where many cells experience this problem simultaneously. As a result, numerical convergence is slow, and in transient simulations, time steps are limited.

There are significant advantages to a simulation of both the vadose zone and regional aquifer in the same model. First, there are no approximations in the location of the water table in such a simulation: it is a direct model result rather than a boundary condition. This is especially true for a transient simulation involving pumping from a water supply well. In contrast, for the confined aquifer approach, the fluid storage properties of the grid cells on the upper surface must be adjusted to mimic the actual physical system, in which the water table falls in response to fluid extraction. Also, contaminants percolating through the vadose zone can immediately travel laterally in the same model run when the vadose zone and regional models are combined. This facilitates the integration of the transport systems of the vadose and saturated zones, making the tracking of contaminants from source to potential receptor more straightforward. It is important to note that the current approach of decoupling the vadose zone and regional aquifers is adequate and allows for efficient generation of model results. However, the development of combined models would represent an important advance in our ability to simulate contaminant transport beneath the Pajarito Plateau and elsewhere.

The present study is a first step toward developing improved numerical techniques for such problems. Although no fundamentally new numerical techniques have been discovered yet, the combined UZ/SZ models developed for the TA-16 site will serve as a test-bed for future numerical model development. Several steady state and transient simulations have been developed on the three-dimensional numerical grid, and, although the numerical convergence of such models was slow, they do provide a baseline for assessing improvements to the numerical techniques.

In the combined UZ/SZ models of TA-16, the same numerical grid, infiltration boundary conditions, and hydrologic properties were employed as in the vadose zone nominal case described in Section 6.3.4. The key difference is in the fate of water in the portion of the regional aquifer explicitly simulated at the bottom of the model. The water table is now a simulated result, and water travels laterally within the regional aquifer when it reaches the water table. Water enters and leaves the model within the regional aquifer at the Western and Eastern boundaries, respectively.

Fixed pressure boundary conditions with injection or withdrawal only of water are applied at all nodes at or below the water table. Therefore, the elevation of the water table is set along these boundaries, and is computed within the model domain. Model convergence was also determined to be sensitive to the form of air boundary condition applied on the upper surface of the model. A fixed air pressure was used along the upper surface to allow the air-flow within the system to become established in response to the movement of the water table.

Generalized Dual Porosity Formulation: Many porous media contain distributions of permeability and porosity at scales smaller than the typical control volume of a grid cell in a numerical model. For example, fractures, clay lenses, or mineralized regions of lower permeability may be present within the control volume. Models typically require that a single value of all hydrologic and transport properties be set at each cell. Therefore, this property set must capture the details of flow and transport behavior in an approximate fashion. However, representing such a porous medium with an equivalent set of properties is often difficult. For example, a fractured system with a porous, but low permeability matrix in the vadose zone may exhibit transport velocities controlled by the fractures. However, moisture measurements may be controlled by the matrix rock. Furthermore, solutes can migrate into the matrix via molecular diffusion, thereby delaying and spreading the arrival at a downstream location. Likewise, in a system of sandy soil with clay lenses, it may be important to capture the interchange of solute and fluid between the two media.

There have been several options developed to handle such situations. In dual permeability models, the fracture and matrix media are discretized on the same numerical grid via a one-to-one pairing of grid points for each medium. Flow occurs in each continuum, and a coupling term allows transport to occur between the media. In this way a grid developed for a numerical model can be used to model a fracture/matrix system. A more efficient numerical approach is the so-called dual porosity model, for which the fracture domain allows flow to occur in the fracture domain, with connected matrix nodes acting as storage volumes connected to the fractures. The numerical solution for this system is efficient because the equation set to be solved can be decomposed into a series of small one-dimensional systems to obtain the solution in the matrix, with a fracture domain that is solved as a system of equations no larger than if the problem were a single continuum.

Despite the advantages of these approaches, they too fall short in some instances. Typically, these models have only one or two matrix nodes for each fracture node. With this approach, sharp concentration or pressure gradients in the matrix cannot be resolved. This is particularly an issue for solute transport in fractured systems, where diffusion into the matrix and perhaps sorption on the bulk rock is often important. It is possible to formulate dual porosity models with many matrix nodes for each fracture node, but then the total number of unknowns becomes prohibitive for large, three-dimensional models. In addition, it may be conceptually incorrect to formulate each hydrogeologic unit in a complex system using the dual porosity approach. For example, the Pajarito Plateau contains some units, such as the Otowi member of the Bandelier tuff, for which a continuum, matrix dominated flow model is probably appropriate, and fractures play a small role. In contrast, rocks such as the Basalt units clearly require a model formulation that includes fracture flow as well as interaction with the rock matrix.

To attack such a system, we have developed a flexible approach called the Generalized Dual Porosity Model (GDPM) approach. In this model, a numerical grid generated for the system is used as the overall flow and transport grid, and the user can set, on a node-by-node basis, the level of dual porosity model desired, including simply a continuum assumption with no matrix nodes. Therefore, for our Pajarito Plateau system, the Basalt units are called out as dual porosity media, and the number of nodes in the matrix is specified for each unit for which the dual porosity approach is taken. For the Bandelier Tuff, a single continuum is assumed, and additional unknowns are added only for the matrix nodes in the Basalt units. This flexibility in tailoring the dual porosity model allows more nodes to be devoted in the matrix at each grid point, since the Basalt units comprise only a small fraction of the total grid. For example, only about 20% of the nodes in the TA-16 grid are treated as dual porosity. Adding 10 matrix nodes for each fracture node results in an increase in total unknowns of only a factor of three, keeping the problem tractable.

In the present study, we developed a few GDPM model simulations that will be useful in future studies of the TA-16 system. These simulations proved to be a “proof-of-concept” exercise rather than contributing directly to the results presented in this report. Therefore, we do not present these model results in this report. However, if we extend the modeling to include chemical transport to complement the fluid flow and particle tracking results, the GDPM model will become an important addition to the suite of model formulations that can be used to simulate the migration of contaminants at TA-16. Furthermore, the modeling approach will be used in other studies of Laboratory derived contaminants in the subsurface.

Permeability Reduction at Interfaces: One of the primary assumptions implicit in the formulation of a flow and transport model that is based on a stratigraphic framework model is that the stratigraphy exerts an overriding effect on the flow parameters and processes. If this is true, then the hydrologic properties at a numerical grid point can be populated based on the stratigraphic unit that point falls in. In fact, the approach used in this modeling study is that the finite element grids themselves need to be built based upon the need to replicate the layered stratigraphy present in the subsurface. While this approach is undoubtedly a valid starting point, there may be important features of the hydrologic system that are not captured adequately. For example, the numerous observations of perched water and possibly lateral diversion of downward percolation of fluid beneath the Pajarito Plateau are difficult to capture if mineral alteration or heterogeneities within a hydrostratigraphic unit are the cause. Without a means to change the model parameterization locally through the use of low-permeability barriers, it is difficult to reconcile the perched water with the currently measured hydrologic properties of the current hydrostratigraphy. Mean hydraulic conductivity values for the Bandelier tuff are several orders of magnitude larger than the highest proposed recharge rates for the plateau. This fact implies that if only mean values are used everywhere in a vadose zone model, the rocks will transmit all fluid under unsaturated conditions, and no perching or lateral diversion will occur.

Nevertheless, beneath TA-16, saturated conditions have been found within the Otowi member, and elsewhere perched water has been identified within the basalt units and the Puye Formation. This is a consistent and repeatable observation beneath the Plateau. For example, careful characterization of the rock in the vicinity of the perched water in wells such as LADP-3 (Broxton et al., 1995) has uncovered fine-scale permeability contrasts that explain the perched water occurrence. In LADP-3 in Los Alamos canyon, Broxton et al. (1995) report the presence of a several inch thick clay layer at the base of the Guaje Pumice Bed on top of the Puye Formation. They postulate that this clay may be a paleosoil that today acts as a permeability barrier that diverts downward percolating fluid.

A key issue in the development of unsaturated zone numerical models is how to practically handle such barriers. Although relatively thin layers can be incorporated directly into the finite element grid, there are practical limitations to this approach, including computational inefficiencies and the lack of detailed data at the scale required to construct a model of extreme

grid resolution (centimeter scale grid spacing). The current limit of grid resolution is such that we can handle the units presently characterized in the geologic model, but finer-scale heterogeneities cannot be built into the grid directly.

An alternative approach has been taken in this study, namely an approach that considers the *interfaces* between hydrogeologic units to be important transition regions where hydraulic properties such as the saturated permeability may be different than those in either of the units above or below the interface In this formulation, the presence of a partial barrier to downward fluid migration is handled by assuming that a reduction factor can be applied to the permeability for those parts of the model. Assuming this factor to be much less than unity means that the intervening clay layer has a large influence on the permeability field at that interface.

The numerical implementation of this conceptual model is present in the FEHM code. In most finite difference or finite element codes, including FEHM, when any two connected nodes in the model connected to one another have a different permeability, a harmonic average permeability is applied for that connection. The new feature added to the code is to allow the user to specify a constant multiplier called the permeability reduction factor to any connection on an interface between two hydrostratigraphic units where this effect is present. In this way, the permeabilities within each unit are their original values, but the permeability applied for water passing through the interface is reduced. When the reduction factor makes the permeability at the interface small enough, lateral diversion or perching can occur, depending on the dip of the interface and the local recharge rate.

Because the application of a reduction factor may seem like an ad hoc concept, we present a simple example that allows calculation of the reduction factor. Consider the model geometry in Figure 6-7. On the left-hand figure, two units of somewhat different permeability are adjacent to one another. Considering for the moment the flow to be one-dimensional, steady-state, saturated flow, the pressure drop $P_2 - P_1$ from point 2 to point 1 can be obtained by realizing that the flux within each material is the same, so that:

$$q = \frac{k_2}{\Delta x/2}(P_2 - P_i) \qquad \text{(EQ 1)}$$

$$q = \frac{k_1}{\Delta x/2}(P_i - P_1) \qquad \text{(EQ 2)}$$

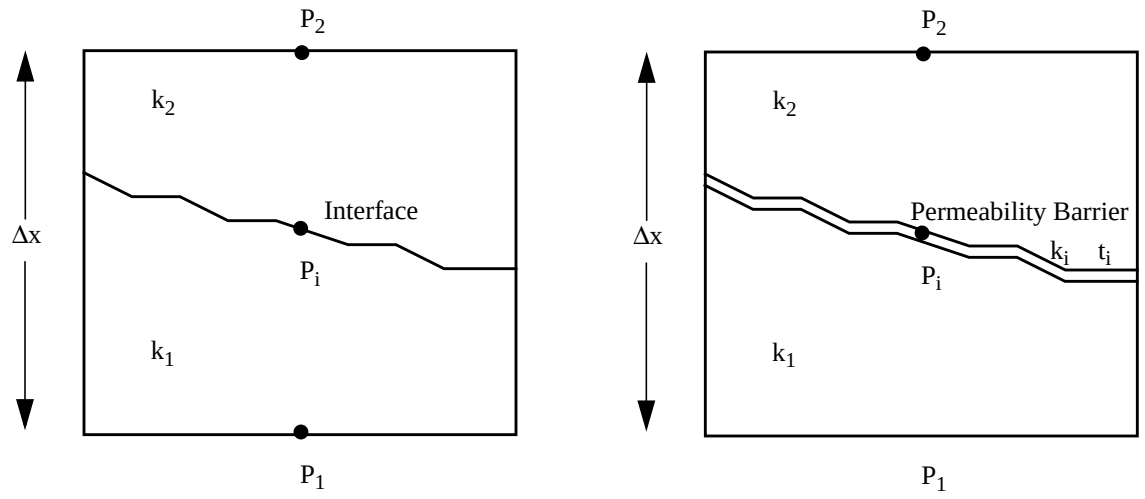

Figure 6-7. Schematic diagram of the conceptual model geometry for the interface between two hydrogeologic units. a) model without low-permeability barrier. b) model with low-permeability barrier.

Where q is the water flux, k_1 and k_2 are the hydraulic conductivities, and P_i is the pressure at the interface. These equations can be combined to eliminate this intermediate pressure, resulting in:

$$q = \frac{k_{harm}}{\Delta x}(P_2 - P_1) \qquad \text{(EQ 3)}$$

where

$$k_{harm} = \frac{2k_1k_2}{k_1 + k_2} \qquad \text{(EQ 4)}$$

Notice that the composite permeability across this interface is the harmonic average of the two permeabilities. This is the reason that codes such as FEHM apply a harmonic average for connected nodes that have different permeability values. Now consider the right-hand diagram of Figure 6-7. A similar derivation can be applied for flow in a system containing a thin layer at the interface between the units of thickness t_i and hydraulic conductivity k_i. The result, after algebraic manipulation, is:

$$q = \frac{k_{comp}}{\Delta x}(P_2 - P_1) \quad \text{(EQ 5)}$$

$$k_{comp} = \frac{1}{\frac{1}{2k_1} + \frac{t_i}{\Delta x k_i} + \frac{1}{2k_2}} \quad \text{(EQ 6)}$$

The composite permeability k_{comp} across the interface now contains a term that includes the permeability and thickness of the low-permeability layer. When this layer is not present, the permeability reduces to the harmonic average of k_1 and k_2, but in cases in which k_i is low enough, the low-permeability layer effectively controls the composite permeability across the interface.

Returning to the example of the Guaje/Puye interface, some reasonable parameter values illustrate the point. Using the base-case values of permeability for these two units, the harmonic average permeability (the relevant value in the absence of the clay layer) is 3 x 10^{-13} m^2. When we include the clay layer, we need to apply a characteristic dimension for the term Δx, which in a numerical model is the typical grid spacing at this interface. If we assume a 5 cm clay layer, Δx = 2 m, and k_i = 1 x 10^{-17} m^2, we obtain an effective permeability across the interface of 4 x 10^{-16} m^2. Comparing this value to the harmonic average permeability, we find that the permeability reduction factor for this example is 3 x 10^{-13}/4 x 10^{-16} = 0.0013. Clearly, the possibility exists that thin layers can exert a strong influence on the flow system.

In this study of flow and transport beneath TA-16, we restrict our attention to the Otowi/ Puye interface, and treat the permeability reduction factor as an uncertain parameter that is varied systematically to examine the impact on flow. Because the three-dimensional model is somewhat coarse, the interface between the Bandelier tuff and the Puye formation can be either associated with the Otowi member or the Guaje Pumice Bed. Therefore, the interface is considered to be between the Puye formation and either the Guaje Pumice Bed or the Otowi member.

6.3.4 Three-Dimensional Flow Model Results: Nominal Case

A series of simulations were carried out with the three-dimensional model to examine predicted *in situ* moisture contents, travel times, and transport directions within the vadose zone. The modeling is designed to address the nature of transport in the deep vadose to augment the calibration carried out in the one-dimensional simulations. In particular, transport times for solutes to reach a given depth must agree with observations of deep HE transport at the site, and lateral

diversion of water from Cañon de Valle under the mesa must be reproduced, as the R-25 observations suggest occurs.

We first present the results of a simulation we refer to as the "nominal case," a baseline which we then compare with the results from other simulations. The black dots in Figure 6-4 are the locations of nodes designated as high infiltration nodes, coincident with the trace of Cañon de Valle in the model. The nominal case consists of an equivalent continuum model (ECM) approach for every hydrogeologic unit, with an infiltration rate of 300 mm/y in Cañon de Valle and 1 mm/y elsewhere. The 300 mm/y value is consistent with values cited in Robinson et al. (1999) for Los Alamos Canyon, and serves as a starting point for these simulations at TA-16. In this simulation, we include no reduction in permeability at any interface, and assume that the water table, as defined in the 1999 site geologic model, is an infinite sink for water. Figure 6-8 is a fence diagram of the predicted fluid saturation in the rock. The fluid saturation pattern correlates closely to the rock hydrologic unit encountered, as the different units possess different hydrologic properties. In addition, wetter conditions occur beneath Cañon de Valle because of the focused recharge assumed for the canyon. A deficiency of this model is that the rock is unsaturated everywhere above the water table, in contrast to the large region rock under saturated conditions that was detected in R-25.

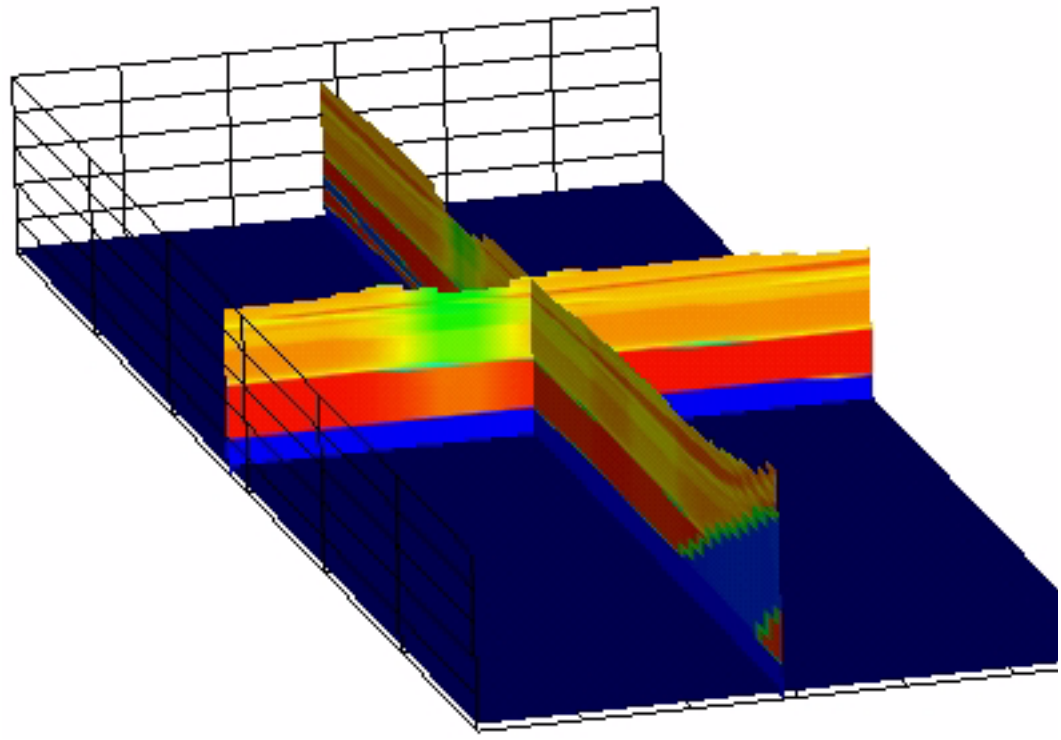

Figure 6-8. Fence diagram of fluid saturation, nominal case. 300 mm/y in Cañon de Valle, 1 mm/y elsewhere.

Particle streamlines are a modeling tool for interpreting the nature of the fluid pathways (velocities, directions of flow) in a flow model. For a conservative, nonsorbing contaminant such as HE, particle travel times are a proxy for the travel time of the contaminant, although we are ignoring other potential processes such as solubility limitations and dispersion. Table 6-1 lists the coordinates and locations of a series of particles used to map the subsurface flow predicted by the different model simulations, and Figure 6-4 (the white squares) illustrates the locations of these particle starting locations in relation to key facilities and PRS's. Figure 6-9 shows the predicted particle pathways for the nominal case. A key element of the conceptual model is the presence of HE-contaminated water at significant depths in R-25. Recall that we concluded, based on the low presumed infiltration rate on the mesa at R-25, that the HE most likely reached R-25 as laterally diverted flow from Cañon de Valle. The particle pathways show very little lateral diversion for the nominal case, suggesting an additional deficiency of this rendition of the model. Finally, Figure 6-10 shows the travel time versus depth for a few of the particles. Note first the much smaller travel time to depth for particles entering with the Cañon de Valle fluid versus those entering on the mesa. For example, transport times to reach the bottom of the Otowi member are on the order of 150 y for Particle 6 (Cañon de Valle at MDA P), 200 y for Particle 10 (Cañon de Valle near R-25) and 10,000 y for Particle 7 (released at the location of R-25). Infiltration rate is obviously the strongest contributor to this result. The time required for the Cañon de Valle particles to transport to depth appear to be consistent with this infiltration rate, although more rapid transport to depth is certainly not precluded based on the available data.

Table 6-1. Coordinates of particles used in three-dimensional simulations

Particle Location	Particle Number	x in ft x in m	y in ft y in m	Elevation in ft Elevation in m
90's Line Pond	1	1612015	1763879	7578.74
		491342.2	537630.3	2310.
Middle of MDA R	2	1613059	1764848	7513.12
		491660.4	537925.7	2290.
260 outfall - head	3	1613241	1764404	7545.93
		491715.9	537790.3	2300.
260 outfall @ CdV	4	1613766	1764848	7480.315
		491875.9	537925.7	2280.
CdV @ Burn Grnd Spr	5	1614264	1764639	7414.698

Table 6-1. Coordinates of particles used in three-dimensional simulations

Particle Location	Particle Number	x in ft x in m	y in ft y in m	Elevation in ft Elevation in m
		492027.7	537862.0	2260.
CdV @ MDA P	6	1615702	1764641	7349.081
		492466.0	537862.6	2240.
R-25	7	1615058	1764090	7513.123
		492269.8	537694.6	2290.
Martin Spring	8	1614829	1761932	7447.507
		492199.9	537036.9	2270.
Fish Ladder Spring	9	1616851	1763187	7316.273
		492816.2	537419.4	2230.
CdV near R-25	10	1615157.5	1764599.8	7414.698
		492300.0	537850.0	2260.

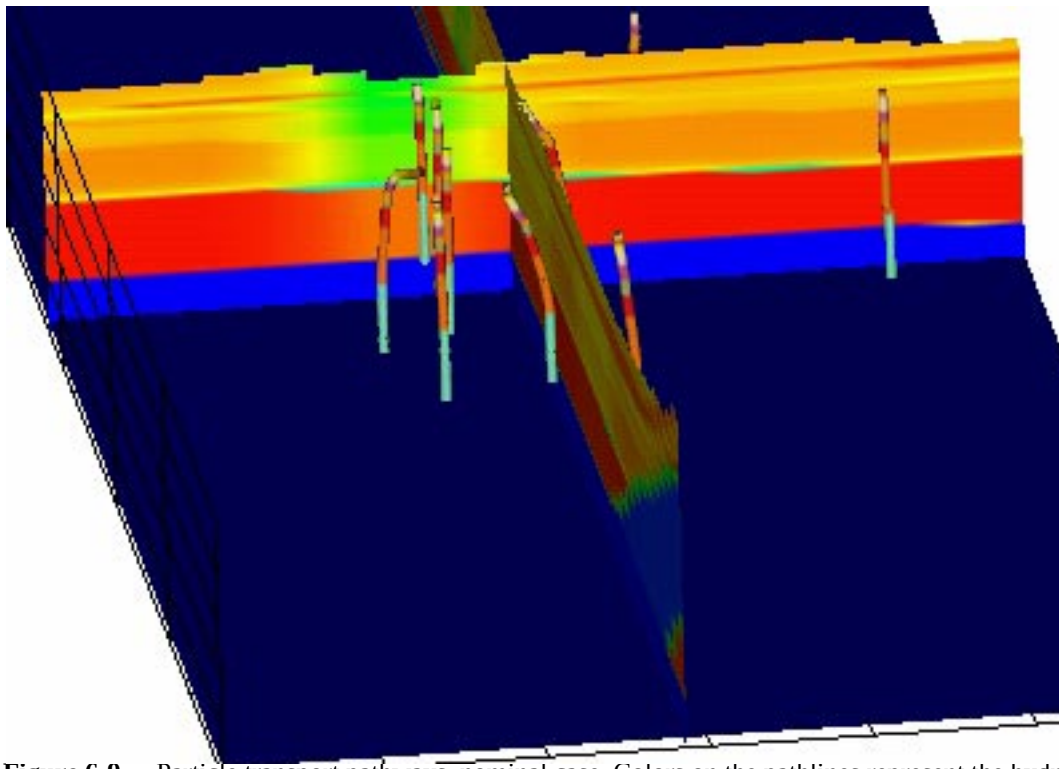

Figure 6-9. Particle transport pathways, nominal case. Colors on the pathlines represent the hydrogeologic units through which the particles are traveling.

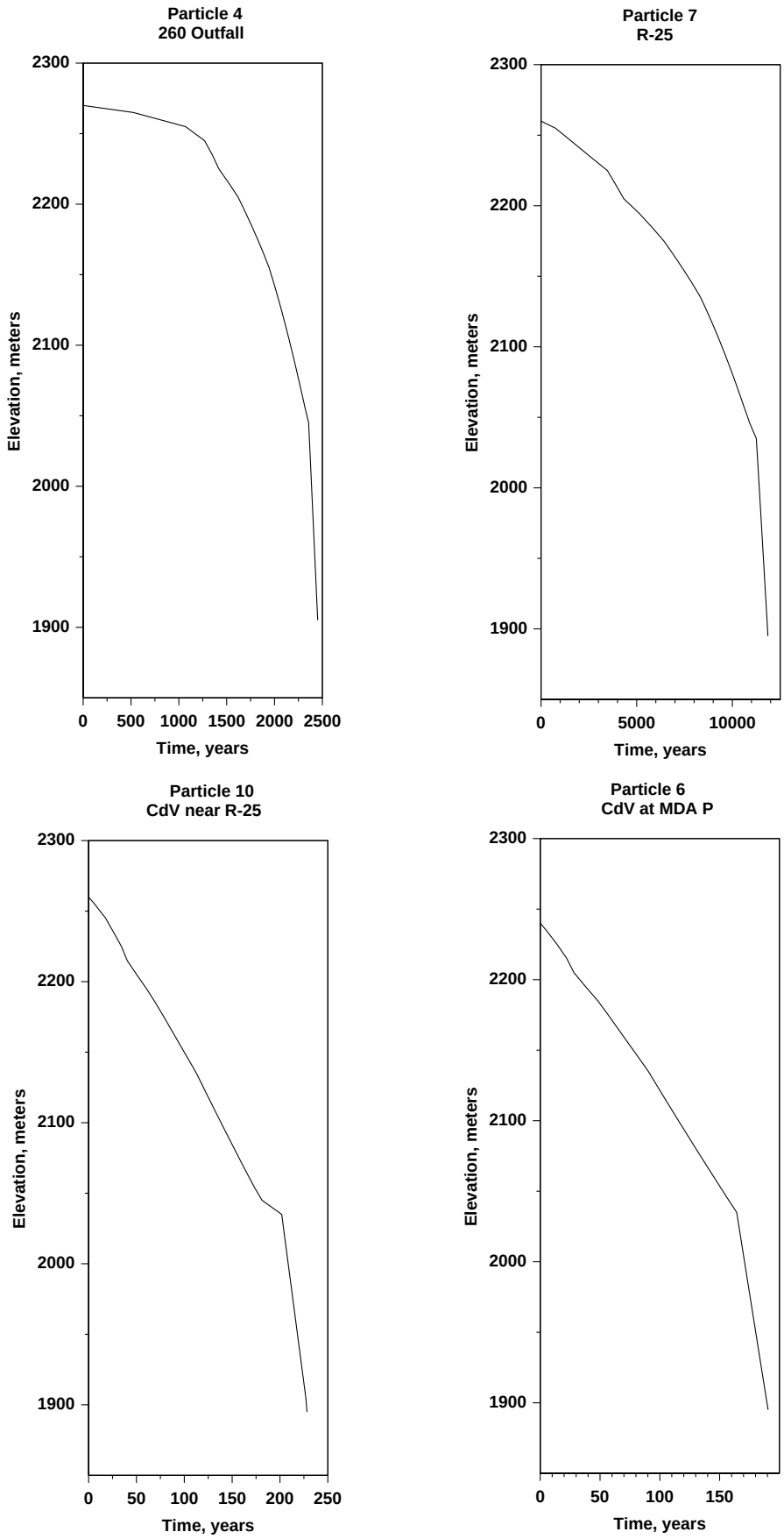

Figure 6-10. Travel time versus depth for several simulated particles, nominal case.

6.3.5 Influence of Cañon de Valle Infiltration Rate

There is large uncertainty in the infiltration rate along Cañon de Valle, given the lack of data necessary to derive estimates of this critical parameter. Therefore, the model possesses uncertainty that can be explored through a sensitivity analysis of infiltration rate. Figures 6-11 and 6-12 show the saturation distributions for Cañon de Valle infiltration rates of 1000 and 2000 mm/

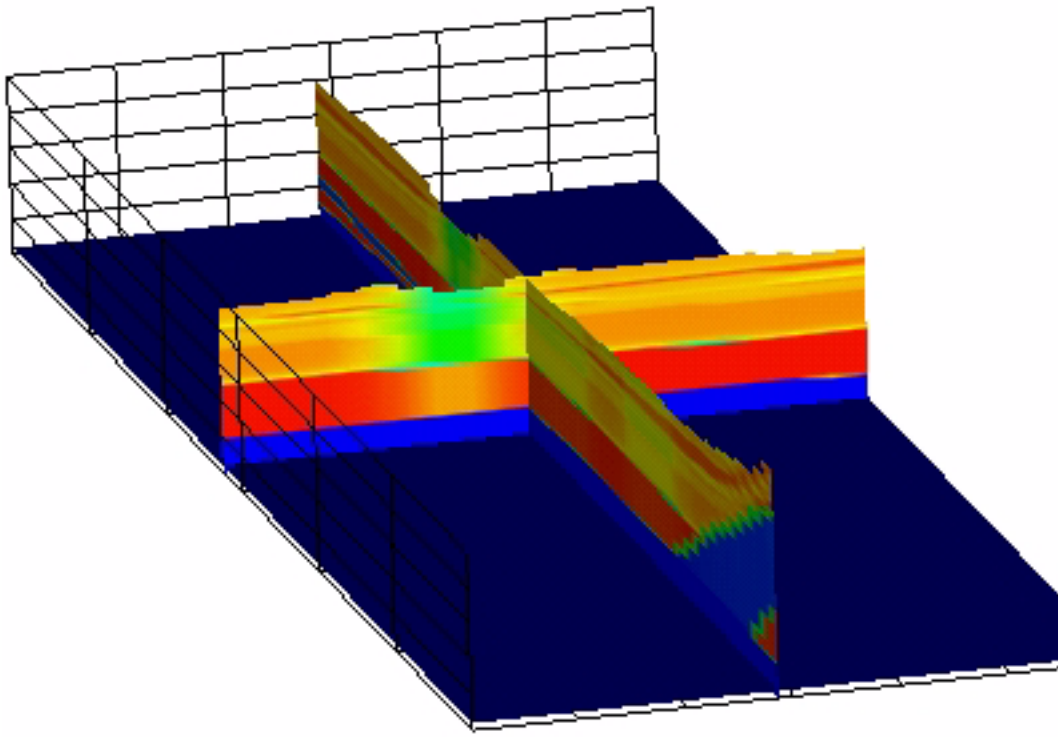

Figure 6-11. Fence diagram of fluid saturation, nominal case. 1000 mm/y in Cañon de Valle, 1 mm/y elsewhere.

y, respectively. Higher canyon infiltration rates result in wetter conditions beneath the canyon. In addition, transport pathways exhibit somewhat more lateral diversion due to the inability of some units to transmit fluid vertically (Figures 6-13 and 6-14 , respectively). The lateral diversion occurs at interfaces of units with contrasting hydrologic properties, including those within the Tshirege member and at the base of the Otowi member (either the Otowi member or the Guaje Pumice bed). The interface of the Otowi member and the Puye formation clearly exhibits saturation buildup within the Guaje Pumice bed, although in these models moisture is still significantly below saturation, and the underlying Puye formation remains unsaturated. Therefore, even though the trends with increasing infiltration rate are in the right direction (saturation buildup, more lateral diversion), significant observations about the subsurface hydrologic system are still not captured with the model. Figures 6-15 and6-16 show the travel times to depth for Cañon de Valle particles

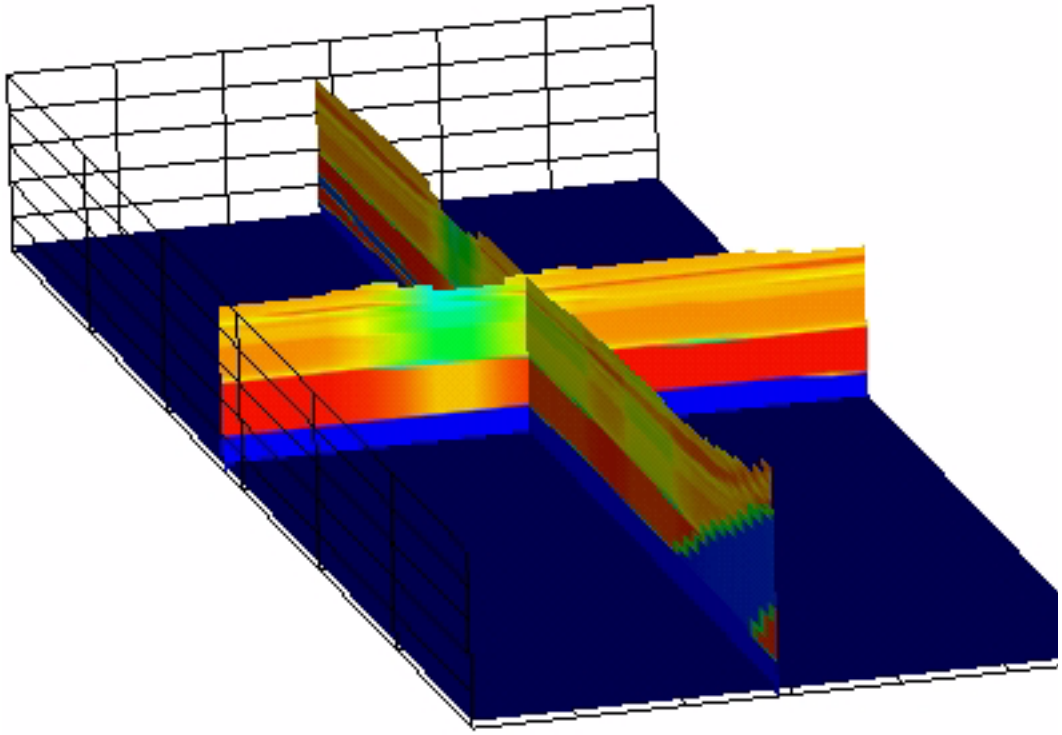

Figure 6-12. Fence diagram of fluid saturation, nominal case. 2000 mm/y in Cañon de Valle, 1 mm/y elsewhere.

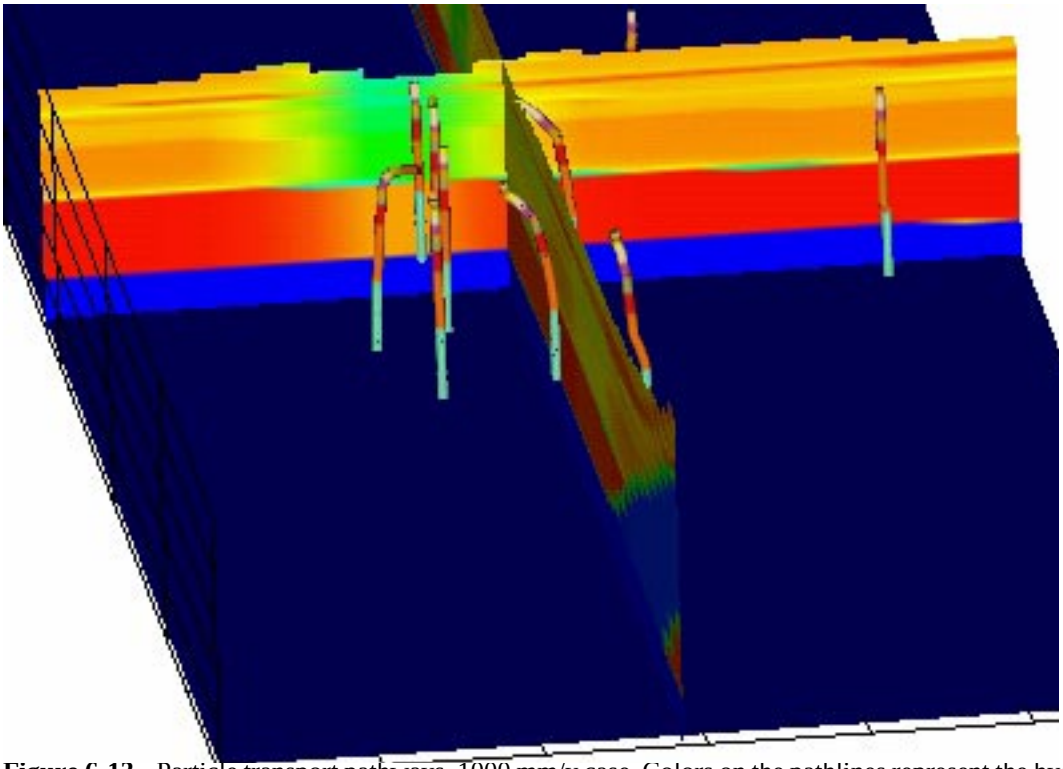

Figure 6-13. Particle transport pathways, 1000 mm/y case. Colors on the pathlines represent the hydrogeologic units through which the particles are traveling.

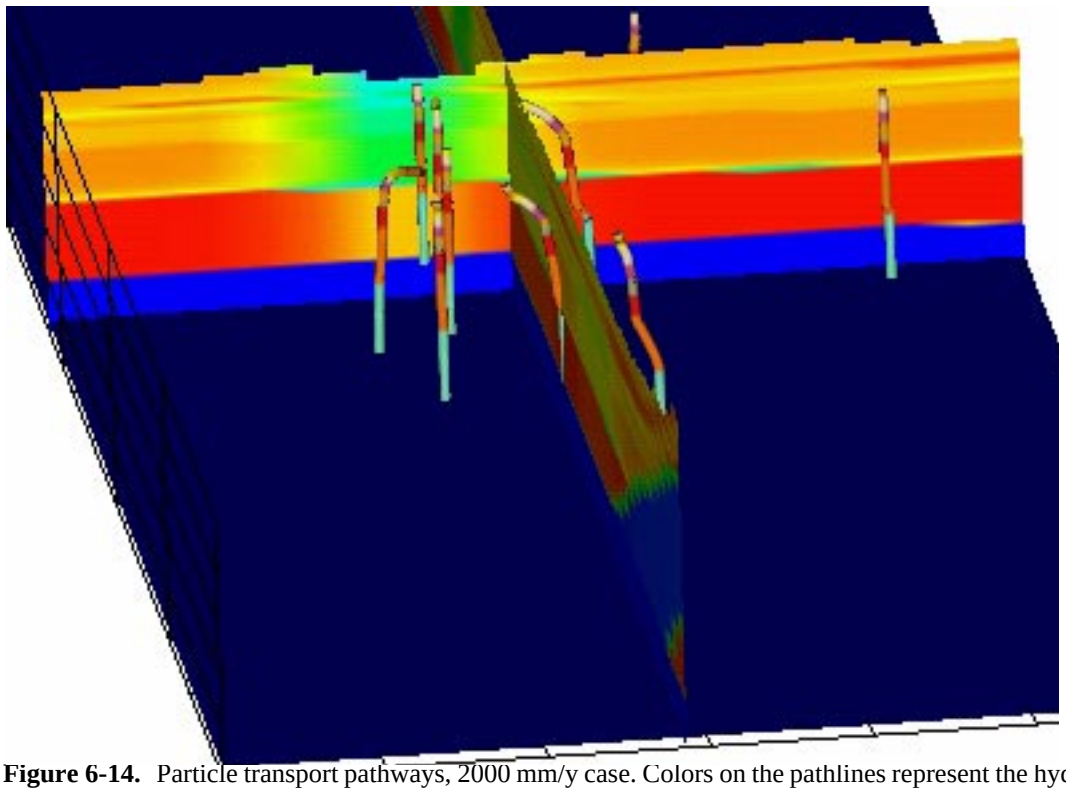

Figure 6-14. Particle transport pathways, 2000 mm/y case. Colors on the pathlines represent the hydrogeologic units through which the particles are traveling.

for the higher infiltration scenarios. As expected, the travel times decrease with increasing infiltration rate in the canyon. The magnitude of these travel times are also consistent with the observations, but they also suggest that under these conditions, transport all the way to the regional aquifer could occur in the last 50 years. This result reflects the uncertainty in when the HE actually reached the depths at which it was detected in R-25 and some of the other shallower wells at TA-16.

Given the importance of infiltration rate on the migration of HE contaminants at TA-16, it is clear that additional data are required to constrain the infiltration rate. Several approaches are possible, each of which yield independent estimates. First, an overall water budget for Cañon de Valle would allow for an accounting of the various mechanisms of water transport, including run-on/run-off, ET, precipitation, and infiltration. An enhancement of the existing monitoring system at TA-16 would allow a study similar to that of Gray (1997) for Los Alamos canyon to be executed for Cañon de Valle. The downside of such an effort for estimating infiltration is that the estimate is indirect and possibly plagued by the problem of subtracting two uncertain numbers (precipitation and ET). Alternatively, wells drilled into bedrock from the bottom of Cañon de Valle would provide moisture profile data that can be used to constrain infiltration rate. Figure 6-17 shows the

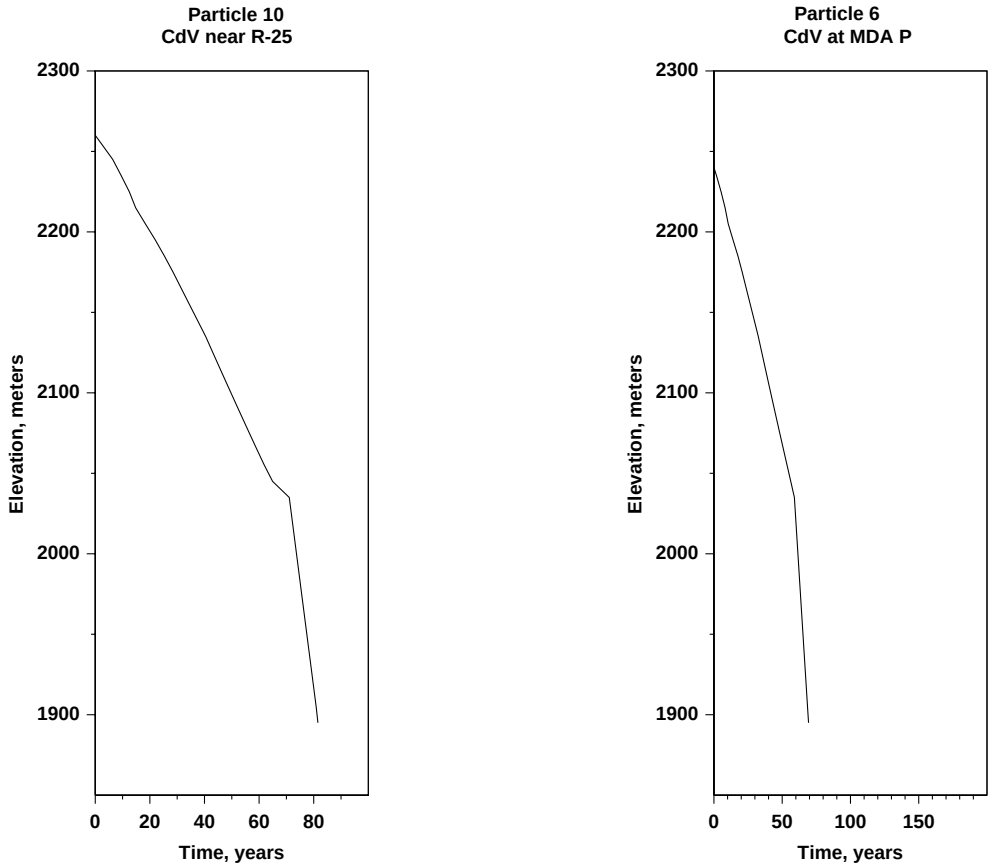

Figure 6-15. Travel time versus depth for two simulated Cañon de Valle particles, 1000 mm/y case.

predicted fluid saturation profile in the uppermost rock units for the three infiltration rates. This plot illustrates that moisture profiles can be a sensitive data set for estimating infiltration rate. Finally, contaminant fronts, if they terminate within the depth of these boreholes, give a direct estimate of travel times, from which infiltration rate can also be constrained. Of course, given that HE has already migrated to depths greater than these proposed boreholes, a front would not be detected for HE. Sorbing contaminants, perhaps including Be, might provide a better diagnostic tool for estimating infiltration rates. This approach would require an accompanying laboratory characterization program to determine sorption coefficients and basic mechanistic information.

As is usually the case in groundwater hydrology, no single measurement provides all of the necessary information for characterizing the system. A variety of approaches and data sets usually allow the system to be better constrained. As these data are collected, models such as the one presented here are excellent vehicles for synthesizing the information and quantifying our understanding. Reducing the uncertainty associated with the vadose zone flow and transport system at TA-16 will require these additional measurement and modeling steps to be taken.

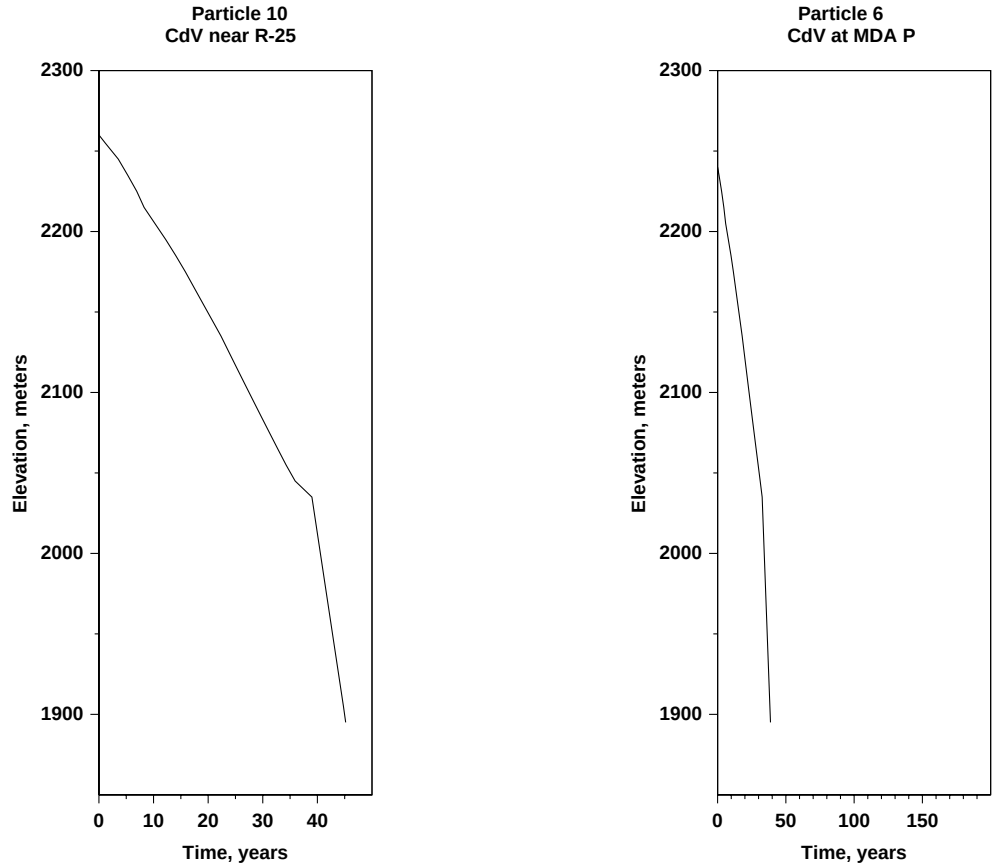

Figure 6-16. Travel time versus depth for two simulated Cañon de Valle particles, 2000 mm/y case.

6.3.6 Permeability Reduction at the Otowi/Puye Interface

Given the large zone of saturation observed in R-25, and the inability of the nominal case model to reproduce it, additional modeling to explore possible reasons for this hydrologic observation is needed. In addition, the extent of lateral diversion of fluid under the mesa from Cañon de Valle is probably also not captured sufficiently in the nominal case. Saturated conditions were first observed in the Otowi member, so the first attempt at reproducing this behavior was to apply the permeability reduction at the Otowi/Puye interface. For the 300 mm/y infiltration rate scenario for Cañon de Valle, reduction factors of 0.001, 0.0003, and 0.0001 were used. Figure 6-18 illustrates that progressively wetter conditions occur above the interface as the reduction factor is reduced. However, a thick zone of saturated rock does not build up when the interface reduction model is applied. Due to the relatively planar, gently sloping nature of this interface as represented in the geologic model, water infiltrating from the canyon bottom, upon reaching the interface, disperses laterally in the direction of maximum ascent of the interface, until it is able to penetrate the barrier and continue percolating downward. This is best illustrated in the three corresponding particle pathways shown in Figure 6-19 for reduction factors of 0.001, 0.0003, and 0.0001,

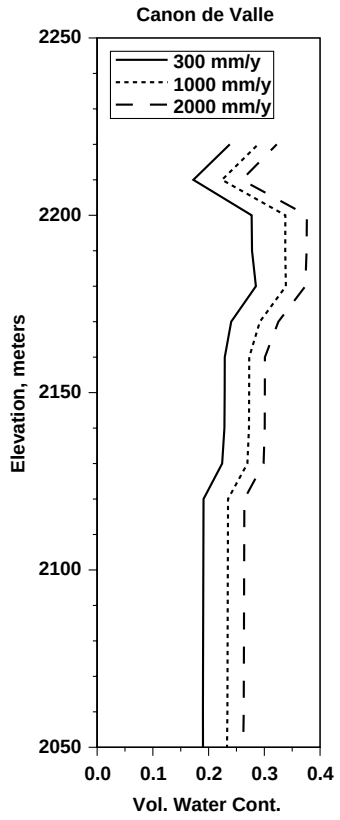

Figure 6-17. Predicted fluid saturation versus depth in a hypothetical well drilled in Cañon de Valle for the various infiltration rate scenarios.

respectively. The direction of fluid migration is generally to the south from Cañon de Valle underneath the mesa, consistent with the observation of HE in R-25. Lateral diversion is extreme for the lowest reduction factor. Although this amount of lateral diversion cannot be ruled out based on the available data, we selected the 0.001 factor for further exploration.

Figure 6-20 show the particle pathways and saturation distributions for the 0.001 reduction factor and infiltration rates of 1000 mm/y and 2000 mm/y, respectively. As expected, progressively more lateral diversion under the mesa occurs at higher infiltration rates. Thus, any of the reduction factors and infiltration rates result in models that are consistent with the observation of lateral diversion, probably because the extent of lateral diversion is not well constrained by data. However, a persistent result that is not consistent with the R-25 observations is that saturated conditions do not build to large thicknesses in the Otowi member, and unsaturated conditions are predicted in the Puye formation for all simulations, in contrast to the data.

It does not appear that any realistic set of reduction factors and infiltration rates will be able to reproduce this element of the flow system under TA-16 using a vadose zone model formulated

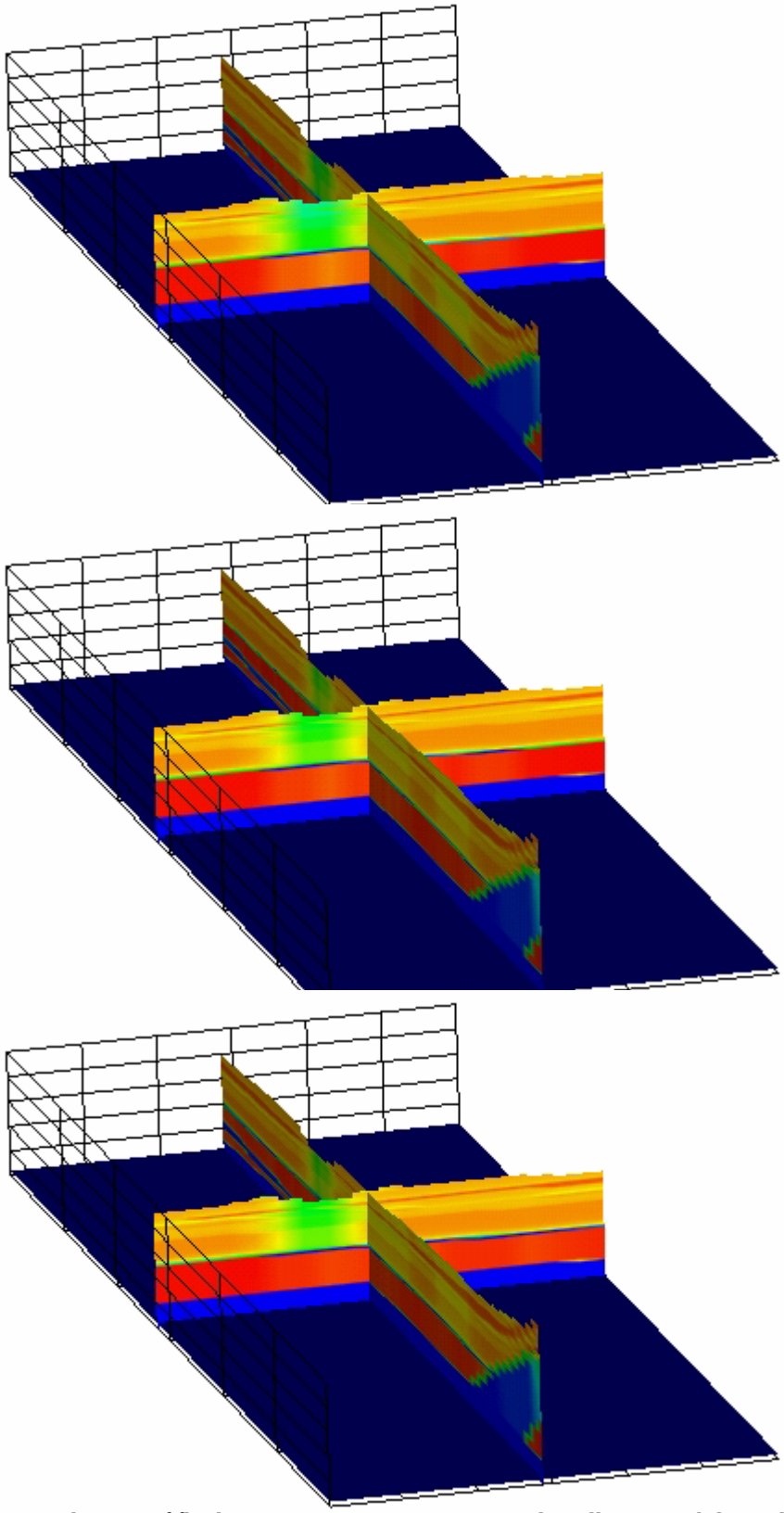

Figure 6-18. Fence diagram of fluid saturation, 300 mm/y in Cañon de Valle, permeability reduction factors of 0.001, 0.0003, and 0.0001 (top to bottom).

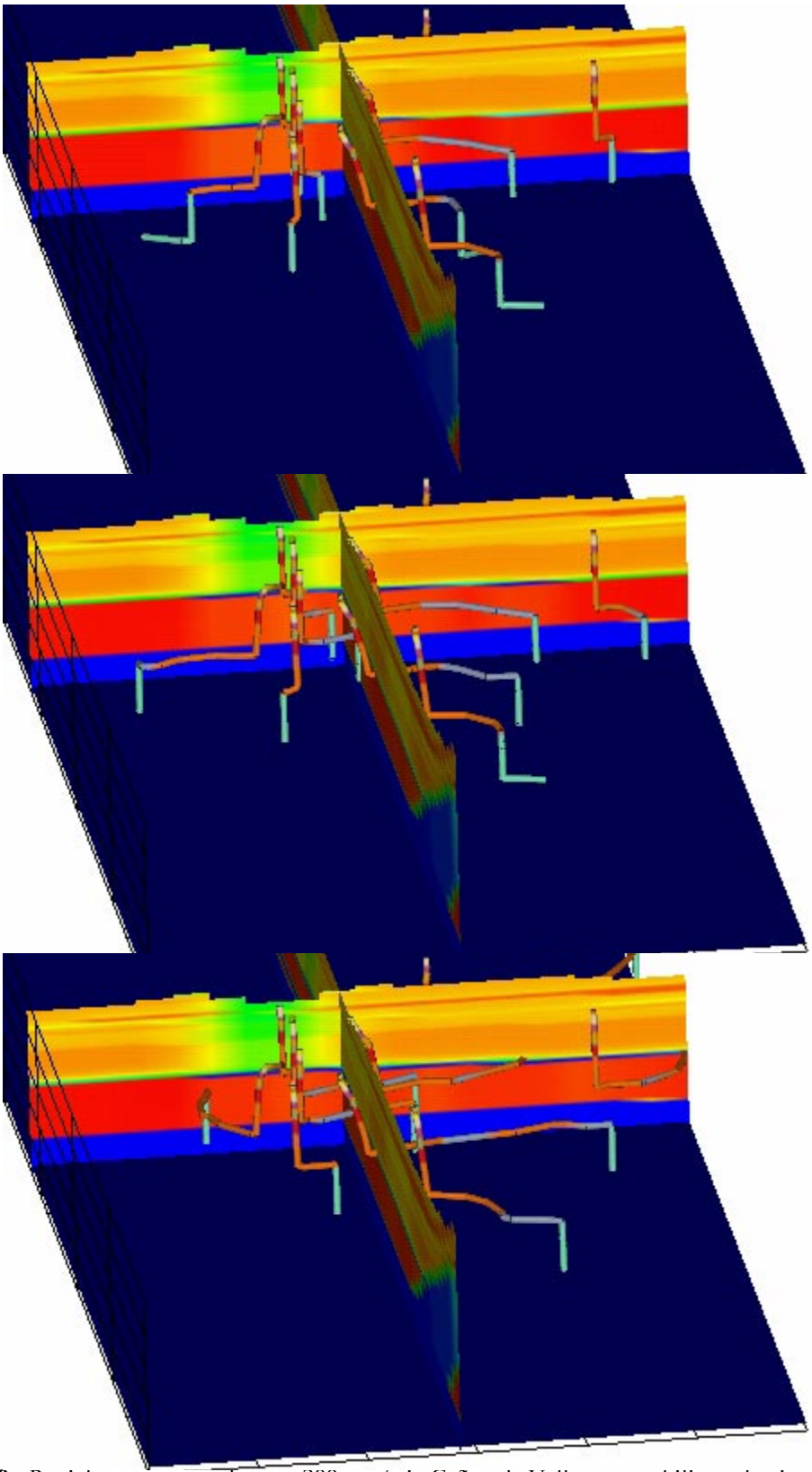

Figure 6-19. Particle transport pathways, 300 mm/y in Cañon de Valle, permeability reduction factors of 0.001, 0.0003, and 0.0001 (top to bottom). Colors on the pathlines represent the hydrogeologic units through which the particles are traveling.

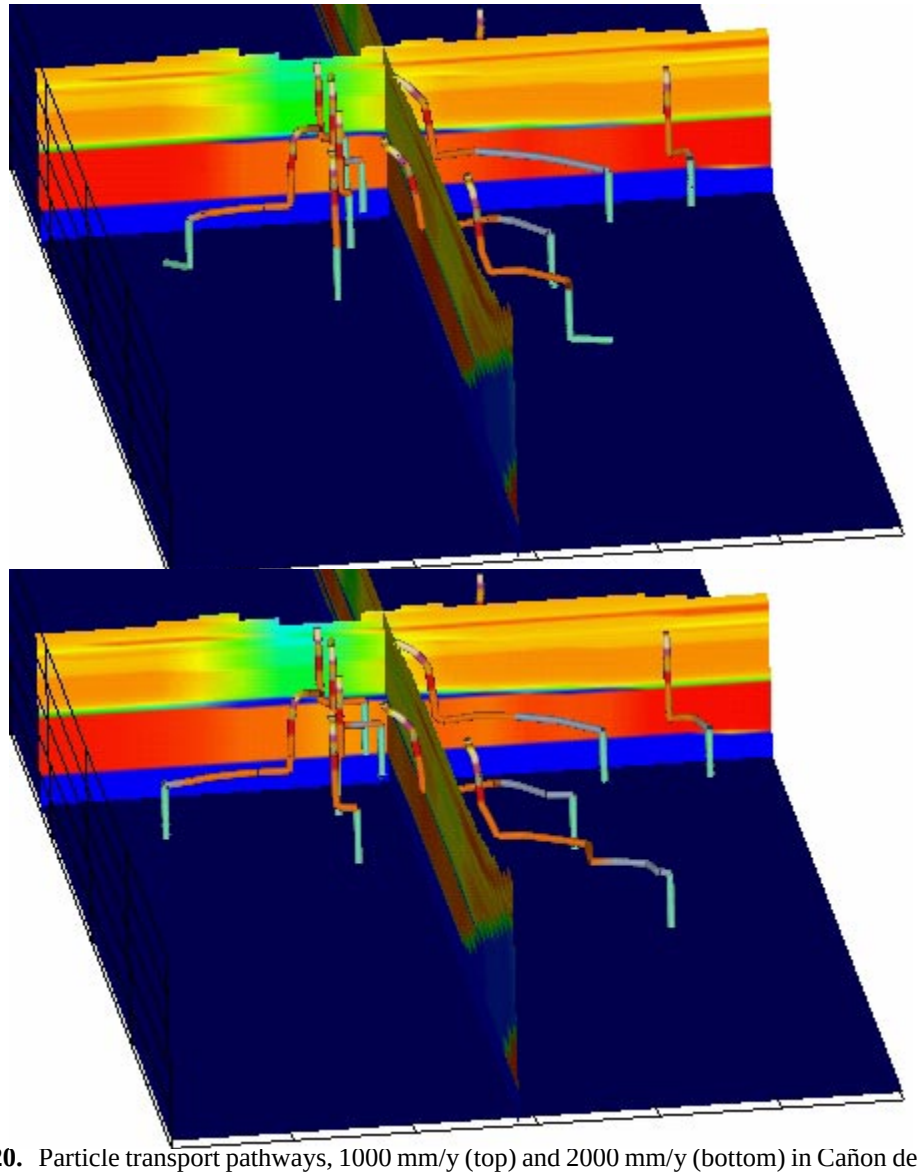

Figure 6-20. Particle transport pathways, 1000 mm/y (top) and 2000 mm/y (bottom) in Cañon de Valle, permeability reduction factor of 0.001. Colors on the pathlines represent the hydrogeologic units through which the particles are traveling.

as we have formulated it. Possible reasons include geologic model uncertainties, permeability variability not directly correlated to the geologic model, or a deficiency in our understanding of the water table in this portion of the Plateau. Geologic models constructed based on sparse data typically have relatively smooth interfaces between stratigraphic units, as this is the simplest, and hence most reasonable, way to form geometric surfaces from such data. In contrast to this type of representation, actual interfaces may possess smaller scale variability. Undulating surfaces could create “bowls” of low-permeability barriers that would accumulate water, perhaps resulting in thicker zones of saturation. Next, permeability, though generally correlated to stratigraphy in the Bandelier tuff, may be only an approximate method for capturing variability in hydrologic

properties. Specifically, low permeability zones in the Puye formation could provide additional barriers to flow that would result in saturated zones above what is thought to be the water table of the regional aquifer. An argument against this idea for TA-16 is that no such zones were immediately obvious from well logs of R-25. The final possibility, an alternate explanation of the nature of the water table at this site, is explored in the next section.

6.3.7 A Combined UZ/SZ Model for TA-16

The representation of the water table of the regional aquifer under TA-16, as it exists in the geologic model, is strongly influenced by the interpretation of well logs in R-25 and earlier studies of SHB-3. Each well has large zones of saturation that are interpreted as perched water, placing the regional aquifer at much greater depths. However, the evidence for whether a saturated zone represents perched water or the top of the regional aquifer is subject to uncertainty. Using visual observations of core and cuttings during drilling, it is difficult to ascertain whether rocks are wet, fully saturated, or unsaturated. In R-25, the description consisted of a saturated zone starting in the Otowi member, extending down into the Puye formation. Then, the observation of alternating zones of wet and dry cuttings was the basis for interpreting the saturated zone as perched, rather than the top of the regional aquifer. However, the possibility exists that the cuttings and core interpreted as dry actually represents a zone encountered in R-25 of lower permeability and porosity, which would contain less moisture even if it is actually saturated. Proceeding on the possibility that this interpretation was inaccurate, we propose an alternative model in which the top of the regional aquifer is actually much higher than it is currently represented in the geologic model.

The hydrogeologic setting at the TA-16 site lends credence to this alternate explanation. The proximity of the site to the Pajarito Fault zone raises the possibility of some unique local characteristics. There is a distinct possibility of higher recharge along and near the fault zone and a change to the hydrologic characteristics of the fractures relative to other locations beneath the Plateau. The fault zone may also be a barrier to flow from the west due to the presence of fault gouge and other changes to the native rock. These factors may suggest that the water table to the west of and at the Pajarito fault zone is higher than the current water table map predicts. Until wells scheduled to be drilling within the fault zone are constructed and data are collected, it is possible that the TA-16 site is in a transition zone in which the water table is much higher in the western portion of the model, and drops more precipitously to the east.

A model exploring this possibility has been constructed for the TA-16 site. Using the same numerical grid and hydrogeologic representation, this model explicitly simulates the combined UZ/SZ system through the application of boundary conditions on the western and eastern boundaries of the model. In the east, it is assumed that the current representation of the water table is valid, but the water table at the west boundary is much higher than currently represented (2280 m elevation, rather than the - m as predicted by the current model). The resulting saturation distribution for the nominal case (300 mm/y infiltration in Cañon de Valle, no interface reduction) is shown in the left hand plot in Figure 6-21. The water table extends significantly into the Puye

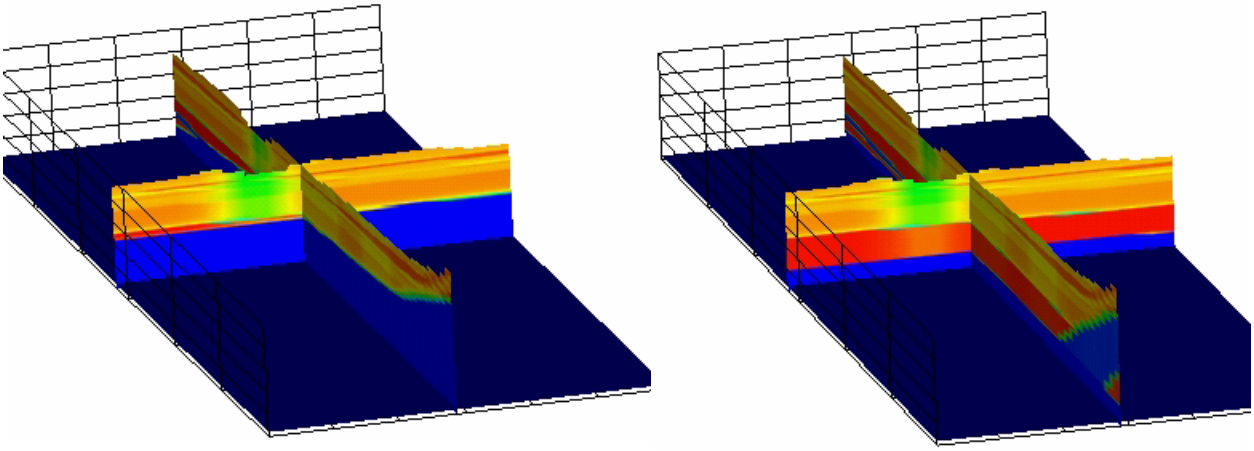

Figure 6-21. Fence diagram of fluid saturation, combined UZ/SZ model (left), compared to the nominal case (right).

formation for this model, and the slope of the water table is much steeper from west to east. For this particular simulation, the water table is not quite high enough at R-25 if one assumes that the water table is in the Otowi formation. Nevertheless, with further adjustment of the boundary condition (not performed in this preliminary analysis), the elevation of the water table could be matched at R-25. Figure 6-22 shows the travel time for transport to depth for the particles initiated on the mesa at the 260 outfall and in Cañon de Valle near MDA P. Transport times to the elevation of the water table match that of the nominal case Figure 6-10, but in the UZ/SZ model the particle then travels within the aquifer, resulting in the divergence of the two curves due to lateral transport.

Another use of the combined UZ/SZ model approach is that pumping well scenarios can be constructed to examine water table drop and potential capture of contaminants in the regional aquifer. In this study, a hypothetical water wells was placed in the model approximately 900 m from the eastern boundary of the model. Water was withdrawn from the aquifer from a series of vertically aligned grid cells starting about 100 m below the original water table. The simulation

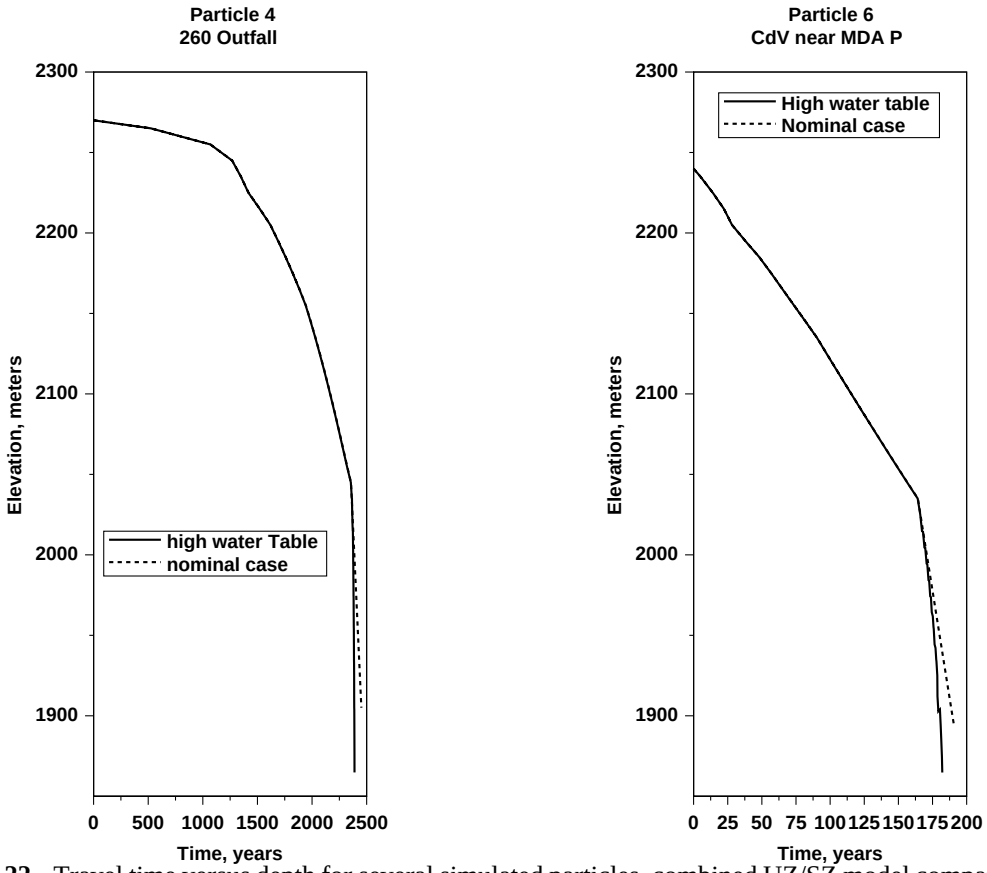

Figure 6-22. Travel time versus depth for several simulated particles, combined UZ/SZ model compared to the nominal case.

was run to 100 years to approximate a steady state flow simulation with pumping, after which particles were released. Figure 6-23 shows the paths of particles in plan view for a pumping rate of 50.5 kg/s. The lateral migration to the east is a result of transport in the aquifer. Interestingly, no particles were captured by the pumping well. The relatively small drawdown around the pumping well, combined with the fact that water extraction took place at significant depths below the water table, allowed particles to travel past the pumping well rather than being captured. However, a much more complete series of simulations is required before making any definitive conclusions about the possibility of contaminants bypassing pumping wells in this fashion. For example, in contrast to this result, Section 6 illustrates that contaminants are captured under the confined aquifer model assumptions used in the regional aquifer model. Future work will implement the combined UZ/SZ model approach in a more systematic fashion to examine this issue more thoroughly.

Regarding the difference in conceptual models proposed to explain the TA-16 hydrologic data, a likely outcome of additional modeling would be the merger of the higher water table with

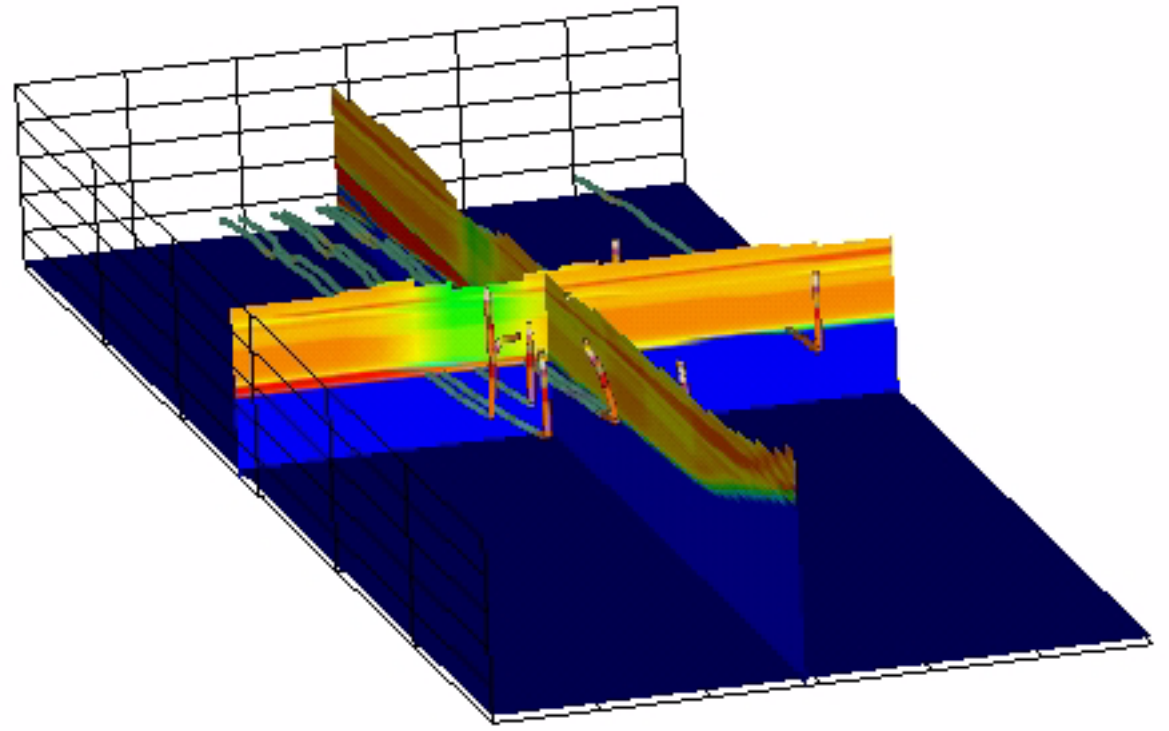

Figure 6-23. Particle pathlines for the combined UZ/SZ model, illustrating the near-vertical transport to the water table, followed by easterly transport in the regional aquifer.

the lateral diversion model for the Otowi/Puye interface. Such a model would produce a higher water table and lateral diversion, both of which could explain the available data. Additional data are required to explore the nature of the hydrologic connectivity of the uppermost saturated region with deeper formations. Hydrologic testing in the multiple completions zones in R-25 will undoubtedly provide important new clues. Additionally, planned characterization wells in the Pajarito Fault zone will allow us to confirm or refute the theory of an elevated water table in the vicinity of this zone.

7.0 - Regional Aquifer Transport Model

7.1 Previous work

Preliminary simulations of HE transport in the regional aquifer were described by Keating (1999). These simulations were generated using the numerical mesh for the basin-scale model (Keating et al. 1999) with a grid resolution of 250m (x direction), 250 m (y direction), and 50 m (z direction, most shallow layers). Two scenarios were used as the basis for the simulations: 1) Initial HE distribution limited to the immediate vicinity of R25; and 2) HE distributed near R25 and beneath the upper reaches of Canyon de Valle. Transport was assumed to be conservative (i.e. no chemical reactions) and advection-dominated (no dispersion). In all simulations, the contaminant plume was predicted to be entirely captured by PM4 and PM2, wells located to the east of TA16. Travel times for 50% capture were predicted to range from 80 to 1438 years, depending on assumptions about porosity. Very short travel times (i.e. 80 years) corresponded to cases of porosity = 0.01, a very unlikely value for the sedimentary rocks that comprise this aquifer. For more typical values of porosity (0.1), the fasted travel time predicted was 760 years.

One important result of this study was to highlight the importance of the hydraulic properties of the Puye Formation, the shallowest hydrostratigraphic unit in the aquifer in the vicinity of R25. According to the site-wide geologic model, the Puye is subdivided into two hydrostratigraphic zones (fanglomerate and Totavi Lentil) (Carey et al. 1999). This model defines the Totavi Lentil, a relatively coarse river gravel deposit, to be a thin, continuous layer beneath the fanglomerate. In the HE transport simulations, the Totavi provided a relatively fast and continuous pathway for particle transport between the HE source area in TA16 and the PM well field. It is unknown, however, whether or not such a continuous, coarse pathway exists. One conclusion of this work was that increased attention to heterogeneity within the Puye Formation was critical to our ability to accurately predict travel times in the regional aquifer.

7.2 Improvements to the numerical model

7.2.1 Stochastic hydraulic conductivity fields

As described above, preliminary HE transport results highlighted the dominant role of the permeable Totavi Lentil hydrostratigraphic unit, which, as defined by the site-wide geologic model

(Carey et al. 1999) provided a continuous conduit for relatively fast transport away from TA-16. In fact, the spatial continuity of the Totavi Lentil is not certain, and discontinuous models of this unit have been proposed (Reneau, 1995) in accordance with knowledge of basin rift dynamics and migration of the ancestral Rio Grande. Unfortunately, the lateral continuity of facies within sedimentary rocks will be difficult to quantify with borehole information from the relatively sparse wells on the plateau.

To address the inherent uncertainty in spatial definition of hydrofacies within the Puye Formation, we have begun work on a stochastic facies-based model of hydraulic conductivity variation for this important unit. The elements of the approach were are developing are as follows: (1) identification of key hydrofacies within the Puye, (2) estimation of the *statistics* of facies dimensions (e.g. minimum, maximum, mean thickness; minimum, maximum lateral continuity) and spatial relations between facies, using outcrop and borehole data, and (3) generation of facies-based stochastic hydraulic conductivity fields within the Puye, using Markov transition probability software (Fogg et al. 1998). This year, we focused on compiling field-based information from the literature and collecting new field data from exposures of the Puye near LANL. This compilation is summarized in the Appendix.

We were not able to collect as much new data as expected due to the Cerro Grande fire, which greatly limited our access to those canyons where the Puye is well exposed. The composite dataset on facies in the Puye is, at present, is insufficient to adequately parameterize a facies-based stochastic model. However, we were able to incorporate the limited available data into a relatively simple stochastic model (*Gómez-Hernández* 1991); this model allows us to examine the influence of fine-scale heterogeneity within the Puye on HE transport in the regional aquifer. As more data are collected from the Puye, we will develop a more realistic facies-based stochastic model.

7.2.2 *Pajarito Plateau numerical mesh*

In order to investigate the possible importance of fine-scale heterogeneity within the Puye, we require a greater resolution in the numerical mesh than that used in the preliminary study (Keating et al. 1999). Vertical resolution is particularly important, particularly since the coarse gravel layers observed in outcrop may be hydrologically important and are 10m thick or less (see Figure 7-1). With present computer resources, it was impossible to further refine the basin-scale model sufficiently; instead, we created a separate numerical mesh for the Pajarito Plateau with increased vertical resolution (250m (x direction), 250 m (y direction), and 12 m (z direction)).

Figure 7-1. Photograph of an outcrop of the Puye Formation.

The locations of lateral boundaries for the submodel were specified to be coincident with hydraulic low or no-flow boundaries (topographic divide to the west of LANL; Santa Clara Canyon to the north; Frijoles Canyon to the south). Estimates of flow across these boundaries from the north, west, and south were calculated using the basin scale model (see Figure 7-2); flow was applied to sub-model boundaries conserving total amount of flow in each individual hydrostratigraphic units present along the boundary face. The numerical mesh for the submodel is shown in Figure 7-3.

In addition to water entering/leaving the submodel along lateral boundaries, recharge is applied to the water table in accordance with the model developed by Keating et al. (1999). Water is allowed to flow out of the model along the eastern boundary (the Rio Grande) and the eastern corner of the north boundary (Santa Clara Creek) at specified head nodes. Predicted fluxes

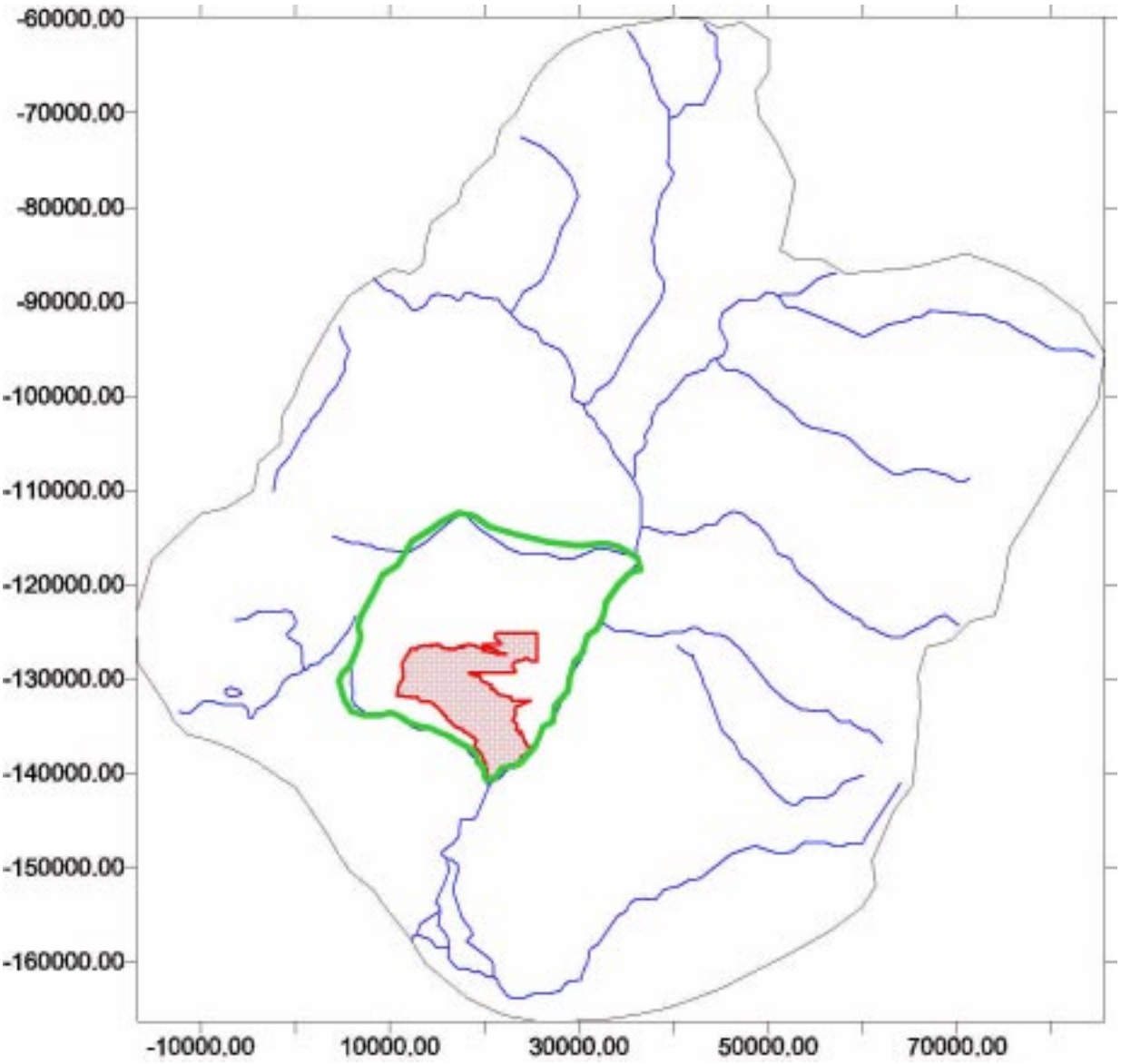

Figure 7-2. Basin scale model, showing submodel boundaries (green line) and the Laboratory boundary (red).

entering or leaving along these river boundaries were compared to estimates derived from streamflow data; these comparisons are discussed below in the model calibration section.

The FY99 site-wide geologic model (Carey et al. 1999) was used to establish the geometry of hydrostratigraphic zones in the submodel.

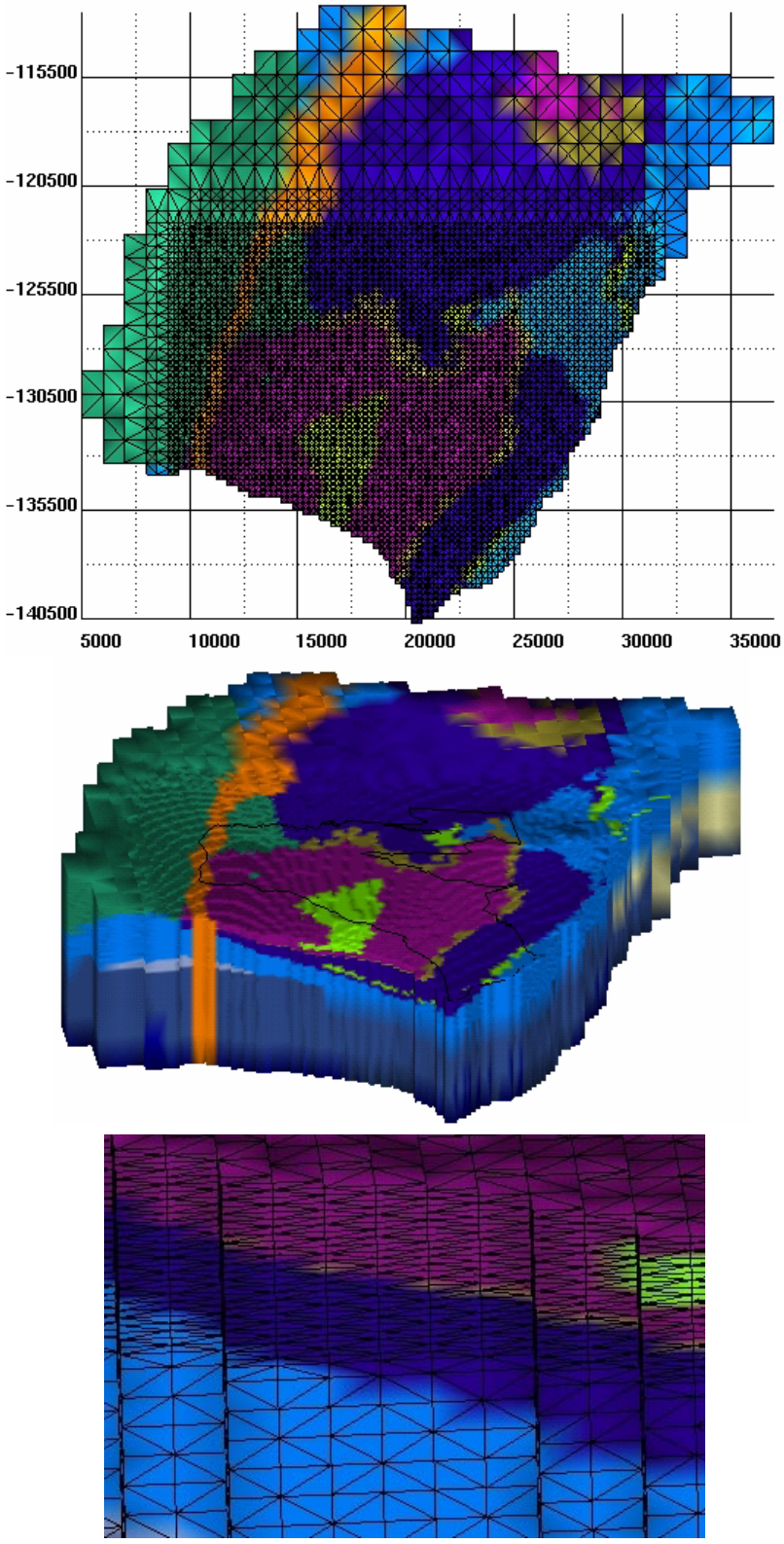

Figure 7-3. Top: Map view of numerical mesh for submodel. Colors indicate location of hydrostratigraphic zones. Middle: Edge view of southern boundary of submodel (looking north), showing vertical resolution of grid. Bottom: Zoom in of middle.

7.3 Flow and transport simulations

7.3.1 Groundwater flow

The transport simulation results described below are based on a simulated steady state flow field for the Pajarito Plateau, assuming that pumping rates in municipal supply wells continue into the future at approximately the same rates as were measured in 1996. Since transport results will be very dependent on the accuracy of the flow field simulations, it is important to evaluate the consistency of the flow model with available data (permeability, water level, and flux data). Flow model development has been funded by the Hydrogeologic Workplan; detailed description model development and calibration is available in other reports (Keating et al. 1998; Keating et al. 1999; Keating et al. 2000).

We evaluate model performance based on two factors: 1) agreement with pre development (no pumping) water levels and fluxes and 2) prediction of water level declines due to pumping over the last 50 years. Calibrating steady state and transient models to these datasets, using automated parameter estimation software (PEST, (Watermark Computing 1994)) provides the best possible constraints on critical model parameters such as permeability, specific storage, and recharge rates. All model parameters values are required to be consistent with available data (Keating et al. 1999). Tables 7-1 and 7-2 present calibration results and best-fit parameters; Figure 7-4 presents the

Table 7-1. Water level comparison, pre-development steady-state simulations

	Observation	Measured	Calculated	Residual
LANL/LA County wells	g-1	1763	1760.2	-2.8
	g-2	1768	1768.4	0.4
	g-3	1786	1784.1	-1.9
	g-4	1793	1790.9	-2.1
	g-5	1800	1793.0	-7.0
	la-1	1708	1709.1	1.1
	la-2	1704	1715.6	11.6
	la-3	1700	1718.9	18.9
	la-4	1764	1752.2	-11.8
	la-5	1759	1740.7	-18.4

Table 7-1. Water level comparison, pre-development steady-state simulations

	Observation	Measured	Calculated	Residual
	la-6	1734	1730.5	-3.5
	pm-2	1796	1793.7	-2.3
	pm-3	1797	1791.0	-6.0
	r-31	1781	1786.0	5.0
	dt-9	1808	1801.1	-6.9
	tw-1	1763	1776.0	13.0
	tw-2	1795	1807.9	12.9
	tw-3	1783	1803.8	20.8
	tw-4	1851	1847.1	-3.9
	h-19	1899	1902.3	3.3
	dt-5a	1820	1806.8	-13.2
	dt-10	1807	1803.4	-3.6
	r-25	1900	1899.0	-1.0
Off-site wells	Well 1	1678	1695.6	17.6
	Well 2	1694	1695.6	1.5
	Well 3	1698	1695.5	-2.5
	Well 4	1715	1695.5	-19.5
	Well 5	1715	1695.5	-19.5
	Well 6	1711	1695.5	-15.5
	Well 7	1687	1681.8	-5.2
	Well 8	1796	1816.9	20.9
	Well 9	1682	1684.4	2.4
	Well 10	1662	1652.5	-9.5

Flux Comparison, kg/s

	Discharge to Rio Grande	590	543.0	-47.0
	Discharge to Santa Clara Creek	0	7.2	7.2

Water level decline comparison (m), transient simulations. Measured and calculated declines span the maximum period of record for any particular well.

Well	Measured decline	Calculated decline	Error
g-1	27.9	29.3	1.4
g-2	35.6	31.9	-3.7
g-3	30.8	16.5	-14.4
g-4	8.6	15.1	6.6
g-5	18.1	15.6	-2.4
la-1	15.5	13.2	-2.3
la-2	19.9	14.3	-5.6
la-3	5.4	14.4	9.0
la-5	12.0	11.7	-0.3
pm-2	11.2	12.1	0.9
pm-3	8.3	12.1	3.8
tw-2	11.0	11.7	0.7
tw-3	11.7	12.2	0.5
tw-4	1.8	8.0	6.2

Table 7-2. Groundwater flow model parameters

Parameter	Value	95% Confidence Limits	
		lower	upper
Permeability log10 (m^2)			
Deep Precambrian basement	-15.3	fixed	fixed
Paleozoic/Mesozoic (deep)	-15.1	-19.2	-11.0
Paleozoic/Mesozoic (shallow - fractured)	-12.2	fixed	fixed
Cerros del Rio Basalts - Tb1	-11.9	-14.4	-9.5
Cerros del Rio Basalts - Tb2	-11.3	-12.0	-10.6
Cerros del Rio Basalts - Tb4	-13.8	-16.4	-11.2
Tschicoma	-13.0	fixed	fixed
Pajarito fault zone	-14.9	fixed	fixed

Table 7-2. Groundwater flow model parameters

Parameter	Value	95% Confidence Limits	
		lower	upper
Santa Fe Group (horizontal)	-13.0	-13.3	-12.7
Santa Fe Group (vertical)	-13.0	-14.0	-12.0
Deep Santa Fe Group (horizontal)	-14.0	fixed	fixed
Deep Santa Fe Group (vertical)	-16.0	fixed	fixed
Puye, fanglomerate	-13.5	-16.1	-11.0
Puye, Totavi Lentil	-11.0	-12.2	-9.8
Santa Fe Group, Los Alamos aquifer (horizontal)	-13.4	-13.7	-13.1
Santa Fe Group, Los Alamos aquifer (vertical)	-15.1	-15.9	-14.4
Bandelier Tuff	-13.0	fixed	fixed
Storage parameter			
Specific Storage (m^{-1})	-4.1	-4.4	-3.7
Recharge model parameters			
dz	108.936	fixed	fixed
z_{min}	7159.7	6106.7	8394.3
α	0.198109	8.58E-02	0.457516

predicted flow field for pre development conditions and associated residuals. In the vicinity of R-25, where accurate representation of the flow field is critical for simulating HE transport, errors, model predicted water levels were within 5 m of measured levels. As shown in Table 7-1, water level declines due to pumping were more difficult to predict accurately. For the PM2 well, the supply well with the longest period of record approximately down-gradient of R25, predicted declines were within 1 m of measured. Overall, the degree of agreement with predicted and measured water levels in this portion of the laboratory is very good.

Predicting HE transport beginning in 1945 and continuing hundreds of years into the future requires making assumptions about future pumping rates. For these simulations, we assume that 1996 pumping rates for all LANL area wells are sustained hundreds of years into the future. As

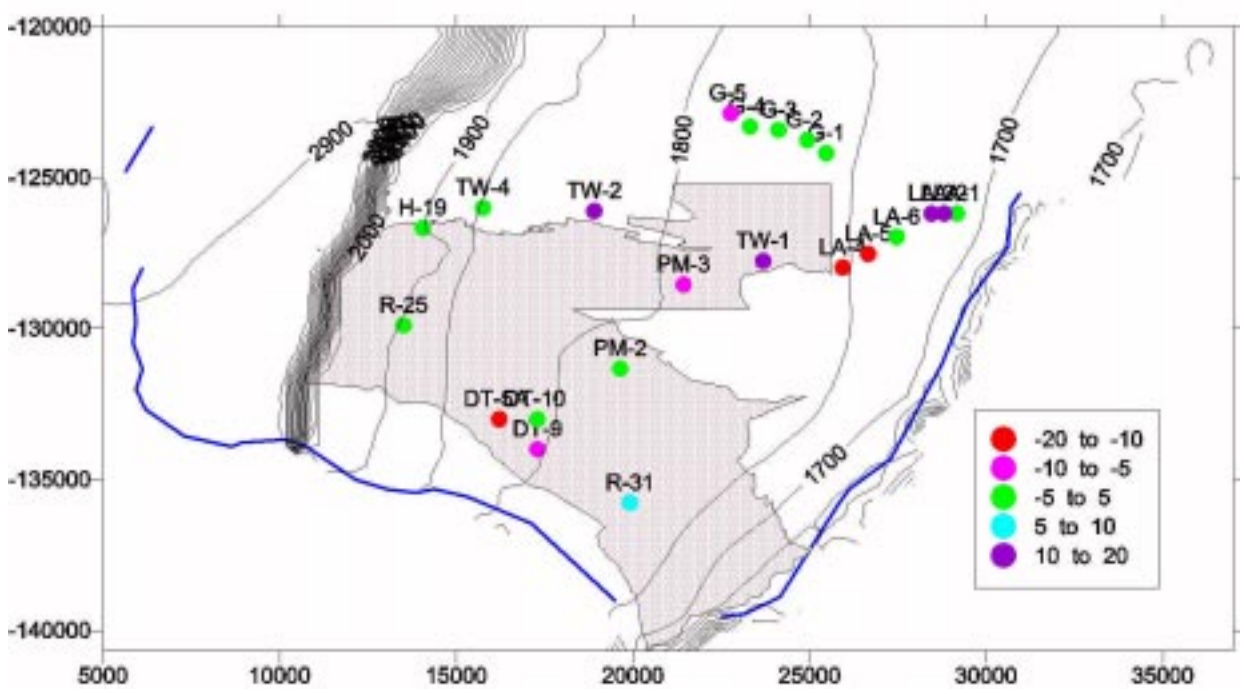

Figure 7-4. Predicted head distribution and associated residuals.

shown in Figure 7-5 the model predicts future water levels to be significantly lower than present water levels. One interesting trend is that the water table is predicted to flatten out; for example, the hydraulic gradient between R25 and PM2 is predicted to change from .019 at present to .007 in the future. The relatively large water level declines near the western edge of the model are presumably caused by low influx of water from the west compared to the total water withdrawn from supply wells. It is possible, however, that continued pumping on the Pajarito Plateau would eventually cause water to be drawn eastward across the topographic divide (western model boundary). In this case, the present hydraulic gradient might be sustained over a longer time. The transport simulations discussed below, however, are based on the assumption that increased flux across the western boundary will not be induced in the future.

7.3.2 HE Transport

To address sensitivity of the transport results to various degrees of heterogeneity within the Puye Formation, we generated a number of stochastic hydraulic conductivity fields for this hydrostratigraphic unit. All other hydrostratigraphic units were modeled assuming uniform permeabilities according to Table 7-2. For the Puye, we required the mean hydraulic conductivity of the random field to be identical to that used in the flow field simulations. Initial sensitivity

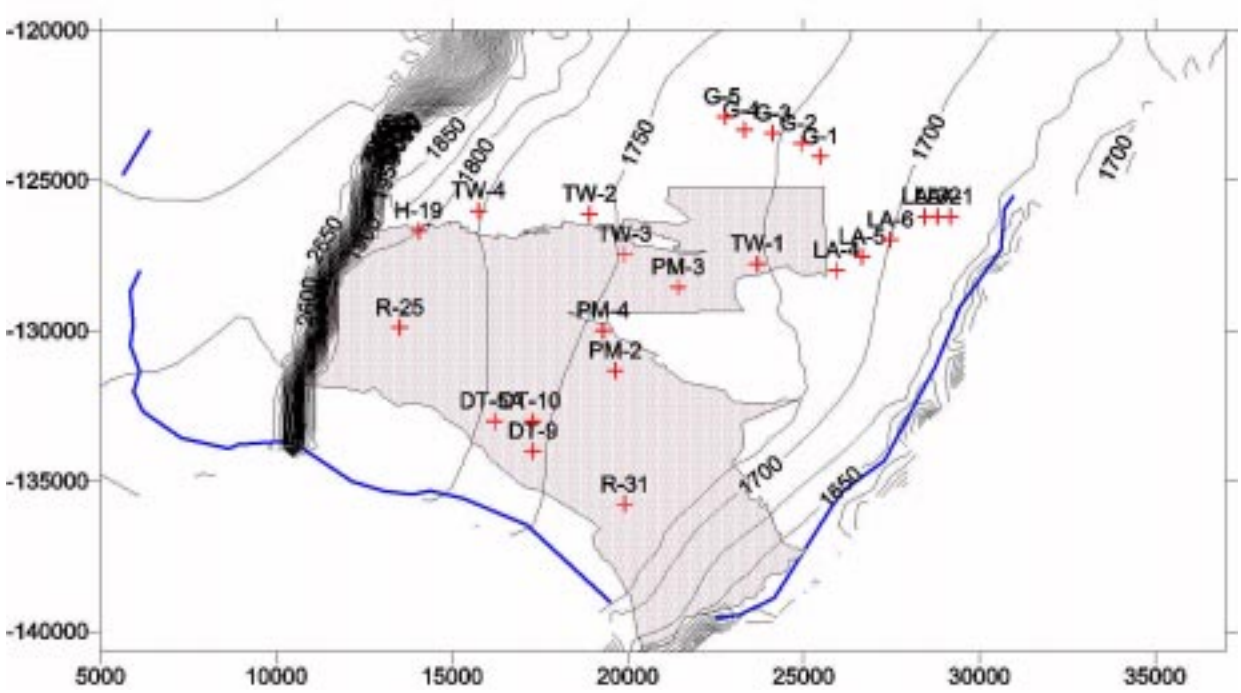

Figure 7-5. Predicted future water levels under pumping conditions.

analyses showed that the introduction of stochastic fields within the Puye did not change predicted heads at any point within the model domain corresponding to an observation water level, therefore, it was unnecessary to re-calibrate the flow model for each stochastically generated field for the Puye.

To simulate conservative transport of HE from its source at the water table at R-25, we used the particle tracking algorithm in FEHM. Particles were released into the system in a 100 X 100 m block centered at the water table at R-25. For all hydrostratigraphic units other than the Puye, we specified dispersivity values of 100 m (longitudinal), 10 m (transverse), and 0.01 m (vertical). For transport within the Puye, we relied on the heterogeneous hydraulic conductivity field to simulate the effects of dispersion and, therefore, specified very low values of dispersivity.

7.3.3 Stochastic distributions of hydraulic conductivity

We generated unconditional statistically homogeneous fields on the grid using a Gaussian sequential simulator, GCOSIM [Gómez-Hernández 1991]. The values of parameters required for the random generator, such as mean and variance of log hydraulic conductivity (<Y>=<log K_s> and σ_Y^2), correlation lengths, are estimated based on permeability measurements (Appendix, Table 12-2) and from estimates of facies geometries for the coarse Totavi Lentil facies (Appendix,

Table 12-4). Since the number of measurements is limited and the estimated values have relatively large uncertainties, therefore it is necessary to analyze the sensitivity of modeling results to the input parameters. We conduct several sets of numerical experiments to explore the importance of each parameter on simulation results. The setup for these experiments is shown in Table 7-3. Case

Table 7-3. Parameters used for generating 10 types of stochastic fields

Case numbers	<f>	σ_f^2	λ_x	λ_y	λ_z	ϕ
0	-11.793	0	500	500	20	0.1
1		0.276				
2		0.5				
3		1.0				
4		0.276	250	250		
5			1000	1000		
6			500	500	12	
7					30	
8					20	0.15
9						0.20
10						variable

0 assumes a uniform hydraulic conductivity (K) for the Puye Formation. Case 1 is the “base case” random field, with variance and correlation lengths calculated according to our initial data from the Puye. This case, along with cases 1-7, assumes a relatively low value of porosity (0.1) and so travel times predicted using these cases are very conservative (fast). Since travel times scale linearly with porosity, these predicted travel times can easily be scaled up or down.

Case 1 probably underestimates the variance of K, since 1) we have very few pump test results, and 2) tests are rarely done in the least conductive layers. To examine the possible effect of larger variance, we generated fields (2) and (3). To examine the possible influence of larger correlation lengths (i.e. more lateral connectivity within facies of the Puye), we generated cases (4) and (5). Cases (6) and (7) explore sensitivity to assumptions about vertical thickness of beds. Cases (8), (9), and (10) examine the sensitivity to porosity. Cases 8 and 9 assign uniform values of porosity to all units; Case 10 correlates porosity of each model element to its hydraulic

conductivity according to the Kozeny-Carmen equation (Bear, 1972). Figure 7-6 shows the resulting permeability fields for three representative cases (1, 3, and 4).

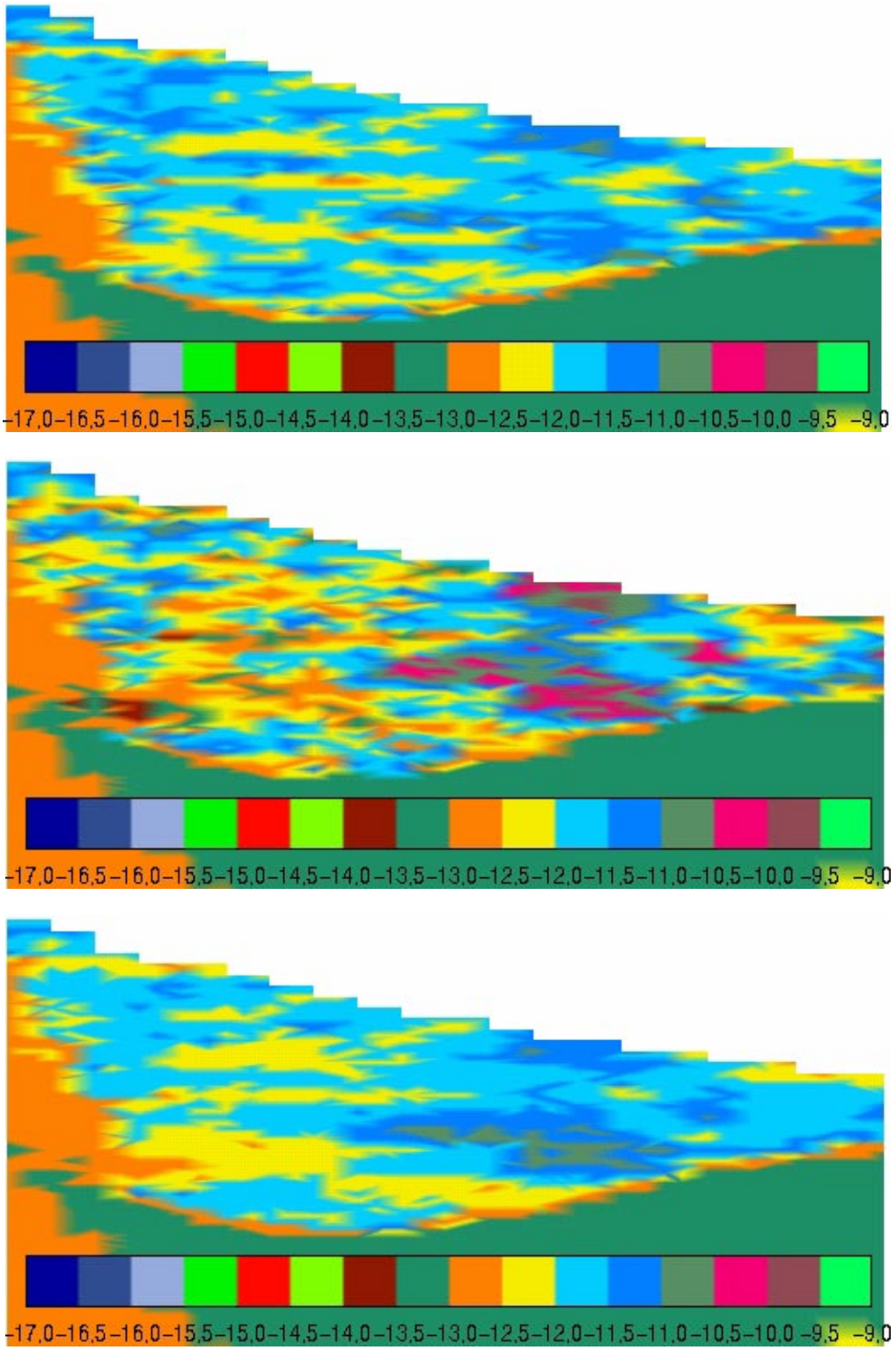

Figure 7-6. Stochastic hydraulic conductivity fields for cases 1, 3, and 4. Permeability values (m^2) are indicated by color.

For robust estimates of transport behavior using stochastic fields, it is required for each case to generate a large number of 'realizations', solve flow and transport equations for each realization, and calculate statistics, such as ensemble mean and (co)variance, based on solutions from all realizations. However, due to time constraints, for most of the cases, we ran only one realization. We conducted multiple simulations for one case (9).

7.3.4 Transport simulations and results

For all cases, all particles released were captured by some combination of PM2, PM4, and the Rio Grande. In most cases, PM4 captured most of the particles. Figure 7-7 presents

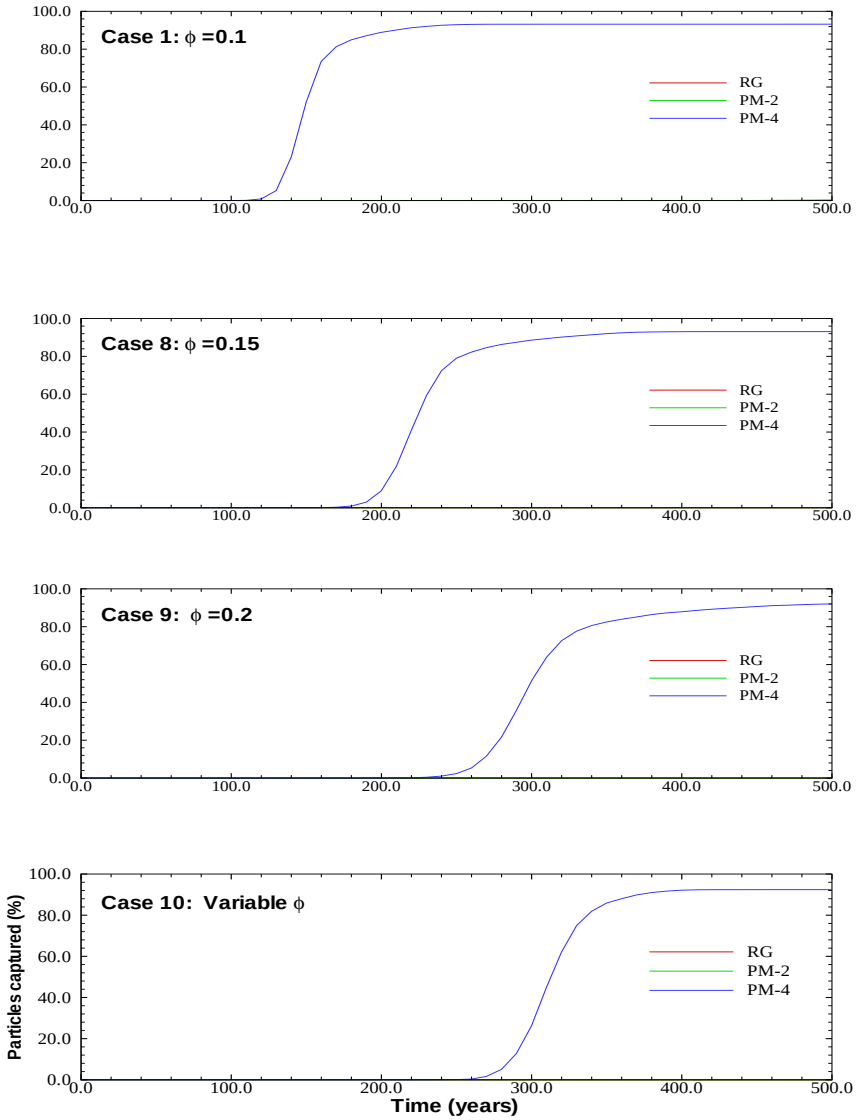

Figure 7-7. Predicted breakthrough curves for Cases 8, 9 and 10, showing effect of porosity

breakthrough curves for Cases 8, 9, and 10, showing the increase in travel times caused by increasing porosity. The increase in mean arrival time is linear, as shown by Figure 7-8. The most realistic case of these is case 10, where porosity is related to hydraulic conductivity. For all of these cases, PM4 was the only supply well that captured particles.

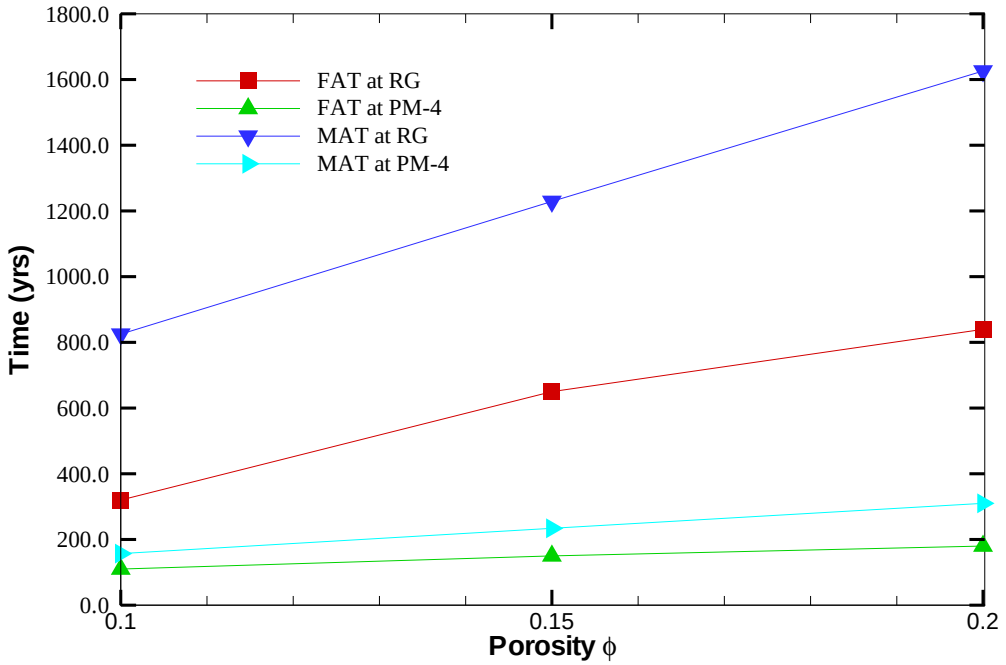

Figure 7-8. Effect of porosity on first arrival time and mean arrival time.

Figure 7-9 shows calculated breakthrough curves for cases 1,4, and 5. These cases vary only by the assumed horizontal correlation lengths, in other words, how laterally continuous any given sand or clay bed might be within the Puye Formation. This figure demonstrates a relative insensitivity of the results to this parameter. Figure 7-10 demonstrates a similar lack of sensitivity to assumptions about vertical correlation length, although there is a slight trend for longer travel times if vertical correlation is relatively high (30m).

Figure 7-11 shows breakthrough curves for cases 0,1,2,and 3, demonstrating model sensitivity to variance in K. As mentioned above, the variance assumed for Case 1 was calculated using available data; however, this may be an underestimate. No particles reach PM2 in the uniform (zero variance) case; as variance increases an increasing proportion of particles reach PM2.

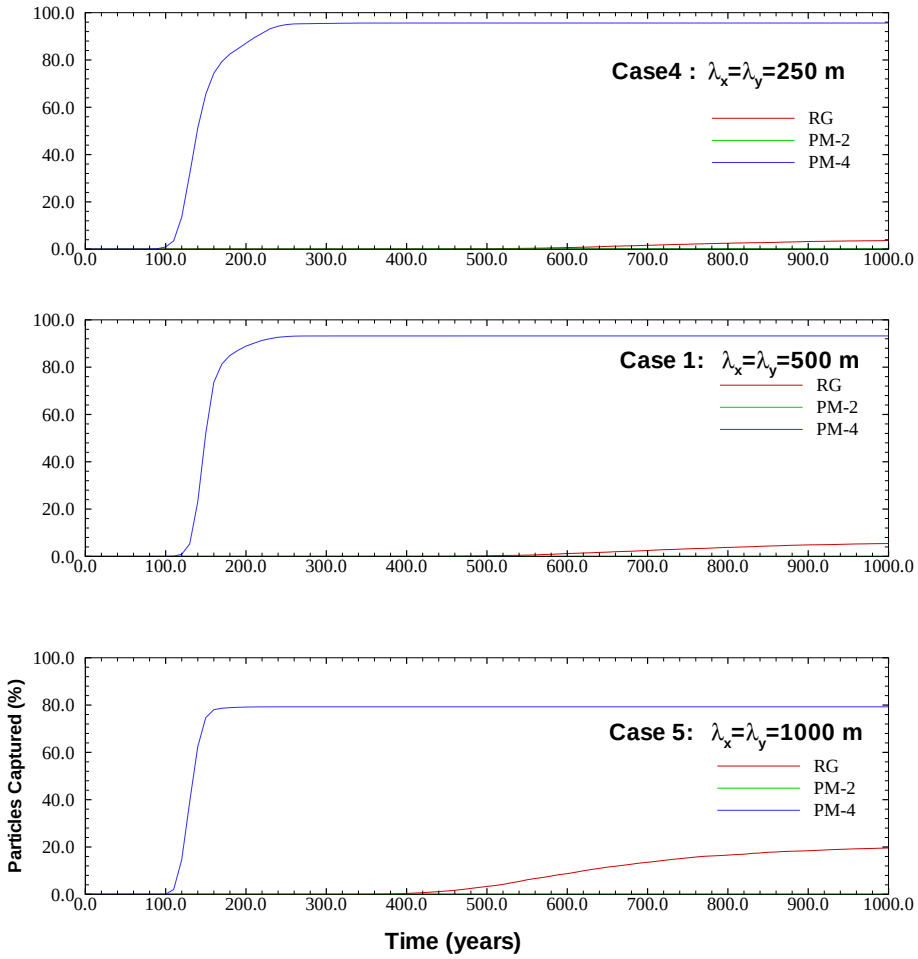

Figure 7-9. Predicted breakthrough curves for Cases 1,4, and 5, showing effect of horizontal correlation length.

Table 7-4 presents time of first arrival, mean arrival time, and standard deviation of arrival times for all cases. Predicted mean arrival times for PM2 range from 169 to 744 yrs; times for PM4 range from 110 to 595. The minimum arrival times correspond to cases where a uniform porosity value of 0.1 was used. This value of porosity is very low for sedimentary rocks; therefore, these travel times provide very conservative estimates. A more typical value of porosity is 0.2; since travel times scale linearly with porosity; travel times are more likely to be twice those calculated for Cases 0 – 9.

We consider Cases 9 and 10 to be the most realistic case, given the present dataset available to constrain the transport model. The only difference between these cases is assumptions about porosity. We conducted 19 simulations for different stochastic realizations for Case 9. Calculating the ensemble average behavior of the system based on many realizations of hydraulic conductivity

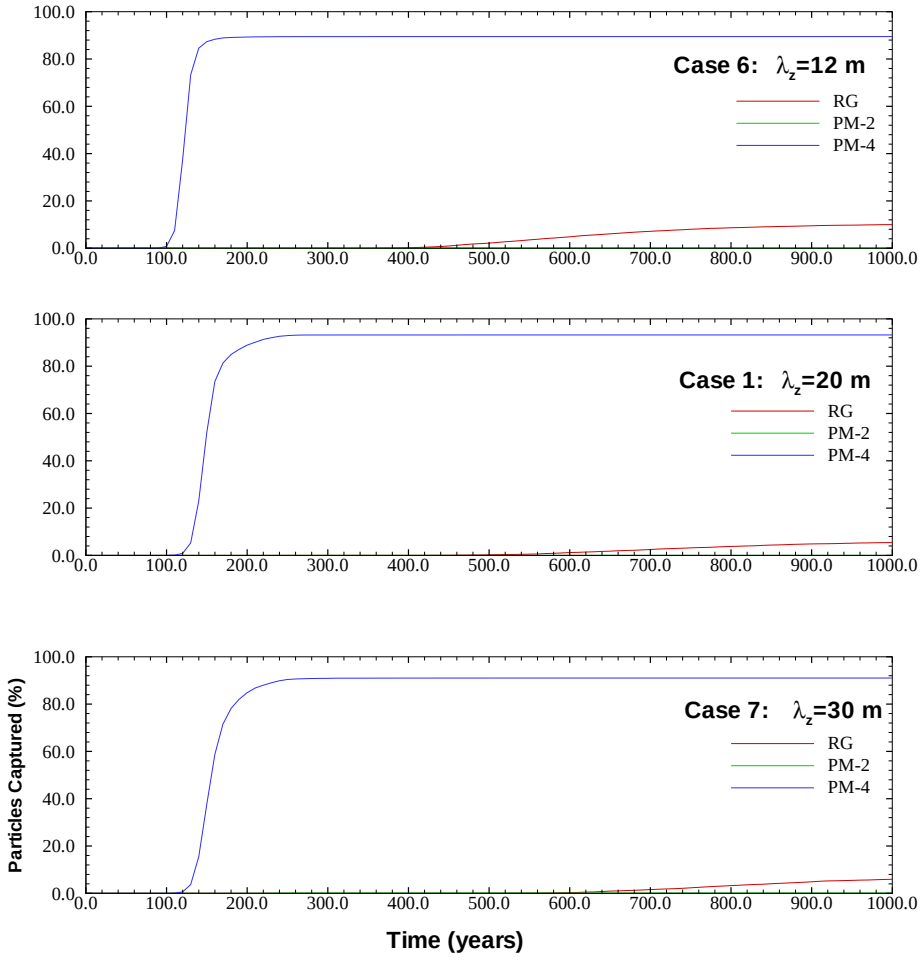

Figure 7-10. Predicted breakthrough curves for Cases 1,6, and 7, showing effect of vertical correlation length.

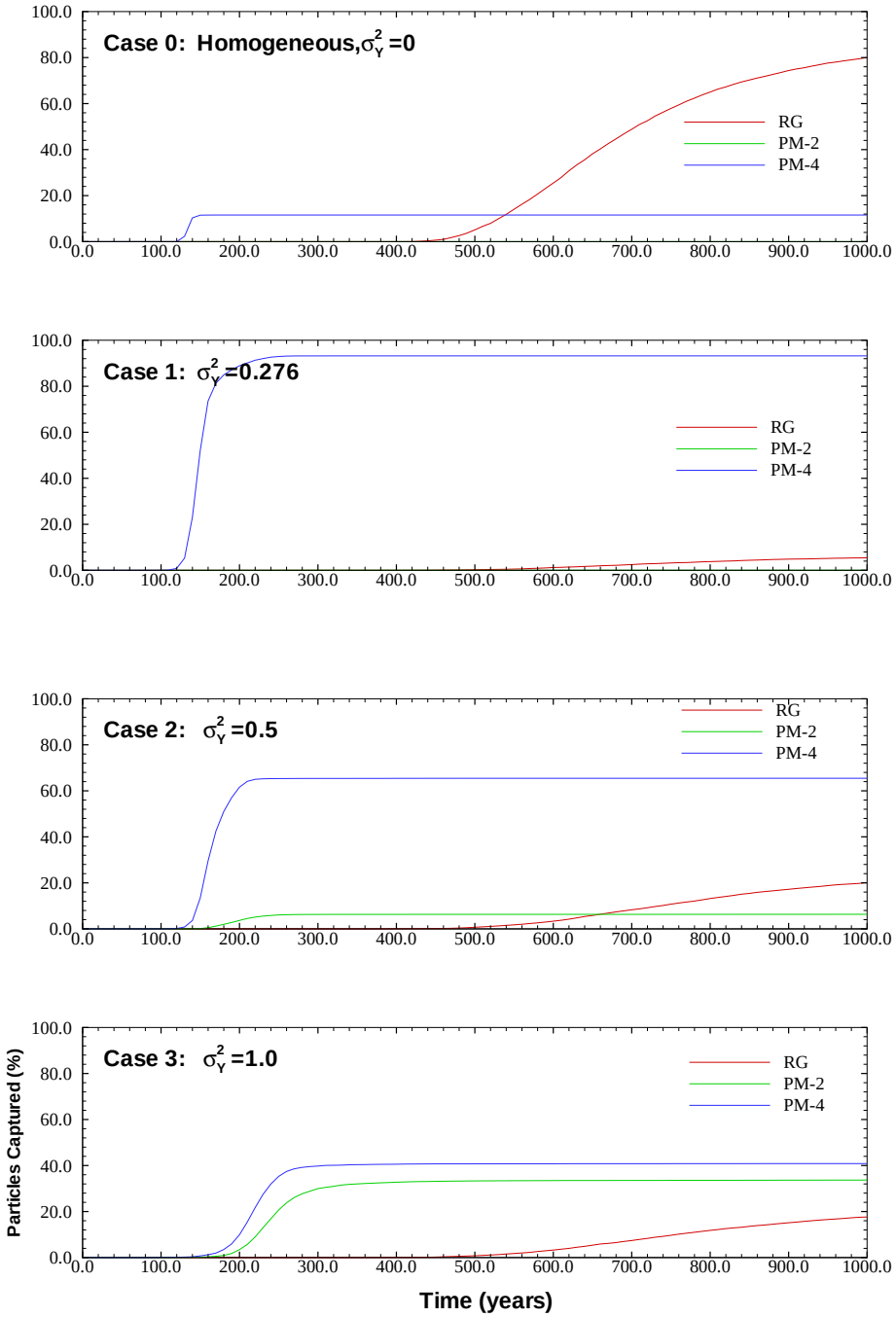

Figure 7-11. Predicted breakthrough curves for Cases 0,1,2,and 3, showing effect of variance.

fields is the best way to achieve confidence in model results. Ensemble breakthrough curves are presented in Figure 7-12; the average "mean breakthrough time" for the 19 cases was 286 years

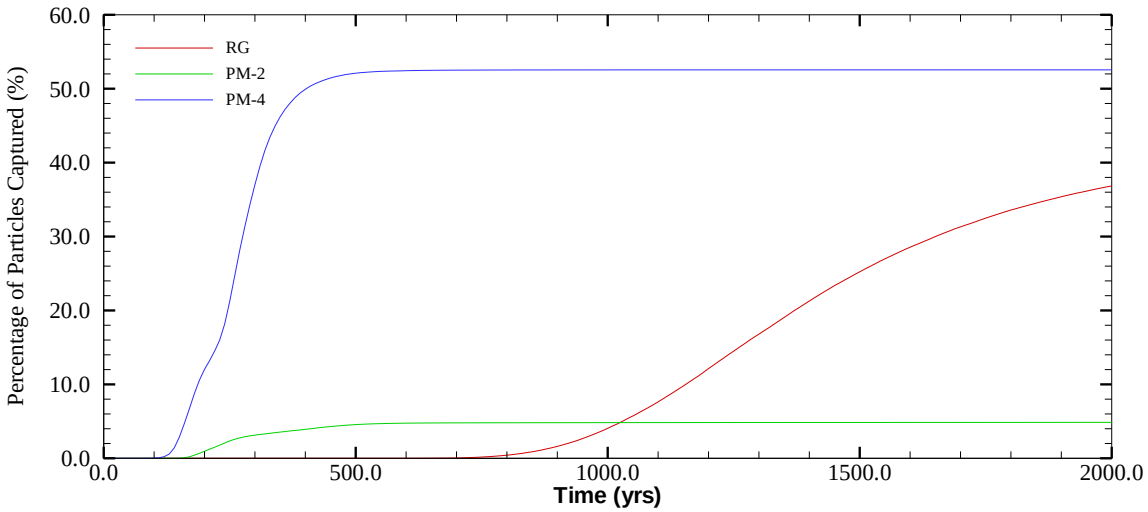

Figure 7-12. Ensemble breakthrough curve for Case 9, computed from 19 realizations.

(PM4) and 477 (PM2).

Table 7-4. Travel times calculated using 10 different models of hydraulic conductivity within the Puye Formation

Case	0	1	2	3	4	5	6	7	8	9	10
First Arrival, years											
RG	270	320	390	340	340	350	360	370	650	840	920
PM-2	110	250	120	110	200	na	na	200	na	430	na
PM-4	80	100	100	90	80	100	90	100	150	180	210
Mean arrivals, years											
RG	760.5	825.2	901.9	935.7	794.4	688.6	675.2	928.6	1229	1626	1569.6
PM-2	200.1	269.9	205.7	259	304.2	na	na	249.9	na	430	na
PM-4	145.1	157.4	170.9	226.9	151.6	135.9	127.9	163.8	234	310	318.1
Standard deviations of arrivals											
RG	252.4	254.8	312.7	379.7	226.1	211.1	213.1	247.7	345.6	478	392.6
PM-2	135.1	20	62.2	81.1	79.6	na	na	69.5	na	0	na
PM-4	28.9	21.5	22.7	50.7	32.1	12.8	14.8	25	32.2	42.7	23.9
Percentage of particles captured											

Table 7-4. Travel times calculated using 10 different models of hydraulic conductivity within the Puye Formation

Case	0	1	2	3	4	5	6	7	8	9	10
RG	50.8	6.8	28.3	25.5	4.3	21.4	10.9	9	7	7.7	7.6
PM-2	14.7	0.02	6.6	33.8	0.1	0	0	0.1	0	0.02	0
PM-4	38.5	93.2	65.5	40.9	95.6	79.6	89.3	91	93	92.3	92.4

Figures 7-13- 7-15 show the migration of the HE plume for three cases (0, 3, and 5). We

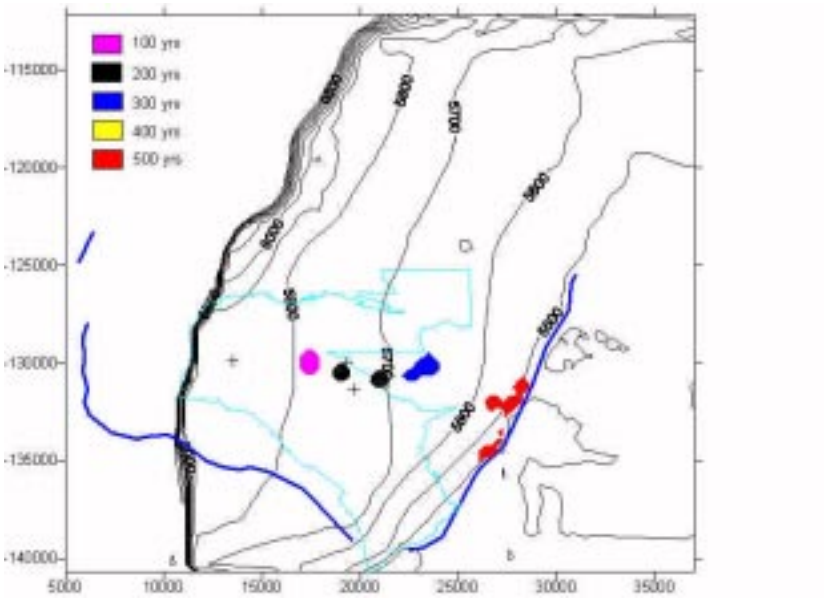

Figure 7-13. Migration of HE in the regional aquifer, case 0. Different colors correspond to different times. Plume extent is defined by the 10^{-8} relative concentration contour.

report relative concentrations, that is, the ratio of the concentration in the aquifer to the maximum concentration at the water table near the source. In these figures, plume extents are defined by the 10^{-8} relative concentration contour. Since these plots represent concentrations relative to a pulse of tracer, they cannot be used directly to determine HE concentration at the downstream locations. In this presentation, they are used to display the direction of transport and the dispersive spreading. Case 3 results shows a slight increase in spreading caused by the large variance in K. In general, the spatial extent and direction of the plumes is fairly similar. Table 7-5 reports the maximum relative concentration predicted to occur at various times for each of these three cases. This table demonstrates that 100 yrs after HE reaches the water table, the maximum concentration will be 5 orders of magnitude less than the original concentration in the pulse. After 500 years, concentrations will be reduced by 7 orders of magnitude. These reductions are caused by a

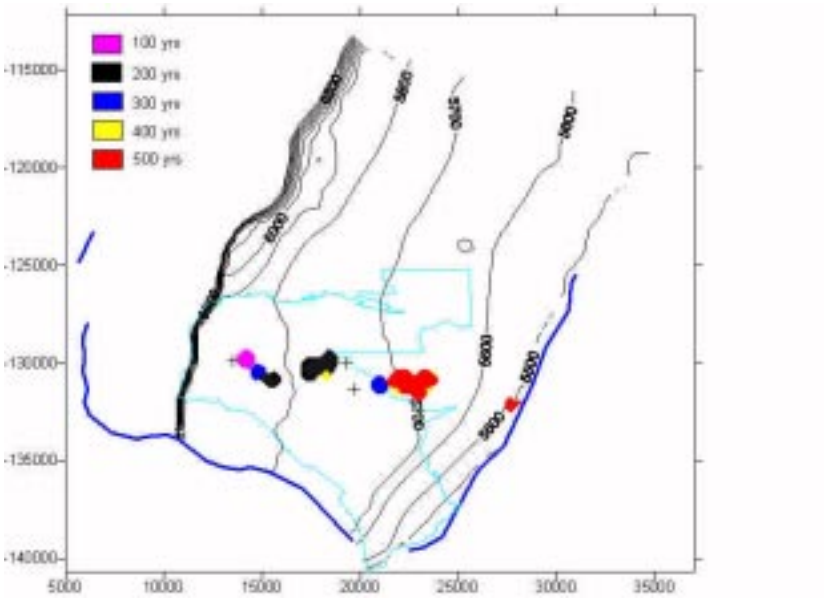

Figure 7-14. Migration of HE in the regional aquifer, case 3. Different colors correspond to different times. Plume extent is defined by the 10^{-8} relative concentration contour.

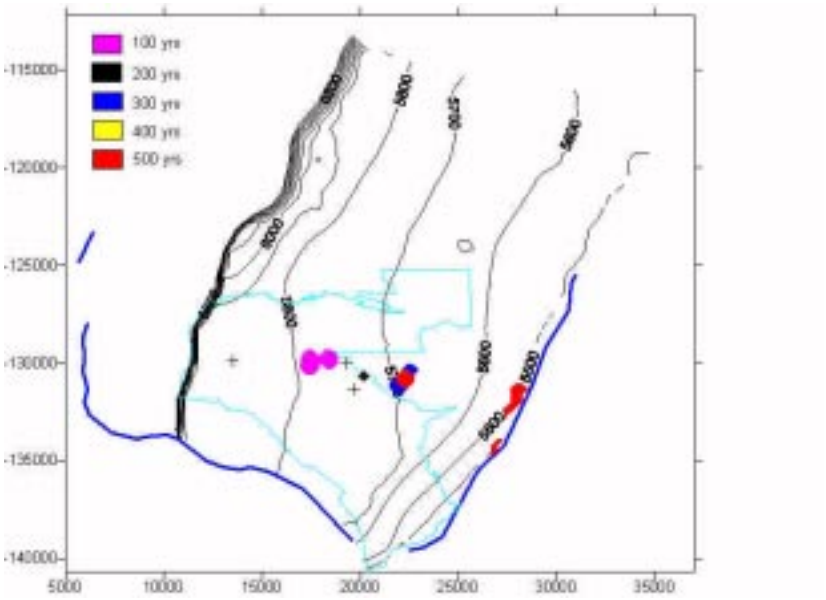

Figure 7-15. Migration of HE in the regional aquifer, case 5. Different colors correspond to different times. Plume extent is defined by the 10^{-8} relative concentration contour.

combination of HE removal (by PM4 and/or PM2), dispersion, and dilution with uncontaminated recharge water. Although they do not directly represent dilution factors in the aquifer, these results can be combined with the source term and vadose zone models to compute concentrations in

response to HE inputs other than a pulse. When the FEHM results are incorporated directly into the systems model in the next iteration of modeling, these concentration fields will be used to predict actual HE concentrations in the aquifer.

Table 7-5. Maximum relative concentration predicted to occur at any location within the aquifer (global) and at the water table for three cases.

	100 years		200 years		300 years		400 years		400 years	
	global	wt	global	wt	global	wt	global	wt	global	wt
Case 0	3.27E-05	1.03E-08	2.64E-05	2.79E-08	1.70E-05	4.88E-08	3.17E-07	0	1.95E-07	1.95E-07
Case 3	2.86E-05	1.63E-08	1.63E-06	2.07E-07	6.83E-07	9.75E-08	3.30E-07	2.90E-07	3.30E-07	9.80E-08
Case 5	7.86E-06	2.44E-07	1.29E-06	3.25E-08	3.17E-07	9.75E-08	1.10E-07	9.75E-08	9.75E-08	9.75E-08
Case 9*	2.60E-06	9.70E-07	9.40E-07	7.70E-07	3.50E-07	2.40E-07	2.20E-07	1.00E-07	2.70E-07	1.60E-07

By developing a stochastic approach to simulating heterogeneity within the Puye Formation, we are able to examine a relatively large number of cases and provide meaningful bounds to the range of possible travel times between R25 and the PM well field. As new data are collected to refine our model of facies within the Puye formation, some of these cases may be proven unrealistic and others may need to be added. Nevertheless, by considering these 10 cases we can evaluate the degree of uncertainty in our estimates of times of first arrivals to PM wells.

For the most conservative estimates (assuming a very low value of porosity), HE could be expected to reach PM4 within 80 years of reaching the water table below R25. For this “worst case scenario”, mean arrival time is predicted to be 150 years. The most realistic cases (9 and 10) predict travel times for first arrival of approximately 180 – 210 years from the time HE reaches the water table, with mean arrival occurring around 300 years. Because porosity is the parameter most directly controlling the breakthrough times, modeling and experiments designed to determine porosity are critical. Because the porosity of interest is the effective porosity of the medium with respect to contaminant transport, laboratory measurements on cores are not useful for determining this parameter. Instead, interwell tracer experiments are required, in which the breakthrough curve of a solute under pumping conditions is determined. Accompanying modeling at the scale of the field site would aid in the interpretation and provide a partial demonstration of the validity of the transport modeling approach being taken to characterize transport in the regional aquifer.

8.0 - Probabilistic Systems Model for Groundwater Contaminant Transport

The systems model developed in this section applies probabilistic concepts to assessing the uncertainty in parameters and their impact on groundwater contaminant transport. Once the basic model is set up, Monte Carlo sensitivity analyses can be performed to define which sub-models and which uncertain parameters are most important to study in order to reduce the uncertainty in the behavior of the system. The commercial software package GoldSim (Golder associates, 2000), is designed to perform this type of study efficiently and in a manner that lends itself to graphical model building and presentation. In this section we use the GoldSim code to construct a model for HE transport from TA-16. We also include barium in the analysis, as it is an additional contaminant of interest at the site. The model development is intended to be iterative, in that the current systems model should provide guidance on future data collection and process-level modeling that can have the greatest impact on reducing uncertainty. The present study documents the first iteration of the TA-16 modeling. Consequently, the systems model and the process-level models were for the most part developed in parallel, with model developers interacting to make the models as consistent as possible.

The GoldSim modeling approach is also being explored in the Environmental Restoration project, so the experience developed in constructing the TA-16 model is also expected to have direct benefit to this Project. For an example of the use of GoldSim to study groundwater contaminant transport, see Haagenstad and Birdsell (2000).

8.1 Background & Methods

The TA-16 GoldSim groundwater transport model includes two vadose-zone pathways, one that represents sources from ponds located on the mesa top and the other from the alluvial aquifer located in Cañon de Valle, as shown in Figure 8-1. Royal Demolition eXplosive (RDX) and barium travel through these two vadose-zone pathways to combine and flow through the regional aquifer into Los Alamos County Municipal Well PM-4. RDX was selected as a worst-case HE contaminant because of its relatively high solubility, conservative (nonsorbing) behavior, and resistance to biodegradation. Barium was selected because it is the dominant inorganic contaminant at TA-16 and because it represents a species with strong adsorption. The model uses an unlimited source term and stochastic distributions to describe RDX source concentrations,

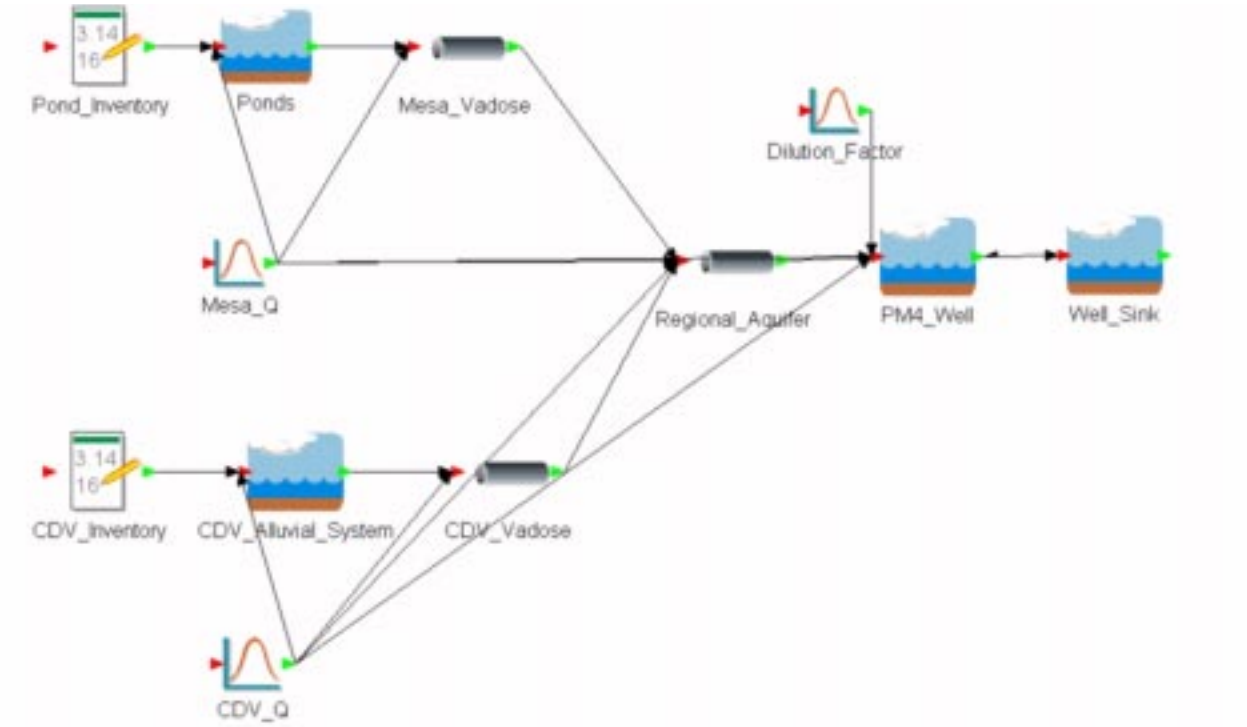

Figure 8-1. GoldSim model flowchart for TA-16. The figure shows the graphical elements and pathways used to model RDX and barium transport at TA-16.

vadose-zone flow rates, regional aquifer flow rates, porosities, and well dilution factors. The results are based on analysis of 100 Monte Carlo realizations for a 1000-year transport period.

The first vadose-zone pathway considers transport of RDX and barium from two ponds located on top of the mesa, the 90's line pond and the 260 outfall. These ponds received substantial loads of high explosives and barium during their operational history. The ponds are modeled as a single source with a surface area equal to that of the two ponds, as measured from aerial photos. The concentration of barium is controlled by its solubility limit, which is well defined and is consistent with recent sampling and geochemical modeling at TA-16. Hence, barium solubility is a deterministic parameter in the model. The RDX solubility limit is also well defined, however, existing analytical data from TA-16 are substantially lower than the solubility limit. This may be due to a less than complete contact of the infiltrating water with HE, of the dilution of solubility-limited fluid with dilute fluid. To handle this complexity, a stochastic uniform distribution with minimum values based on concentrations measured at the building 260 sump and maximum concentrations equal to the solubility limit is used to constrain RDX concentrations in the source areas. The pond is modeled as a well-stirred reactor.

Flow from the pond travels vertically through the vadose zone, which is modeled as a 744-ft long, one-dimensional pipe filled with tuff. In GoldSim, pipes provide a computationally efficient way of solving the advective-dispersive transport equation. The vadose pipe is filled with tuff which has a uniform porosity distribution based on laboratory analyses of TA-16 tuff units, and a saturation of 0.5. The flow rate is sampled from a uniform distribution with a minimum value of 40,774 m^3/yr and a maximum of 753,271 m^3/yr. The minimum is based on field observations of RDX contamination at 43.9 m in well 16-2669, located adjacent to the 90's line pond. We assumed the migration took 50 years, the approximate historic disposal period, to calculate this travel time. The maximum value is based on a bromide tracer test that was performed at the 260-outfall pond. In this test, bromide was transported a vertical distance of 30.48 m to SWSC spring in about 6 months. Because this travel time may represent only near-surface transport velocities and not downward migration rates throughout the entire vadose zone, the bound is considered to be conservative. When the water contacts tuff, barium is allowed to adsorb. A deterministic partition coefficient is used to control the amount of barium adsorption. The value used is based on barium adsorption on Yucca Mountain, Nevada tuffs and we used half that value because the Los Alamos tuffs are not zeolitized and thus, are probably not as sorptive. RDX is assumed to be a conservative (nonsorbing) contaminant.

The second vadose-zone pathway considers the transport of the two contaminants from the alluvial aquifer in Cañon de Valle. The alluvial system is modeled as a well-mixed reactor with the surface area approximately equal to that of the alluvial aquifer along the perennial flow reach in Cañon de Valle. The contaminant inventories and solubilities are constrained in the same way as the mesa ponds. After leaving the alluvial system, the contaminant flows vertically through the approximately 500-ft thick vadose zone below the canyon. The vadose-zone is again modeled as a one-dimensional porous medium with the same stochastic porosity distribution as the mesa, except that it is fully saturated. The choice of full saturation is based the relatively large amount of water that enters and is lost to subsurface flow in Cañon de Valle. Since the flow rate is being selected, rather than computed based on the assumption of saturated flow, the impact of this assumption on travel times is relatively minor compared to the uncertainty applied to the flow rates in the stochastic simulations.

Flow from the two vadose pathways combines to enter a one-dimensional pipe pathway that represents the upper portion of regional aquifer. The aquifer is made up of the Puye Formation, which is assumed to have a stochastic porosity distribution and is fully saturated. The length of this

pathway is 5811 m, the approximate distance from the vadose sources to the PM-4 well. The flow rate in the regional aquifer pathway is equal to the sum of the two vadose flow rates. Estimates of mean travel times based on three-dimensional FEHM simulations of the regional aquifer from TA-16 to PM-4 (see Section 7.0) are used to constrain regional aquifer transport in the GoldSim model. The cross sectional area of the regional aquifer element in the GoldSim model was adjusted so that the arrival of analytically detectable HE in the mean breakthrough curve for the aquifer corresponded approximately to the FEHM results.

After exiting the regional aquifer pipe, the PM-4 municipal well element is assumed to capture the entire contaminant plume. A simple stochastic dilution factor is used to represent possible reductions in contaminant concentration resulting from mixing in the PM-4 well bore. The well is represented as a simple, continuously stirred reactor that instantaneously transmits water to the surface. A sink element receives the “pumped” water, which allows water and contaminants to flow into and out of the PM-4 element.

8.2 Probabilistic systems model results & discussion

The transport of RDX and barium will be discussed as flow occurs from the source areas, though the vadose zone, through the regional aquifer, and finally, through the PM-4 well. Starting with the mesa pathway, predictions of RDX concentrations at the bottom of the vadose zone show rapid transport with breakthrough curves reaching concentration limits in less than forty years (Figure 8-2). These results are significant because they indicate that mesas may provide important sources of contamination to the regional aquifer. However, it is important to note that the results are based on the assumption that the flow rates used in the model are representative of the entire vadose zone. The flow rates used in the model are based on “tracer” movement in the upper part of the vadose zone only. Unfortunately, no data on deeper movement in the mesas exists, but the presence of significant thicknesses of Otowi member suggests the possibility of matrix flow and transport for part of the transit to the water table. Therefore, these results should be conservative. Barium transport in the mesa is apparently minimal (Figure 8-3). Concentrations for all of the realizations do not reach analytically detectable levels in the 1000-year time frame. The magnitude of the concentrations reflect low solubility of barium, and the long travel times are the result of sorption.

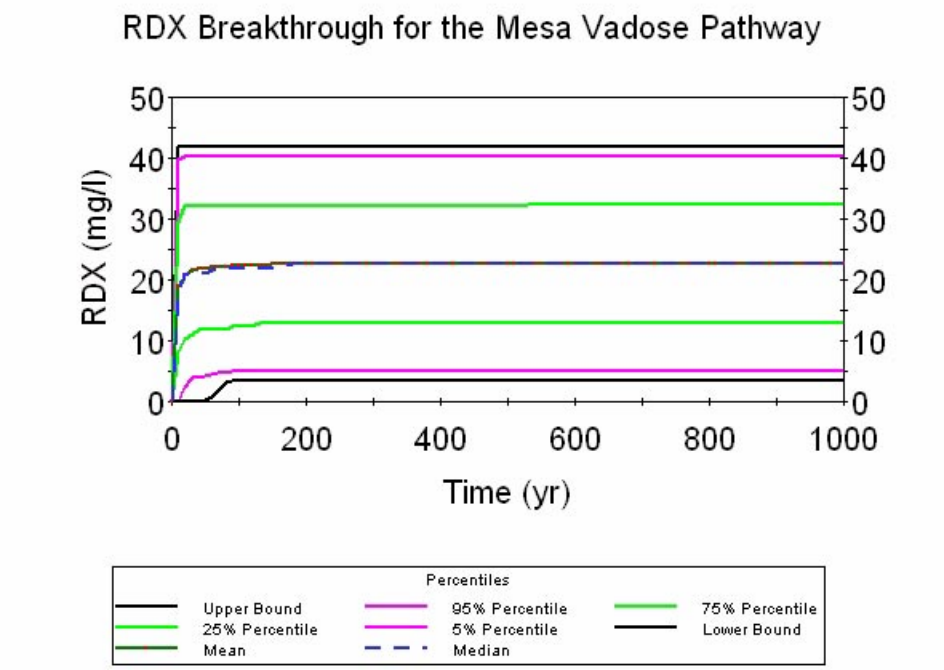

Figure 8-2. Summary curves of RDX breakthrough at the end of the mesa vadose zone pathway.

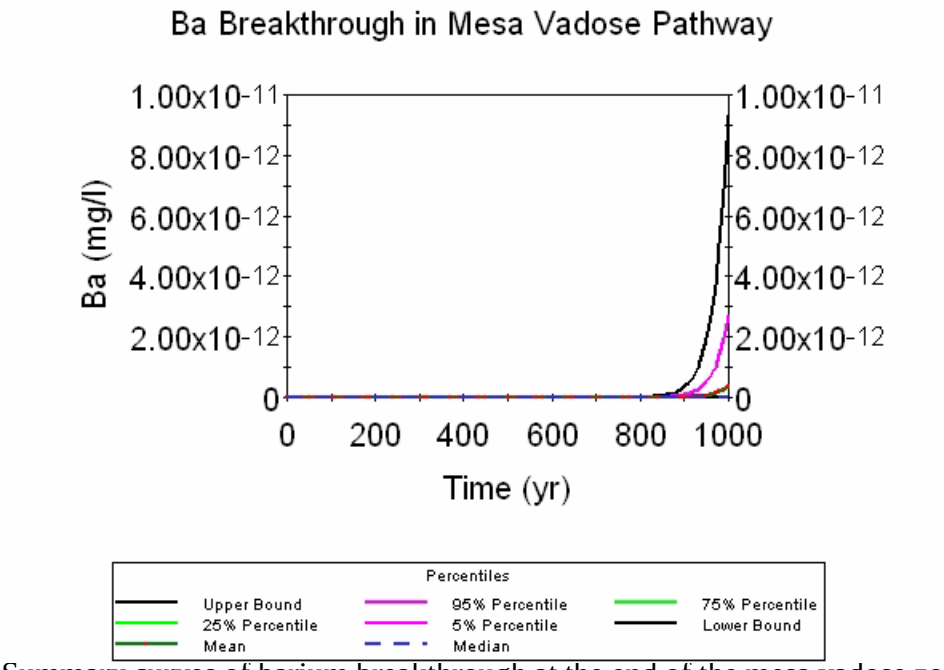

Figure 8-3. Summary curves of barium breakthrough at the end of the mesa vadose zone pathway.

Concentrations of RDX through the Cañon de Valle pathway are similar to those from the mesa pathway (Figure 8-4). However, steady state concentration levels occur slightly earlier than in the mesa pathway. The barium results for Cañon de Valle (not shown) are almost identical to the mesa pathway, but are about an order of magnitude lower. Thus, even though there are large

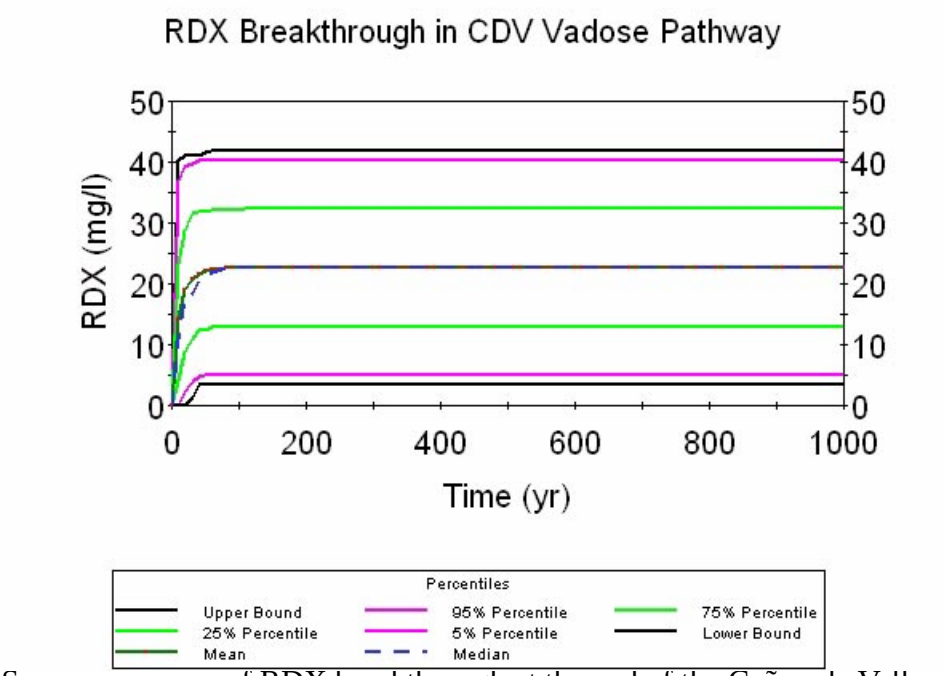

Figure 8-4. Summary curves of RDX breakthrough at the end of the Cañon de Valle vadose zone pathway.

sources of barium in the alluvial aquifer of Cañon de Valle, the modeling results suggest that barium will have little to no impact on the regional aquifer.

Concentrations of RDX at the end of the regional aquifer flow path represent inputs from both mesa and Cañon de Valle sources. Figures 8-5 shows the full curves, whereas Figure 8-6 shows an expanded concentration scale to display the first arrivals more clearly. Over the 1000-year simulation period, regional aquifer concentrations are reduced substantially from those in the vadose pathways. First arrivals of RDX at the end of the regional aquifer pathway range from about 110 to over 1000 years, depending on the stochastic parameters selected by the GoldSim code. Because of the unlimited source inventories, and large RDX concentration limits, some of the realizations show fairly rapid and large concentration increases after first arrival. These breakthrough curves reflect the more conservative parameters that are built into the model. No barium breakthrough occurred over the 1000-year period, which is consistent with the results from the vadose pathways.

The PM-4 pumping well results are a highly simplified representation of what may happen during pumping. They show that substantial reductions in RDX concentrations can occur if the well pumps from both contaminated and uncontaminated parts of the regional aquifer (Figure 8-7). However, one of the significant uncertainties in the model is the magnitude of the dilution factor

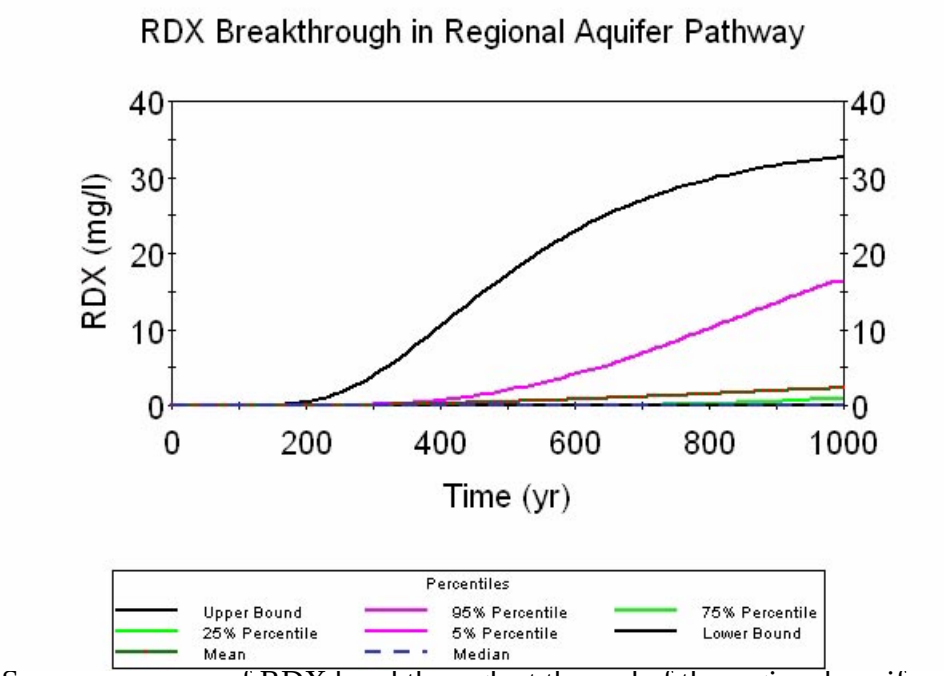

Figure 8-5. Summary curves of RDX breakthrough at the end of the regional aquifer pathway.

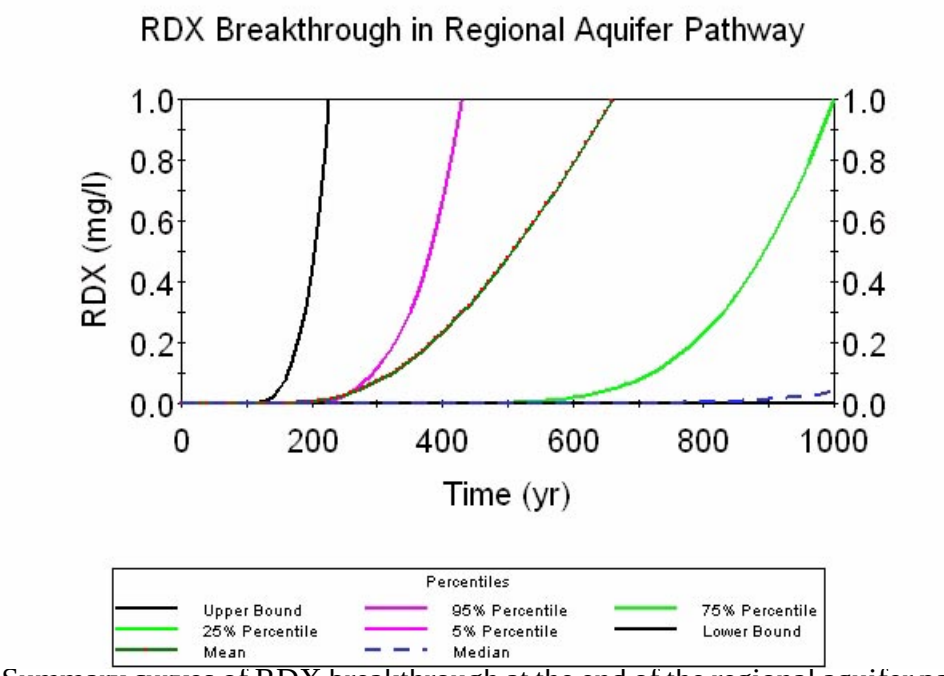

Figure 8-6. Summary curves of RDX breakthrough at the end of the regional aquifer pathway. The Y-axis scale was adjusted to better show first arrival times.

for the actual aquifer/well-bore system. Under high transport rate conditions with minimal wellbore dilution, analytically detectable RDX is predicted to appear in pumped water in about 150 years (about 100 years from now, since about 50 years have already passed). However, most of the

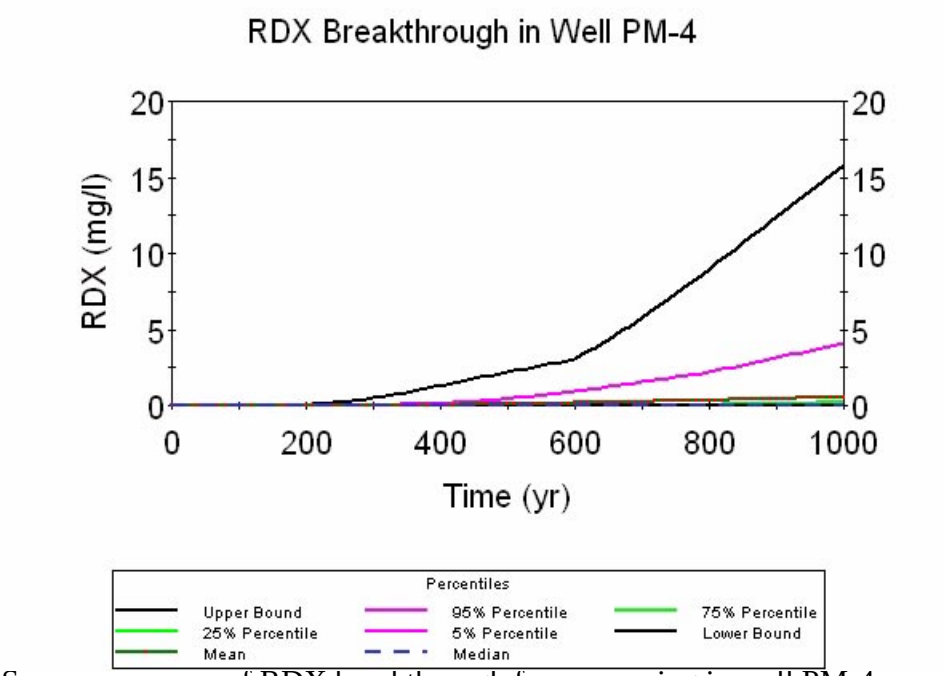

Figure 8-7. Summary curves of RDX breakthrough from pumping in well PM-4.

realizations indicate that RDX concentrations will reach detectable levels only after several hundred years, or do not reach detectable levels at all.

8.3 Sensitivity and uncertainty

Results presented for the GoldSim model show a wide range of possible behaviors, much of which is due to the ranges used in the various stochastic distributions in the model. However, under the current conservative estimates applied in this initial modeling effort, predicted concentrations reaching well PM-4 for the worst cases are higher than acceptable from a human health standpoint. However, we stress that in several instances, conservative assumptions have been made, and that further work will likely reduce the highest predicted concentrations. Furthermore, the modeling suggests that concentrations will not begin to rise in PM-4 for many decades, illustrating that this is a long-term issue rather than one that demands immediate action.

The range of breakthrough curves reflect how well we understand flow and transport in the vadose and saturated zones in the vicinity of TA-16. Top-down modeling approaches such as the one used here can typically be refined (reducing uncertainty) from the initial simulations by collecting and applying additional information about how the system behaves. A high-level sensitivity analysis of the current model shows that some of the model parameters have particularly

large impacts on the results. These parameters can then be refined through additional characterization and process modeling work (e.g., FEHM simulations). One set of sensitive parameters includes the RDX and barium inventories. On-going work at TA-16 by the LANL Environmental Restoration Project will provide improved inventory estimates that may allow us to relax the unlimited inventory assumption. If the forthcoming inventory estimates are low enough, the model estimates will show much lower concentrations predicted for the regional aquifer and PM-4 water. In addition, ongoing surface clean-up efforts should improve the predictions.

The other set of sensitive parameters include the flow rates for the various model elements. The stochastic distributions of flow rates are based on best available data and in some cases are probably realistic site-specific values. For example, the bromide based flow rate for the vadose zone pathways is an extremely rapid one and likely represents fast-path type transport along preferential flow paths such as fractures. It therefore provides a good conservative bound for transport at TA-16. However, the flow rates used for the regional aquifer element are less certain, which is why the FEHM results were used to constrain behavior in that element. As additional process level modeling is conducted and new wells are drilled in the regional aquifer, we should be able to refine the flow and transport behavior in the saturated zone element. Finally, the last high sensitivity parameter set includes the cross-sectional areas of the vadose and regional aquifer pathways. This parameter is strongly related to the flow rate and in fact is what was adjusted in the regional aquifer element to approximate the FEHM results. It is an important parameter in the vadose zone as well. We assumed that the cross-sectional area was the same as the footprints of the ponds and alluvial aquifer. The actual area of recharge through the vadose zone could be smaller than that used in the model because of localized or preferential flow, or could be larger because we did not include some of the historic ditches and ponds that are no longer at the site. Like the flow rates, reduction of the cross-sectional area uncertainty can be achieved through on-going site characterization work and additional process modeling.

8.4 Future systems model work

With respect to the GoldSim model, improvements and refinements of the model can be made based on additional modeling and site characterization information collected in late FY00 and FY01. The model can also be refined using currently available process model results. We were able to incorporate some of those results into the current model, but would like to better integrate

the FEHM work described in this report in the next iteration of the modeling. It would also be valuable to expand the contaminant species list to include TNT in order to include another important high explosive, and one that biodegrades. The model can also be modified to predict occurrence of contaminants at future wells drilled near TA-16, including R-27, which is scheduled to be drilled near the Cañon de Valle-Water Canyon confluence.

9.0 - Conclusions and Recommendations

We have demonstrated that the methodology proposed to examine flow and contaminant transport in the groundwater beneath the Pajarito Plateau can provide important insights into the potential impact associated with particular contaminants. Although the present study focused on HE in groundwater from TA-16, the methodology should be useful for other contaminants. A two-pronged effort of process-level and probabilistic systems modeling is the recommended course of attack for understanding the system and performing focused studies to determine future impact.

The advantage of the approach developed is that overall direction of the characterization and modeling effort is based on concrete a metric, in this case the potential concentration and time of a contaminant in a water-supply well. If one relies only on process-level studies, there is a greater chance that modeling activities become unfocused lack of perspective concerning which uncertain parameters are in greatest need of study. A similar problem occurs in purely data-driven characterization: field studies are just as susceptible to the problem of lack of focus. Process-level modeling is best used to synthesize the data acquired from field and laboratory investigations, and to provide the scientific basis for developing the simplified submodels that comprise the system model.

An important element of the probabilistic systems modeling approach is that it must be iterative. A single iteration does not capitalize on one of the biggest advantages of the approach, the ability of the results to guide future modeling and data collection activities. A more practical issue is that in the first iteration, we may not have enough of the right type of data, and the process-level models will not be refined enough, to enable us to make an argument of minimal impact. In the present study, conservative assumptions about the HE source term and transport properties were required. Consequently, the worst of the Monte Carlo realizations yielded maximum concentrations at well PM-4 which, if taken out of context, might be regarded as alarming. The proper perspective is that these concentrations are unlikely to occur for at least many decades, and that many realizations predict much lower concentration. The worst cases reflect the actual outcome only if several pessimistic parameters simultaneously turn out to be true. In an iterative approach, we identify which of these parameters control the results, and work to reduce those uncertainties.

With regard to HE migration from TA-16, the GoldSim modeling revealed that the following uncertainties were most important to the “bottom line:”

- The HE inventory and source term.
- The flow rates for the various model elements.
- The cross-sectional areas of the vadose and regional aquifer pathways.
- Dilution at the pumping well.

Therefore, future modeling and characterization efforts should focus on obtaining a better understanding of these elements. With this in mind, we summarize out recommended activities that should be embarked on in the next iteration of modeling. Accompanying studies to characterize the source term are already being executed by the Environmental Restoration Project.

The first iteration of the vadose zone modeling focussed on capturing the large-scale effects of mesa versus canyon infiltration, lateral diversion, and overall transport velocities through the vadose zone. Transport was studied only with respect to travel time to depth from various locations on the mesa and in Cañon de Valle. This model is a suitable platform for taking the next step, which is to develop a chemical transport model for HE migration. To do this, increased grid refinement in Cañon de Valle and in the vicinity of the 260 outfall and the 90's line pond is required. The grid for such a model has already been generated (Figure 6-6). This model would compute the source term directly by placing the water in contact with the waste at the solubility limit. This contaminated fluid would then mix with other clean fluid, resulting in a process-level description of the HE source, and a better representation of Bullet 1 above. Subsurface concentration data would then be used to constrain the model. Such an approach is likely to result in lower source concentrations, resulting in an improvement in the contaminant concentration at the downstream locations. In addition, the model should be improved in its application of infiltration on the mesa to include local enhanced flux in the area of the contaminated ponds. Near-surface lateral diversion (in the upper-most units of the Tshirege Member) should also be captured in the next iteration of the model.

Further development of some of the modeling approaches is also warranted. The issue of perched water versus regional aquifer water should be further studied, as it impacts the time required for HE to reach the aquifer (Bullet 2). This is best accomplished through the use of the combined UZ/SZ model approach developed in the present study. Improved numerical methods for handling this challenging computational problem should be developed. This model would also allow the issue of contaminant capture by pumping wells to be studied in the most realistic manner

possible, thereby attacking Bullet 4 above. This modeling should probably be carried out in a fundamental, site-independent way, rather than as an “add-on” to the existing TA-16 model. This would give the results a wider applicability to future contaminant studies elsewhere at the Laboratory.

The regional aquifer modeling revealed that heterogeneities and possible correlations between permeability and porosity have a significant impact on the nature of the contaminant plume and the breakthrough curve at a downstream location. This suggests that further model development will improve our ability to constrain the migration times and plume concentrations in the regional aquifer (Bullet 2 and 3). The characterization of the Puye Formation and the development of a facies-based permeability model is therefore a critical modeling need. Additional field investigations and the development of realistic permeability distributions should continue. The Monte Carlo approach employed in the regional aquifer study should be fully implemented in terms of generating a statistically significant number of realizations for each transport case, and a variety of theoretical relationships between porosity and permeability should be employed. A more complete parameter sensitivity analysis is also recommended. For example dispersion coefficients could be varied to study the impact on the breakthrough curves. To study some of these sensitivities, alternative stochastic modeling approaches not involving Monte Carlo simulation could possibly be explored. Finally, as mentioned above, pumping well capture of contamination (Bullet 4), is an area that should be examined in the regional aquifer modeling initiatives.

The next iteration of probabilistic systems modeling should strive to incorporate the results of the current and future process-level models more directly into the calculation. For example, the Monte Carlo results of the regional aquifer model should be abstracted and explicitly incorporated in the GoldSim model, perhaps by using arrival time and dispersion statistics compiled from the simulations. The parameters of the pipe model for the regional aquifer would then be more directly tied to the process-level model. Similar improvements could also be made to link the vadose zone process-level model to the vadose zone pathways. This will probably lead to a more complex pathway model in GoldSim to capture the details more faithfully. Finally, as mentioned in Section 8.4, including some basic degradation reactions and HE breakdown products in the model (and in the vadose zone process-level model) should provide further constraints on the results.

10.0 - Acknowledgements

This work was sponsored by the the office of the Associate Laboratory Director for Strategic and Support Research at Los Alamos National Laboratory. The original discussions leading to the development of the approach taken in this study involved a large number of scientists and project leaders in the Environmental Restoration Project and the Laboratory's Environment, Safety, and Health Division (ESH). We especially thank Charlie Nylander and Diana Hollis for their input at the early stages of this work and the support of related modeling efforts from which the present study directly benefitted, and Ken Eggert and Bev Hartline for providing managerial support. Much of the information used to build the TA-16 GoldSim model was collected by the Los Alamos Environmental Restoration Project by the High Explosives Production Sites Team and is available in the various RFI and CMS documents for TA-16. We would like to thank Don Hickmott for providing discussion and site-specific geochemical and hydrologic information.

11.0 - References

Bear, J. (1972). Dynamics of fluids in porous media. New York, American Elsevier.

Birdsell, K.H., W.E. Soll, K.M. Bower, A.V. Wolfsberg, T. Orr, T.A. Cherry, (1997). "Simulations of Groundwater Flow and Radionuclide Transport in the Vadose and Saturated Zones Beneath Area G, Los Alamos National Laboratory," Los Alamos National Laboratory manuscript LA-13299-MS.

Broxton D.E. et al., 1995. Earth Science Investigations for Environmental Restoration - Los Alamos National Laboratory Technical Area 21, Report LA-12934-MS, Los Alamos National Laboratory, Los Alamos, New Mexico.

Broxton et al., (draft 1999). Interim Completion Report for Characterization Well R-25, Draft Los Alamos National Laboratory report.

Carey, B., G. Cole, C. Lewis, F. Tsai, R. Warren, and G. Wolde-Gabriel, 1999. Revised site-wide geologic model for Los Alamos National Laboratory (FY99), Report LA-UR-00-2056, Los Alamos National Laboratory, Los Alamos, New Mexico.

Fogg, G. E., C. D. Noyes and S. F. Carle (1998). "Geologically-based model of heterogeneous hydraulic conductivity in an alluvial setting." Hydrologeology Journal **6**(1): 131-143.

Golder Associates, 2000. User's Guide GoldSim Graphical Simulation Environment, Version 6.02, Draft #3, Redmond, Washington, Golder Associates, Inc.

Gomez-Hernandez, J. J. (1991). A Stochastic Approach to the Simulation of Block Conductivity Fields Conditioned Upon Data Measured at a Smaller Scale. Stanford, California, Stanford University.

Gray, R.N., 1997. Hydrologic budget analysis and numerical simulations of groundwater flow in Los Alamos canyon near Los Alamos, New Mexico, Master's Thesis, University of New Mexico, Albuquerque, New Mexico.

Haagenstad, M. and K. Birdsell, 2000. Stochastic groundwater flow and transport models for MDA G using GoldSim, Environmental Restoration Project progress report.

Keating, E., E. Kwicklis and B. Robinson (1999).Simulated transport of HE in the regional aquifer from TA-16.LANL.

Keating, E., G. Zyvoloski, C. Gable, M. Witkowski, et al. (1998).A Steady-state regional flow model for the saturated zone in the Espanola Basin.Los Alamos National Laboratory.

Keating, E. H., E. Kwicklis, M. Witkowski and T. Ballantine (1999).A Regional Flow Model for the Regional Aquifer beneath the Pajarito Plateau.LA-UR-00-1029.

Keating, E. H., E. Kwicklis, G. Zyvoloski and V. V. Vesselinov (2000).Simulation model for the regional aquifer.LANL.

LANL (Los Alamos National Laboratory), 1998. Hydrogeologic Workplan, Los Alamos, New Mexico.

Purtymun, W.D., E.A. Enyart, and S.G. McLin, 1989. Hydrologic characteristics of the Bandelier tuff as determined through an injection well system, Report LA-11511-MS, Los Alamos National Laboratory, Los Alamos, New Mexico.

Reneau, S. L. and D. P. Dethier (1995). Pliocene and quaternary history of the Rio Grande, White Rock Canyon and vicinity, New Mexico. NM Geol.Soc.Guidebook, 47th Field conference, Jemez Mountains Region.,. F.Goff, NM Geological Society: 484.RFI Report for Potential Release Site 16-021(c) (1998). Los Alamos National Laboratory report LA-UR-98-4101 (3 volumes).

Robinson, B.A., M. Witkowski, C.J. Elliot, L. Dale, R. Koch, (1999). "Numerical Model of Flow and Transport for Los Alamos Canyon," Los Alamos National Laboratory Environmental Restoration Project Milestone.

Robinson, B.A., H.S. Viswanathan, and A.J. Valocchi, 2000a. Efficient numerical techniques for modeling multicomponent ground-water transport based upon simultaneous solution of strongly coupled subsets of chemical components, *Adv. in Water Resour.*, 23, 307-324.

Robinson, B.A., S.G. McLin, and G.Y. Bussod, 2000b. Hydrologic behavior of unsaturated, fractured tuff: interpretation and modeling of a wellbore injection test and implications for contaminant transport, to be submitted to *J. Contam. Hydrol.* (in prep.).

van Genuchten, M.T., (1980). "A Closed-Form Equation for Predicting the Hydraulic Conductivity of Unsaturated Soils," Soil Science Society of America Journal 44, 892-898

Vaniman, D., G. Cole, J. Gardner, J. Conaway, D. Broxton, S. Reneau, M. Rice, G. WoldeGabriel, J. Blossom, and F. Goff, (1996). "Development of a Site-Wide Geologic Model for Los Alamos National Laboratory," Report LA-UR-00-2059, Los Alamos National Laboratory, Los Alamos, New Mexico.

Watermark Computing (1994).PEST Model-Independent parameter estimation: user's manual, Watermark Computing.

Wohletz, Ken (draft, 1999). "Geological Borehole Logs for the TA-16 260 Outfall Area MDA P". Draft Los Alamos National Laboratory report.

Zyvoloski, G.A., B.A. Robinson, Z.V. Dash, and L.L. Trease, (1997). "Summary of the Models and Methods for the FEHM Application - A Finite Element Heat- and Mass-Transfer Code," Los Alamos National Laboratory manuscript LA-13307-MS.

12.0 - Appendix - Hydrofacies within the Puye Formation

12.1 Geologic History of the Puye Formation

The Puye Formation is a volcanogenic-alluvial fan deposited approximately 2-5 Ma. The Plio-Pleistocene alluvial fan sediments were deposited in response to rift-margin volcanism of the Rio Grande Rift and the development of the Tschicoma volcanic center located in the northeastern Jemez Mountains (Figure 12-1). Progradation of the alluvial fan developed to the east of the

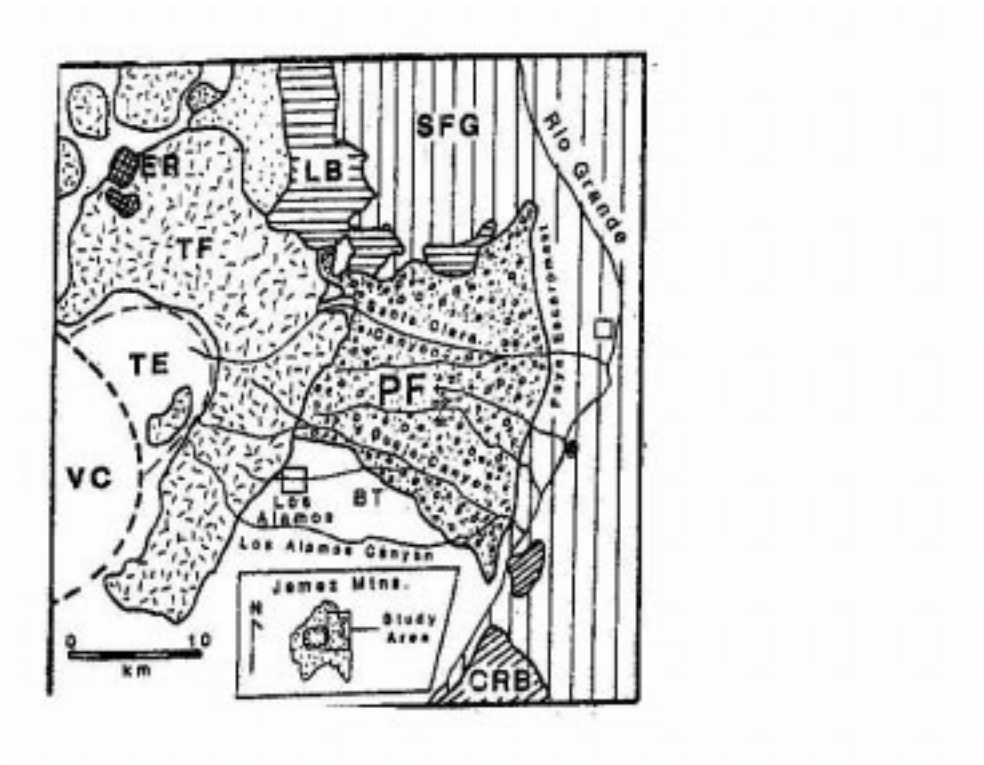

Figure 12-1. Location of the Puye Formation (Waresback and Turbeville, 1990).

Tschicoma volcanic center and advanced continuously with grabben development and establishment of the Rio Grande in the Espanola Basin. Fan migration diminished due to waning sediment supply as a result of ceasing volcanic activity and development of basin-wide pedimentation by the Rio Grande. The Puye is estimated to be a 200km^2 fan which contains >15km^3 of coarse-grained volcaniclastic sediments [Tuberville, 1988 #34].

Puye sedimentation is characterized by sediment deposition as stream channel deposits, sheet flood deposits, flood flows, and sediment gravity flows. These sediments are interbedded

with primary and reworked pyroclastic units such as pumice falls, pumiceous ignimbrites, block-and-ash flows, rhyolitic deposits, and basaltic ash. Lacustrine deposits, formed by damming of the Rio Grande by Cerros del Rio basalts, constitute a significant portion of the distal facies of the fan. The Puye exhibits great lateral and vertical variation, although many of the pyroclastic facies display distinct cyclicity related to volcanic activity [Waresback, 1990 #37].

12.2 Deposit Types found within the Puye Formation

12.2.1 Alluvial Fans

Alluvial fans are cone shaped deposits formed by sedimentation that is enhanced when flows laterally confined by narrow drainages expand rapidly when discharged into a flat valley. Dominant flow processes are stream flows, gravity flows, mudflows, and flood flows. They are generally triangular or fan shaped in map view, wedge shaped in cross section, and are limited laterally (Figure 12-2). Alluvial fans are usually poorly sorted conglomerates and breccias exhibiting crossbedding, reverse and crude grading, and lenticular bedding. Grain size can range from silt and sand to pebbles, cobbles and large boulders. Fan development occurs in rifting continental grabbens, basins, and areas of rapid uplift.

12.2.2 Stream Channel

Stream channel deposits are generally clast-supported conglomerates exhibiting imbrication and lenticular bedding, crossbedding, ripples and dunes. Depositional processes are rapid discharge, traction flow, open channel flow, saltation, and unidirectional flow. Common macroforms seen in channel deposits are longitudinal, transverse, and point bars. Deposits are generally tabular, elongate and straight with lenticular or sheet-like sand bodies. Stream channels can develop in the upper reaches of alluvial plains and are associated with rapid down dropping basins.

12.2.3 Debris Flow

Debris flows are a poorly sorted assortment of clay, silt, sand, pebbles, cobbles, and boulders. There is usually no stratification unless sequences of debris flows have been emplaced on top of each other. Debris flows are matrix-supported, reversely graded, and are generally tabular and lobate bodies of uniform thickness. In alluvial fans, they usually occur in the upper section of the fan. Debris flows are caused when a dense mass of mud and debris becomes saturated and the force of gravity causes the mass to flow down steep slopes and canyons. Volcanic terrains with

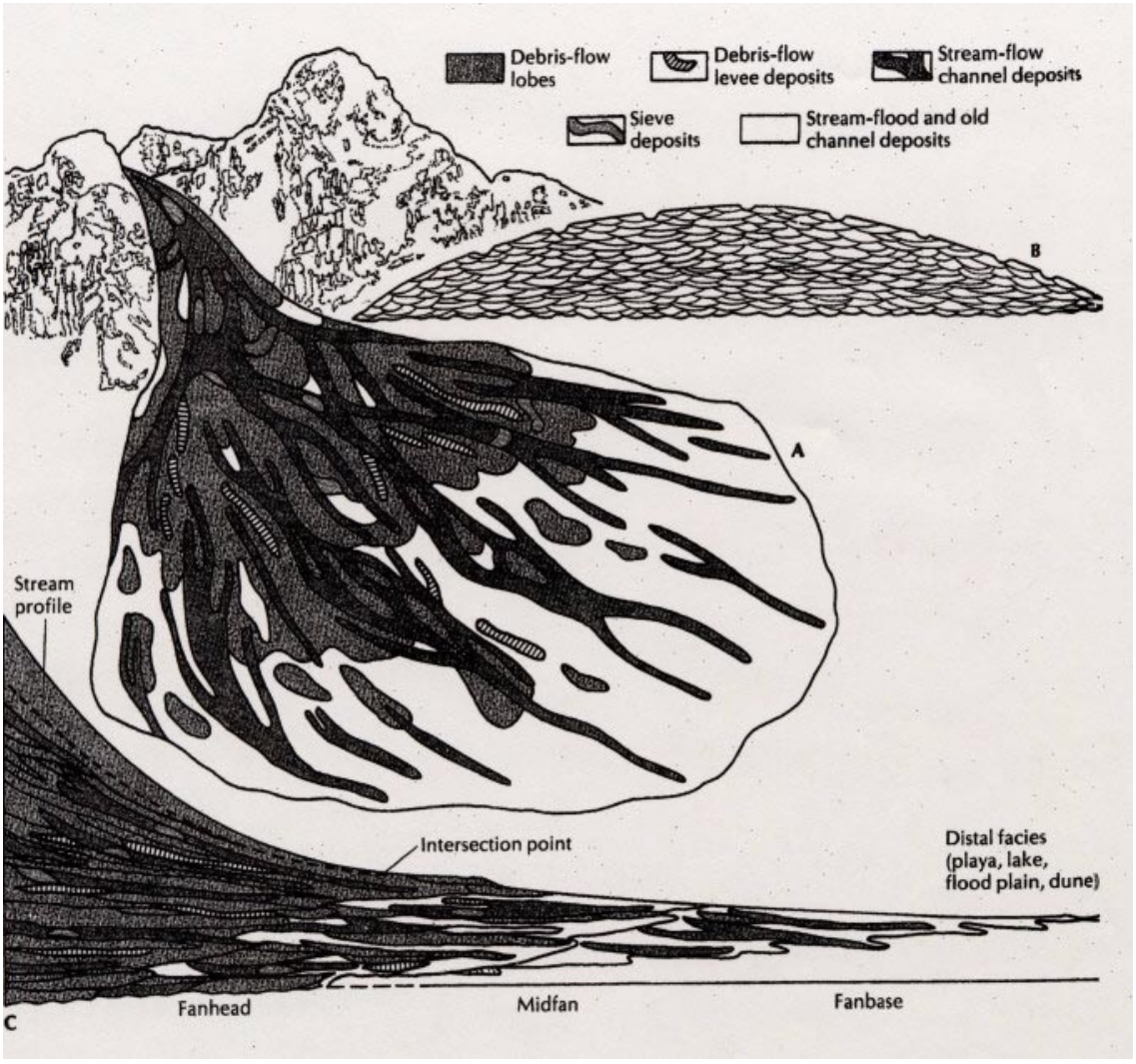

Figure 12-2. Model of alluvial fan sedimentation. (A) Fan surface; (B) Crossfan profile; (C) Radial profile. Vertical profiles are greatly exaggerated (reproduced from Prothero and Schwab, 1996).

large amounts of pyroclastic material, such as the paleo-terrain of the Puye fan, are particularly susceptible to debris flows. Volcanic debris flows are typically clay-poor, and can contain boulder- and cobble-rich zones aligned parallel to flow direction or have more random matrix-supported deposition. Overall, there is not a significant difference between debris flows generated in volcanic and non-volcanic terrains.

12.2.4 Sheetflood/Hyperconcentrated flood flow

Sheetflood deposits form during flood periods when excess water spills over a channel bank and spreads out across the alluvial fan depositing a shallow sheet of sand or gravel with no fines. These deposits are well sorted, well stratified, laminated and crossbedded.

Hyperconcentrated flows represent the transition from debris flow to stream channel deposition. They are generally sand size, massive or crudely stratified, cross bedded and can be normally graded. They usually occur at the top of debris flows and exhibit erosional scours into underlying deposits.

12.2.5 Lacustrine

Dominant flow processes in lacustrine deposits are sediment gravity flows, wave action and suspension settling. Lake deposits are typically laminated mudstones and sandstones displaying ripple marks, hummocky cross stratification, desiccation cracks, soft sediment deformation structures, rootlets, and coarsening upward sequences. Sand body geometry is usually circular to elongate. Lakes generally form in fault grabbens and areas of internal drainage.

12.2.6 Volcaniclastic Sediments

Volcaniclastic rocks are both sedimentary and igneous. They are derived from when pyroclastic material, which is material ejected during a volcanic eruption, is deposited by sedimentary processes.

The following are some of the most common types of volcaniclastic deposits.

Tephra. Tephra is defined as material of any size or composition ejected by volcanic explosions. There are three general classes: 1) vitric tuff and ash dominated by pumice and glass shards 2) crystal tuff and ash dominated by crystals 3) lithic tuff and ash dominated by rock fragments.

Pyroclastic Air Fall. Pyroclastic air fall deposits are derived when ejecta is thrown into the air and settles onto the surface. These deposits tend to rapidly coarsen and thicken toward the source. Air fall deposits contain large, poorly sorted, angular blocks and bombs immediately adjacent to the center of the eruption. Fine ash is deposited down wind. Air fall deposits tend to form uniformly thick blankets of material on all surfaces regardless of topography.

Volcaniclastic Flow. Volcaniclastic flows form when tephra is remobilized and moves downslope. There are three basic types: 1) pyroclastic flows, which also produce ignimbrites 2) pyroclastic surges 3) lahars.

Ignimbrites. Ignimbrites are the most lithified portion of an ash flow deposit. They are produced by hot density currents, which are gravity-propelled clouds of ground hugging tephra and gas. Ig-

nimbrites tend to have poor internal organization, upward coarsening, and alter to welded tuffs. Deposition follows drainages and does not mantle topographic divides.

Pyroclastic Surge. A pyroclastic surge is a rapid, episodic, or discontinuous downslope movement of pyroclastic material, gas, and/or water. Individual deposits are thinner and finer than ignimbrites and richer in crystals and rock fragments. They exhibit well-defined internal organization, planar- and trough- crossbedding. Surge deposits are usually thicker in valleys and thinner over topographic divides.

Lahars. Lahars are mudflows formed of water saturated volcanic material and can be very voluminous and extensive.

Base Surge. Base surges are sediment gravity flows which form when steam saturated eruption columns collapse and travel outward across the surface as a turbulent mix of water vapor or condensed droplets and solid particles. The deposits are moderately to poorly sorted with a rapid decrease in grain size and thickness away from the source. There is commonly crossbedding and fine laminations.

12.3 Hydrofacies of the Puye Formation

The Puye is made up of three distinct units: the Puye fanglomerate, lacustrine facies, and the Totavi Lentil member (Table 12-1). The Puye fanglomerate can be divided into three main facies and nine subfacies. The three main facies are: clast-supported conglomerates which are further divided into channel deposits and sheet deposits; matrix-supported conglomerates which consist of clast-rich deposits and matrix-rich deposits; pyroclastic facies which can be broken down into block-and-ash flows, lower tephra group, middle tephra group, upper tephra group, and phreatomagmatic basalts. The facies observations and descriptions below are taken from Waresback and Turbeville, 1990; Turbeville, Waresback, and Self, 1988; and Turbeville, 1991.

12.3.1 Puye Fanglomerate

Clast-Supported Conglomerates. The clast-supported conglomerates are the dominant lithofacies within the Puye Formation. These deposits are divided into two subfacies based on differences in external structure.

The channel deposits change considerably with grain size, geometry, thickness, internal structure, and position within the fan. Proximal to medial-fan exposures tend to exhibit broad channel-form geometries with individual channel sequences ranging from 30 cm to >6 m thick and showing upward thickening and coarsening with abrupt thinning downfan. Coarse grained, poorly sorted deposits that display normal and reverse grading tend to dominate proximal exposures. Clasts are generally angular to subrounded cobbles and pebbles. Some of the stream-channel deposits are capped by a pebbly sandstone, which forms discontinuous lensoid bodies with horizontal to low-angle stratification.

Distal stream-channel exposures are notably much thinner, 10 cm to 3.5 m; better sorted; and finer grained. They tend to be laterally extensive lenticular bodies, which are commonly polymodal and normally graded with better developed stratification than in other exposures.

Sheet deposits form sandy-pebble conglomerates and pebbly sandstones that are laterally continuous throughout the Puye. Proximal deposits are confined to lower parts of the section while medial and distal deposits can be found throughout the fan sequence. Sheet deposits range in thickness from 10 cm to 3.5 m and are laterally extensive for several hundred meters with only minor thinning. Stacked sand and gravel couplets are common and range from 1 cm to 5 cm in thickness.

Sheet deposits are very similar to braided stream deposits but can be distinguished by laterally extensive sheet-like geometry, absence of deep scours, laterally continuous with uniform horizontal stratification, and lack of apparent grading.

Matrix-Supported Conglomerates. Matrix-supported conglomerates are fluidized sediment-gravity flows produced by a variety of debris-flow deposits. These debris flows are divided into clast-rich deposits and matrix-rich deposits, also referred to as clast-poor deposits.

Clast-rich deposits are sandy-cobble and boulder conglomerates that are more dominant in proximal exposures and upper parts of the fan sequence. Deposits range from 20 cm to >4 m thick, are laterally continuous, exhibit tabular geometry parallel to flow direction, and can continue downfan for several kilometers. Clast-rich deposits are characterized as being unstratified, polymodal, poorly sorted, and having a wide grain-size distribution from clay size particles to boulders >3.5 m in diameter. Coarser grained conglomerates contain reversely graded basal layers and overall reverse coarse-tail grading.

Matrix-rich deposits are generally muddy-sandy pebble conglomerates and pebbly-muddy sandstones which predominate medial and distal fan exposures. Deposits tend to be polymodal, massively bedded, lack basal shear zones or well developed reverse grading, locally exhibit more abrupt decreases in grain size downfan, lack traction structures and erosional scours, and commonly exhibit coarse-tail normal grading. Thickness ranges from 20 cm to >3m. Subaerially emplaced deposits form laterally continuous deposits truncated by sheetflood or braided stream deposits.

Pyroclastic Facies. Primary pyroclastic facies consist of clast-supported dacitic, rhyodacitic, and rhyolitic pumice falls, poorly sorted ignimbrites and block-and-ash deposits.

Block-and-ash flow deposits are dense, nonvesicular lava blocks set in an ash matrix with subordinate amounts of poorly vesicular pumice. These deposits are confined to proximal exposures in the fan.

Tephra deposits in the Puye have been divided into three groups based on distinctive changes in clast type, deposition environment, and source. The three groups are the lower tephra group, middle tephra group, and the upper tephra group. The lower tephra group includes widespread pumice-fall and thin ash flows, thin ignimbrites and tephra redeposited as pumiceous clast-poor debris flows.

The middle tephra group consists of lithic-rich nonwelded ignimbrites, coarse-grained lithic-rich pumice falls and fine-grained capping ash falls. Two large dacite pumice blocks and pumice flow deposits have also been observed in this group.

The upper tephra group is made up of several rhyodacitic pumice fall deposits, abundant lake-deposited pumice and ash, and water lain basaltic ash. Two distinct rhyolite pumice falls are located in the upper tephra group at the top part of the fan sequence. In the central portion of the fan they have been observed to overlie a red clay horizon.

Phreatomagmatic basalts derived from Cerros del Rio volcanic activity interfingers with Puye fluvial gravels and lacustrine sediments in distal portions of the fan.

Lacustrine Facies. Lacustrine deposits, resulting from damming of the Rio Grande by Cerros del Rio basalts, dominate distal fan exposures. Lake deposits are characterized by subaqueously emplaced mudflows, horizontal laminations, abundant tephra, micaceous muds and clays, and lateral grading to stacked pumiceous clast-poor debris flow and sheetflood deposits that form a prominent

apron around the perimeter of the Puye fan. Lake sediments generally lack particles larger than small pebbles. The apron ranges from 2 m to 10 m thick.

Totavi Lentil Member. The Totavi Lentil is a pebble to cobble axial stream gravel deposited by the ancestral Rio Grande. Gravel units range from 1.5 ft to 10 ft thick, exhibit cross and planar bedding, and are interbedded with 1ft to 5 ft thick sand lenses. Imbrication and long axis orientation indicate paleoflow direction to the southwest. Total thickness varies from 16 ft to 150 ft. Fills channels in and locally interbedded with the Puye Fanglomerate. In some areas the Totavi overlies the Santa Fe group. (Dethier, 1997).

12.3.2 Permeability

Very few field-scale measures of permeability for the Puye Formation are available. Table 12-2 summarizes these data, both for five tests conducted in wells screened entirely within the Puye and for six tests in wells screened in multiple units including the Puye. For the latter six tests, the contribution of the Puye Formation to test results is unknown. Lithologic logs from these wells that were tested provide thickness estimates for two facies within the Puye: the “fanglomerate” and the Totavi Lentil. Permeability measurements indicate the fanglomerate is, on average, less permeable than the Totavi Lentil.

A crude estimate of permeability has been done for each of the deposit types found within the Puye Formation (Table 12-3). There are plans for a more detailed study of permeability in the future.

Channel deposits within the fan are dominated by well-sorted pebble-cobble gravels. They are clast-supported conglomerates with medium to coarse sand matrixes and little to no cementing. Based on this, permeability is estimated to be high to medium.

Sheet deposits are also gravel rich with minor to no fines and are estimated to have high to medium permeability.

Clast-rich debris flows are matrix-supported, but because they are clast rich the permeability is estimated to be medium to low. Clast-poor debris flows, however, are dominantly made up of fines and would most likely have low permeability.

Block-and-ash flows and tephra deposits have a varying permeability dependent on the permeability properties of ash and how extensively the ash has been weathered to clays. Fractured basalts have high permeability.

Axial stream gravels are made up of thick sequences of pebble-cobble gravel beds, similar to other channel deposits in the Puye. They would also have high permeability. Lacustrine deposits are dominantly silt to coarse sand, indicating medium to low permeability.

When applied to large-scale hydrofacies, the Fanglomerate would have medium permeability, Totavi Lentil permeability would be high, and permeability of Lacustrine facies would be medium to low.

12.3.3 Size and Geometry

The gravel beds of the Totavi Lentil are defiantly the most permeable unit of the Puye Formation. This makes understanding the size, geometry and continuity of the Totavi very important since those beds will have a great effect on increasing the groundwater flow rate. East-West and North-South dimensions, thickness, and elevation at the top of the bed of Totavi Lentil outcrops were estimated using *Geology of White Rock quadrangle, Los Alamos and Santa Fe Counties, New Mexico* [Dethier, 1997 #212] in order to better understand the size and continuity of the Totavi. Table 12-4 shows the minimum and maximum estimates of outcrops in Ancho, Water, Mortandad, Sandia, and Los Alamos canyons.

12.3.4 Lateral Facies Variations

The following descriptions of lateral facies variations in the Puye are taken from Waresback and Turbeville [, 1990 #37]. Proximal facies are dominated by coarse-grained ignimbrites and block-and-ash sequences which grade downfan to coarse, better sorted clast-rich debris flow deposits. The debris flow deposits then locally grade laterally to hyperconcentrated flood-flow deposits which gradually change to sheetflood and stream-channel facies interbedded with ash-rich clast-poor debris flow deposits. Downfan thinning and fining trends were also observed within these sequences.

Debris flow deposits and lithic-rich ignimbrites show marked lateral variability. Lake deposits interbedded with flow deposits contain abundant pumice and ash. Transitions from inversely graded, clast-rich deposits to fine-grained matrix supported deposits occur in as short a lateral distance as 200 m.

Stream channel deposits compose up to 50% of some sequences in proximal exposures and were observed to decrease in abundance progressively downfan and are replaced volumetrically by better-sorted, thinner, and finer-grained distal braided-stream and sheetflood deposits.

Sheetflood deposits volumetrically dominate in outcrop over distal braided-stream deposits and are approximately proportional to clast-poor debris flow deposits. Downfan, sheetflood deposits exhibit decreases in thickness, improved sorting, better-developed horizontal stratification, and decreases in grain size and angularity. Proximal deposits tend to be more massive while distal deposits show increases in cross-stratal, planar bedsets and horizontally laminated sands and mud.

Several meters of conglomerates and mudstones commonly separate pumice falls in proximal exposures. Distally they become more closely spaced and converge to form thick sequences of primary and reworked pumice and ash.

12.3.5 Cyclic Facies Variations

The following observations of cyclic facies variations were made by Waresback and Turbeville [, 1990 #37]. Majority of the alluvial fan's development is characterized by the stacking of distinctive eruption related depositional sequences on the 5-m to 30-m scale. Cyclic facies resulted from tephra and volcanic-debris flows generated during explosive eruptions and reworking by fluvial processes during inter-eruptive periods.

Proximal exposures contain cyclic sequences of one or more tephra deposits overlain by pumice and ash-rich debris in the lower portions of the fan and by very coarse-grained block-and-ash flow deposits toward the top of the section. Between eruptive events, unconsolidated lava and pyroclastic material was redistributed as clast-rich debris flows emplaced in stacked assemblages.

Clast-supported conglomerates also developed above individual coarse-grained mass-flow sequences, where the upper parts of the debris flow deposits were partially reworked by braided streams. Coarsening or fining upward trends in fluvial conglomerates indicate individual flood cycles. Sheet-like geometries, poor sorting, common normal grading and horizontal bedding of some conglomerates represents periods of intermittent aggradation.

Medial exposures consist of one or more airfall units overlain by ashy debris flow deposits. Thick sequences of alternating clast-rich and matrix-dominated conglomerates developed as debris flows episodically infilled stream channels following eruptions.

In distal exposures, primary pyroclastic deposits are nonexistent or thin and interbedded with stacked pumiceous clast-poor debris flows and sheetflood deposits. Fine-grained, braided stream and intermittent sheetflood conglomerates separate individual clast-poor debris flow deposits. Inter-eruptive depositional sequences are more complex than in proximal exposures. Clast-rich debris flow deposits and coarser-grained stream-channel deposits are lacking in distal fan exposures except toward the top of the overall succession, indicating abrupt fan-wide progradation.

A depositional megasequence is observed in the Puye defined by a large-scale coarsening- and thickening- upward sequence. This is most evident in proximal exposures where the fan is thickest. The megasequence reflects nearly continuous emplacement of the Puye between ~4.0 to 1.7 Ma. The Puye megasequence is capped in proximal and medial exposures by stacked stream-channel deposits.

The overall succession in areas where the megasequence is incomplete can be described by at least two coarsening- and thickening- upward sequences. The lower 70-m of the fan exhibits progradation of coarse-grained streamflow and clast-rich debris flow conglomerates over finer-grained braided-stream, sheetflood and clast-poor debris flow deposits. The other sequence is observed in the 70 m to 110 m interval which consists primarily of stacked deposits of subaqueously emplaced clast-rich debris flow and clast-poor debris flow deposits that grade upfan to subaerially emplaced debris-flow deposits and locally to hyperconcentrated flood-flow conglomerates. In medial exposures, the upper sequence is characterized by rapid vertical transition from coarse clastics to fine-grained mudstone which is overlain by stacked conglomeratic mudstones that occur as uniform, laterally continuous, sheet-like beds ranging from 20 cm to 2.6 m thick. The overall succession is then capped by a thick sequence of channel-fill gravels.

12.3.6 Heterogeneity

The Puye Formation has great variability. Understanding the changes that occur throughout the Puye is very important in order to model water flow throughout the formation. To achieve this understanding, the heterogeneity can be broken down into three scales: large, medium, and small (Table 12-6).

Large Scale. Large scale heterogeneities represent the overall changes throughout the Puye Formation (Figure 12-3, Table 12-7). In this scale, the west to east changes are more significant than ver-

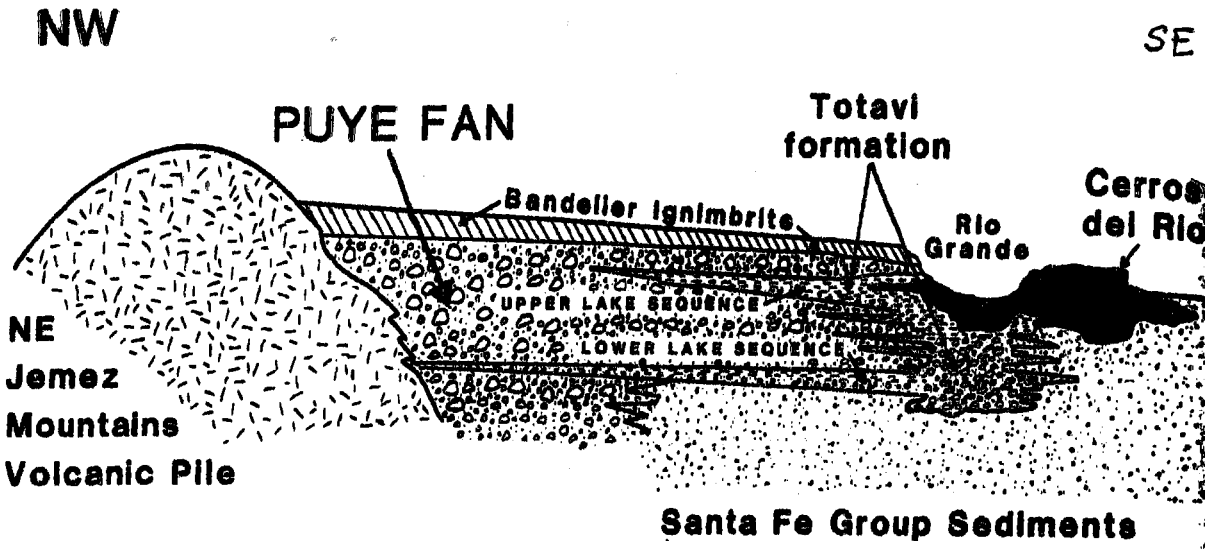

Figure 12-3. Large scale heterogeneity (Waresback and Turbeville, 1990).

tical change as the units vary from the fanglomerate to lacustrine and Totavi units. Heterogeneity occurs at this scale horizontally from 1-10km (.6-6mi) and vertically from .5-4km (.3-2.5mi). On a more detailed level, the fanglomerate can extend horizontally 3-8km (2-5mi) and vertically .4-3.4km (.2-2mi), the Totavi Lentil can extend horizontally 2-7km (1-4mi) and vertically .2-2.4km (.1-1.5mi), and the lacustrine units can extend horizontally 1-6km (.6-3.5mi) and vertically .2-2km (.1-1.2mi). Another observation that can be made on the large scale is whether the Totavi Lentil extends as a continuous sheet or "pancake layer" below the fanglomerate or if it "stair-steps" down west to east. These two theories are currently under debate. Proximal fan is dominated by the fanglomerate. Medial fan contains all three units, and distal portions of the fan are dominated by lacustrine and Totavi Lentil units.

Medium Scale. Medium scale heterogeneities are the larger bedding features seen in outcrop (Figures 12-4 and 12-5). The scale that these transitions occur is horizontally .6-61m (3-200ft) and vertically .6-30m (2-100ft). Some of the heterogeneity that is observed at this scale is the difference between pyroclastic facies such as pumice and ash falls, ignimbrites, block-and-ash flows. These can extend horizontally and vertically 1-5m (3-16ft). Other observations that can be made are grav-

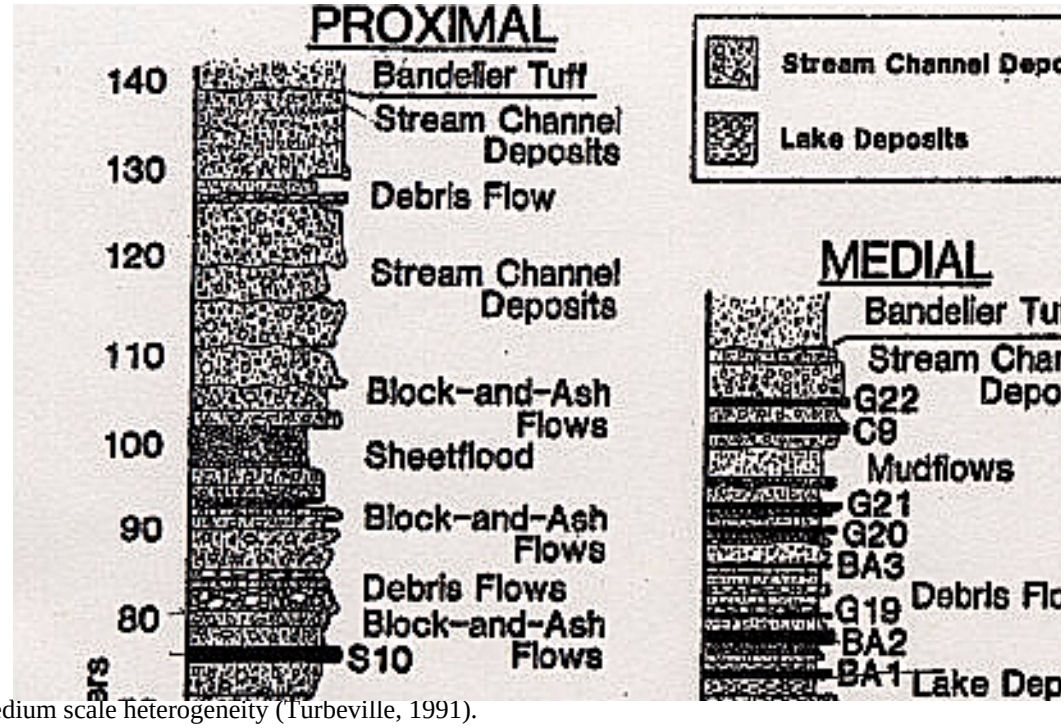

Figure 12-4. Medium scale heterogeneity (Turbeville, 1991).

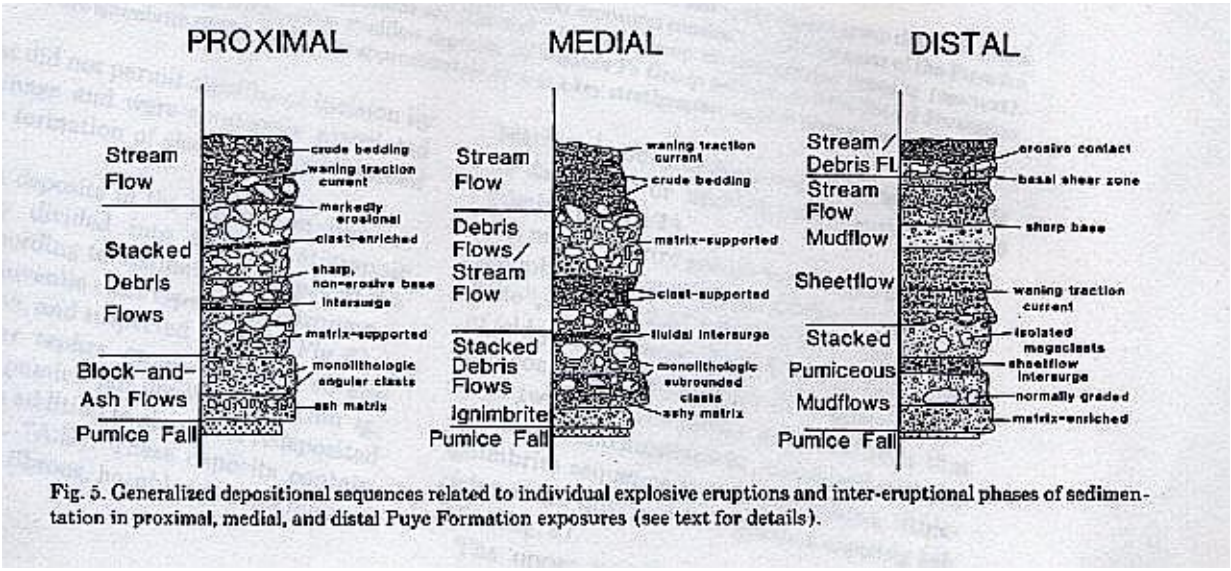

Fig. 5. Generalized depositional sequences related to individual explosive eruptions and inter-eruptional phases of sedimentation in proximal, medial, and distal Puye Formation exposures (see text for details).

Figure 12-5. Medium and small scale heterogeneity (Waresback and Turbeville, 1990).

el beds 1.5-9m (5-40ft), sand beds .6-2m (2-6ft), and boulder rich zones .6-1m (2-4ft). The differ-

ences between stream-channel, debris flow, sheetflood, and mudflow deposits are also made at this scale. Some larger sedimentary structures such as lenses, planar bedding, and cross stratification can be observed on a medium scale. Stream channel, sheetflood, mudflow, and tephra deposits occur throughout all portions of the fan. Block-and-ash flows and clast-rich debris flows are restricted to proximal fan. Clast-poor debris flows occur in medial and distal portions of the fan. Basalts strictly occur in the distal fan.

Small Scale. Small scale heterogeneities are the details seen within the beds of an outcrop (Figure 12-5). They may be too small to be significant in affecting ground water flow, but they are very useful in determining deposit type on a medium scale. These features can be seen horizontally from 0-5ft and vertically from 0-2ft. Heterogeneities observed on this scale are: differences in grain size, silt vs. fine to coarse sand, pebbles, cobbles; grading, normal vs. reverse and massive bedding; matrix vs. clast supported conglomerates; matrix properties such as material, size, cementing agent (silica or calcite), well indurated vs. friable; lithic type, which is very important in determining the difference between fanglomerate stream channel deposits and the Totavi Lentil. Lithic clasts in the fanglomerate channel deposits are volcanic, usually rhyolite and dacite in composition. While Totavi Lentil lithic clasts are dominantly quartzite and other Precambrian material from the Sangre de Cristos. One clay layer was observed in Mortandad Canyon extending horizontally ~2ft and vertically 0-1.5ft. Sedimentary structures that can be observed at this scale are crossbedding, horizontal and ripple laminations, soft sediment deformation features, and erosional scours.

12.4 Field Observations

To further understand the changes throughout the Puye, field studies were done in five locations to observe heterogeneity on large, medium and small scale (Figures 12-3, 12-4, and 12-5). Field studies were restricted because proximal and medial exposures of the fan were located in areas either burned by the Cerros Grande fire or were located on pueblo land. As a result access to Puye outcrops was very limited and mostly distal portions of the fan were observed. Outcrops in Guaje and Rendja canyons represent proximal-medial and medial facies. Truly proximal exposures have yet to be studied. Field notes and photographs representative of the overall appearance of the outcrops were taken at all five locations.

12.4.1 Mortandad Canyon

In Mortandad Canyon thick outcrops of the Totavi Lentil were observed. In some places lacustrine deposits are overlying the Totavi and are interbedded with Cerros del Rio basalts. The Totavi Lentil contains massive pebble to cobble gravel beds ~3-15ft thick. The gravel beds are clast-supported conglomerates interbedded with fine to coarse sand lenses and planar bedded sand units 2-5ft thick. Lithic clasts are dominantly quartzite and Precambrian material. Matrix material is very ash-rich and poorly consolidated. Lacustrine deposits located in the top section of the outcrop are finer grained and exhibit horizontal laminations. Crossbedding and normal grading was observed within the sand units. Gravel beds exhibited minor crossbedding, good sorting and basaltic ash was seen throughout the gravel but was not seen in the sand beds. Total outcrop thickness ranges from 20-100ft (Dethier, 1997), majority of the outcrops in Mortandad Canyon are 60-80ft thick.

The gravel units range from 3-15ft thick and are continuous the entire length of the outcrop. Interbedded in the gravels are 1-5ft thick sand lenses, and near the bottom of the sections is a tabular sand body ~2-3ft thick that continues down the canyon. Overlying the Totavi are 2-4ft thick lacustrine units interbedded with Cerros del Rio basalts.

12.4.2 Los Alamos Highway (SR 502)

Outcrops of the Totavi Lentil were studied along Los Alamos Highway, also referred to as Hwy 502 or SR502. The gravel beds here are very similar to those observed in Mortandad Canyon. The overall outcrop thickness is noticeably thinner than the Totavi outcrops in Mortandad. Total outcrop thickness ranges from 20-100ft (Dethier, 1997). Gravel beds were generally 10-15ft thick and interbedded with cross-stratified medium to coarse sand units. Boulders were present up to 3ft in diameter. Capping the gravel beds, a ~20ft thick finer unit of sediment was observed. This unit is medium grained interbedded with granule sized sand lenses ~1/2 ft thick. At first glance it was thought that this finer unit was lacustrine, but lenticular bodies implies stream channel deposition. Just east of the gravel pit along the highway, the Totavi Lentil appears to interfinger with either the finer sediment units or possibly the Santa Fe Group. On the side of the highway across from the gravel pit, Cerros del Rio basalts cap the Totavi.

12.4.3 Bayo Canyon

Distal fanglomerate and lacustrine facies were observed near the mouth of Bayo Canyon. The fanglomerate showed great variability between and within outcrops. Generally, the

fanglomerate can be described as poorly sorted, silt to boulders up to 3ft in size; deposit types are dominantly debris flow/mud flow, hyperconcentrated flood flow, and stream channel. Cross-stratification and planar bedding was observed in hyperconcentrated flows and stream channel deposits. In one outcrop a mudflow is overlain by a reversely graded pumiceous ignimbrite. Outcrops can be dominated by one deposit type or exhibit many different deposit types throughout a section.

The lacustrine units are fine to medium sand, silt and clay size, well sorted, horizontally laminated. Ripple laminations, soft sediment deformation structures and crossbedding were observed. Lacustrine facies were interbedded in some outcrops with subaquesouly emplaced debris flows, basaltic ash, and very fine-grained tephra deposits. In some areas there was yellow alteration of lacustrine sediments.

12.4.4 Guaje Canyon

Proximal-Medial fanglomerate outcrops in Guaje Canyon are high up above the canyon floor and may not be relevant to fanglomerate below ground. Proximal exposures in the very western portion of Guaje Canyon may have more accessible exposures representative of Puye at groundwater level; however, we did not go up that far in the canyon. The outcrops we did look at were dominantly clast-rich debris flow and hyperconcentrated flood flow deposits with minor clast-poor debris flow and stream channel deposits. Debris flow deposits contain pebble/cobble clasts to boulder up to 4ft in diameter supported by a fine ashy matrix. They are very poorly sorted and exhibit some reverse grading. Debris flow deposits were from 1-4ft thick and would often pinch out or transition into hyperconcentrated flood flow deposits. There was also an angular pumice deposit that appeared to have been reworked by a debris flow. The hyperconcentrated flood flows were medium to coarse sand, ash-rich, moderate to well sorted, exhibiting cross and planar bedding. Some hummocky stratification was also observed.

12.4.5 Rendja Canyon

Some of the best and most accessible proximal-medial exposures of the fanglomerate occur in Rendja Canyon. Like in Guaje, Puye fanglomerate in Rendja Canyon is dominated by clast-rich debris flow and hyperconcentrated flood flow deposits. Stream channel deposits seemed more significant in this canyon than in the outcrop looked at in Guaje. There were little to no clast-poor debris flow deposits. Ash flows were interbedded with the debris and hyperconcentrated flows in some outcrops. Many pumice falls were also observed. In one outcrop a pumice fall had

weathered to a ~6in thick section of pink clay-like material with white pumice lapilli floating in the matrix. Hornblende crystals were seen within the pumice lapilli. As in Guaje Canyon, hyperconcentrated flows are coarse to granular sand size and exhibit crossbedding.

12.5 Well Data

We examined well log data from R-25, R-19, R-12, R-9, R-31, and older wells [Purtymun, 1995 #20] wells. Unfortunately, we discovered that well data have many limitations with respect to the information we were hoping to get from the well logs. Purtymun [, 1995 #20] shows the depths and thickness of the Puye fanglomerate and Totavi Lentil but provides no lithologic descriptions. The R-wells provided depth, thickness, and lithologic information, however in some cases the boundary between what was fanglomerate and what was Totavi was not defined. The lithologic information was useful in showing sand/pebble verse cobble/boulder bed layers and in identifying boulder and argillic clay horizons. Deposit type is near impossible to determine from the log data. Geophysical log data is available for some of the wells and could provide useful sedimentary structure information; however, there is a severe lack of qualified personnel to interpret the data.

Table 12-1. Facies summary

Facies	Sub-facies	Location	Description	Macro-forms	Thickness
Clast Supported Conglomerates	Channel Deposits	proximal to mid-fan exposures	thicker & coarser grained upward in the fan	broad channel-form geometries	individual channel: 30cm->6m sequences
		proximal deposits	coarse grained, very poorly sorted, normal & reverse grading some conglomerates capped by pebbly sandstones which form discontinuous lensoid bodies		

		distal deposits	much thinner, better sorted, finer grained polymodal, normally graded, stratification better developed	laterally extensive, lenticular bodies	10cm- 3.5m
	Sheet Deposits		sheet-like sandy-pebble conglomerates & pebbly sandstones absence of deep scours, uniform horizontal stratification, lack of apparent size grading	laterally continuous with only slight thinning up to hundreds of meters	10cm- 3m individual scours rarely exceed 15cm stacked sand-gravel couplets 1-5cm
		proximal deposits	confined to lower parts of the succession		
Matrix-Supported Conglomerates	Clast-rich Deposits	most prevaliant proximally and in upper parts of the succession	sandy-cobble & boulder conglomerates, unstratified, polymodal, coarser grained cong. contain reversely graded basal layers & overall reverse coarse-tail grading, very poorly sorted	laterally continous tabular bodies	20cm - >4m

	Matrix-rich Deposits	predominate in mid- and distal fan outcrops	lack basal-shear zones or well developed reverse grading, more abrupt decreases in max particle size down-fan, lack traction structures, polymodal, muddy-sandy conglomerates & pebbly-muddy sandstones, commonly coarse-tailed normally graded, lack erosional scours	subaerially emplace: laterally continuous, sheet-like bodies interbedded w/ and truncated by clast supported sheetflood or braided stream conglomerates, most beds are massive	20cm - >3m
		distal exposures	predominance of lacustrine deposits, subaqueously emplaced mudflows		
Pyroclastic Facies	Block-and-ash flows	confined to proximal exposures	dense, nonvesicular lava blocks set in an ash matrix with subordinate amounts of poorly vesicular pumice		
	Lower Tephra Group		widespread pumice-fall and thin ash-flows, thin ignimbrites, redeposited tephra		
	Middle Tephra Group		lithic-rich nonwelded ignimbrite, coarse-grained lithic-rich pumice falls & fine grained capping ash falls, pumice flow deposits, 2 large dacite pumice blocks		

	Upper Tephra Group		several rhyodacitic pumice falls, abundant lake-deposited pumice and ash, water lain basaltic ash 2 Rhyolite Pumice Falls in @ top part of the fan overlies red clay horizon in central portion of the fan		
	Phreato magmatic Basalts	distal fan	interfinger with Puye fluvial gravels and lacustrine sediments, derived from Cerros del Rio eruptions		

Facies	Sub-facies	Location	Description	Macro-forms	Thickness
Lacustrine Facies		distal fan	subaqueously emplaced mudflows, horizontal laminations, abundant tephra and grades laterally to stacked pumiceous CPDF and sheetflow deposits that form a prominent apron around the perimeter of the Puye fan		apron: 2- 10m

Totavi Lentil Member

Facies	Sub-facies	Location	Description	Macro-forms	Thickness
axial stream deposits from ancestral Rio Grande		distal fan	pebble to cobble gravel, lithics dominantly quartzite and other metamorphic rocks, cross and planar beds, sand lenses, fills in channels of and locally interbedded with the fanglomerate, some areas overlies Santa Fe group		gravel beds: 1.5- 10ft sand lenses: 1- 5ft total: 16- 150ft

Table 12-2. Permeability data for the Puye Formation

Well	Permeability (log 10, m^2)	Hydrostratigraphic Unit
TW-8	-12.1	Fanglomerate
R-15	-12.2	Fanglomerate
TW-3	-11.2	Totavi Lentil
TW-2	-11.1	Totavi Lentil
TW-1	-12.0	Totavi Lentil
Test Well DT-9	-10.8	Multiple units including Puye
Test Well DT-5A	-12.1	Multiple units including Puye
Test Well DT-10	-11.3	Multiple units including Puye
PM-5	-12.5	Multiple units including Puye
PM-4	-11.9	Multiple units including Puye
PM-2	-11.8	Multiple units including Puye

Table 12-3. Generalized permeability estimates for facies within the Puye

Deposit Type	Permeability
Channel deposits	high to medium
Sheet deposits	high to medium
Clast-rich debris flow	medium to low
Clast-poor debris flow	low
Block-and-ash flow	medium to low
Tephra	medium
Basalts	high (if fractured)
Axial stream deposits (Totavi Lentil)	high
Lacustrine	medium to low

Table 12-4. Totavi Lentil Outcrop Information (m)

Out crop Name	North-South Dimensions	East-West Dimensions	Thick-ness	Top Elevation

	Min-imum	Max-imum	Min-imum	Max-imum	Min-imum	Max-imum	
Ancho Canyon	20.1	244	80.7	264	18.3	30.5	1755.6
Water Canyon	20.4	223	61	122	12.2	18.3	1524
Mortandad Canyon	61	223	41	548.6	18.3	24.4	1774
Sandia Canyon	41	142	41	771.8	6.1	18.3	1792
Los Alamos Canyon	41	893.7	41	1097.3	6.1	30.5	1823

Table 12-5. Lateral Facies Variations of the Puye Formation

Proximal	Medial	Distal
dominated by coarse-grained ignimbrites & chaotic block-&-ash sequences	grade down fan to coarse, better sorted clast rich debris flows (CRDF)	CRDF locally grade laterally & vertically to hyperconcentrated flood flow deposits & eventually to sheet flood & stream channel dominated facies interbedded with ash-rich clast poor debris flows (CPDF)
stream channel deposits more abundant (as much as 50% of exposures), coarse-grained, poorly sorted, normal & reverse grading	decrease in abundance progressively downfan	replaced volumetrically by better-sorted, thinner, & finer-grained braided stream & sheet-flood deposits
	downslope increase in the proportion of sheetflood deposits	volumetrically dominate over braided stream deposits & become approximal to CPDF deposits
	progressive downfan decreases in the thickness of sheetflood deposits are accompanied by improved sorting, horizontal stratification	

more massive & structureless		downfan increase in cross-stratal, planar bedsets, horizontal laminated sands & muds
pumice falls commonly separated by several meters of conglomerates and mudstones		more closely spaced & eventually converge to form thick sequences of primary & reworked pumice & ash lacustrine sediments more dominate (as much as 70% of exposures)
	increase in lacustrine deposits	
transitions from inversely-graded, clast rich deposits to fine grained ungraded or normally graded, matrix-dominated deposits occur in short lateral distances (as short as 200m)	matrix-rich deposits predominate in medial and distal exposures (as much as 50%)	
block-and-ash flows confined to proximal exposures		

Table 12-6. Heterogeneity of the Puye Formation

Large Scale
overall facies changes throughout the entire Puye Formation
Transitions dominantly occur west to east
Scale[1&2]: Horizontal: 1-10km (.6- 6mi)
Vertical: .5- 4km (.3- 2.5mi)
Heterogeneity
Fanglomerate 3- 8km (2- 5mi)
Totavi Lentil 2- 7km (1- 4mi)
Stair-stepping vs. pancake layer
Lacustrine Facies 1- 6km (.6- 3.5mi)
Location within the fan[2-4]

Proximal: dominated by fanglomerate
Medial: dominantly fanglomerate interbedded with lacustrine and Totavi Lentil
Distal: Lacustrine and Totavi Lentil with minor fanglomerate

Medium Scale

Larger features seen in outcrop
Transitions occur vertically and horizontally throughout outcrop
Scale[1&2]: Horizontal:.9- 61m (3- 200ft)
Vertical: .6- 30m (2- 100ft)
Heterogeneity
Pyroclastic facies 1- 5m (3- 16ft)
Pumice flows, pumice and ash falls, ignimbrites, block-and-ash flows
Gravel beds 1.5- 9m (5- 40ft)
Sand beds .6- 2m (2- 6ft)
Boulder rich zones .6- 1m (2- 4ft)
Clastic deposits .6- 24m (2- 80ft)
Stream-channel, debris flow, sheetflood, mudflow
Sedimentary structures
Lenses, planar bedding, cross stratification
Location within the fan[2-4]
Proximal: channel deposits, sheet deposits, clast-rich debris flow, block-and-ash flows, tephra deposits
Medial: channel deposits, sheet deposits, matrix-rich debris flow, tephra deposits
Distal: channel deposits, sheet deposits, matrix-rich debris flow, tephra deposits, phreatomagmatic basalts, lacustrine deposits, Totavi Lentil
Photographs
Mortandad Canyon #1-3, 7,8,9-13,17,18-20,24&2528-30,31
Los Alamos Highway (SR502) #1-3,4
Bayo Canyon #1,2,3,4,6,7,8-10,11-13

Small Scale

Details within the beds of an outcrop
Transitions occur vertically and horizontally throughout bedding
Scale[1]: Horizontal: 0- 5ft
Vertical: 0-2ft
Heterogeneity
Grain size
Fine to medium sand, pebble, cobble
Grading
Normal vs. reverse
Matrix vs. clast supported conglomerates
Matrix properties
Fine vs. coarse sand, ash
Cementing
Indurated vs. friable
Calcite vs. silica, etc.
Lithic type
Volcanic vs. quartzite
Pumice, fine ash deposits
Clay layers 0- 1.5ft
Sedimentary structures
Crossbedding, horizontal and ripple laminations, soft sediment deformation fea-

tures, erosional scours
Location within the fan
Seen throughout the entire fan
Photographs
Mortandad Canyon #4,5,6,14,1521,22,23,26
Los Alamos Highway (SR502) #4,5,6
Bayo Canyon #5

Table 12-7. Variations within the Puye according to distance from source

PROXIMAL

Deposit Types

Channel deposits

Sheet deposits

Clast-rich debris flows

Block-and-ash flows

Tephra deposits

Characteristics

Single, large-scale coarsening upward, fan wedge is thickest

Overall upward decrease in sheetflood gravels and CPDF deposits that dominate lower parts of the succession

Capped by stacked stream channel deposits

Dominated by coarse-grained ignimbrites and chaotic block-and-ash sequences

Stream channel deposits more abundant: coarse grained, poorly sorted, normal and reverse grading

More massive and structureless

Pumice falls commonly separated by several meters of conglomerates and mudstones

Transitions from inversely-graded clast-rich deposits to fine-grained ungraded or normally graded

Matrix dominated deposits occur in short lateral distances (as short as 200m)

One or more tephra deposits overlain by pumice and ash-rich debris in the lower portions of the fan and by very coarse grained, block-and-ash flow deposits toward the top of the section

Clast-supported conglomerates also commonly developed above individual coarse-grained mass-flow sequences where upper parts of debris-flow deposits were partly regraded by shallow braided streams

MEDIAL

Deposit Types

Channel deposits

Sheet deposits

Clast-poor debris flows

Tephra deposits

Lacustrine facies (minor)

Totavi Lentil (minor)

Characteristics

Capped by stacked stream channel deposits

Rapid vertical transition form coarse clastics to fine-grained mudstone

Fine-grained units overlain by stacked conglomeratic mudstones that occur as uniform, laterally continuous, sheet-like beds ranging from 20cm to 2.6m

Grade down fan to coarse, better-sorted clast rich debris flows

Decrease in stream channel abundance progressively downfan

Progressive down fan decreases in the thickness of sheetflood deposits are accompanied by improved sorting, horizontal stratification

Increase in lacustrine deposits

Matrix-rich deposits (CPDF) dominate in medial and distal exposures

One or more airfall units overlain by ashy debris-flow deposits

Thick sequences of alternating clast-rich and matrix-dominated conglomerates developed as debris flows episodically in filled stream channels following eruptions

DISTAL

Deposit Type

Channel deposits

Sheet deposits

Clast-poor debris flows

Tephra deposits

Lacustrine facies

Totavi Lentil

Characteristics

CRDF locally grade laterally and vertically to hyperconcentrated flood flow deposits and eventually to sheet flood and stream channel dominated facies interbedded with ash-rich clast-poor debris flows (CPDF)

Stream channel deposits replaced volumetrically by better-sorted, thinner, and finer-grained braided stream and sheetflood deposits

Sheetflood deposits volumetrically dominate over braided stream deposits and become approximal to CPDF deposits

Downfan increase in cross-stratal, planar bedsets, horizontal laminated sands and muds

More closely spaced and eventually converge to form thick sequences of primary and reworked pumice and ash

Lacustrine sediments more dominate

Primary pyroclastic deposits are thin and interbedded with stacked pumiceous CPDF and sheetflood deposits

Individual CPDF deposits separated by fine-grained, braided stream and intermittent sheetflood conglomerates

Inter-eruptive depositional sequences more complex than in proximal exposures